# UNIVERSITÀ DEGLI STUDI DI NAPOLI "FEDERICO II"

**DOCTORATE SCHOOL IN BIOLOGY**

Cycle XXXVI

***Health and environmental risks deriving from the reuse of treated wastewater***

***Rischi sanitari e ambientali derivanti dal riutilizzo delle acque reflue trattate***


Coordinator

Prof. Sergio Esposito

Supervisor

Prof. Giovanni Libralato

Co-Supervisor

Dr. Antonietta Siciliano

PhD student

Lorenzo Saviano


Academic Year 2022 – 2023

# Acknowledgements

This PhD project with title “Health and environmental risks deriving from the reuse of treated wastewater” was supported and financed by Istituto Nazionale della Previdenza Sociale (INPS) and therefore I would like to express my deepest gratitude towards it.

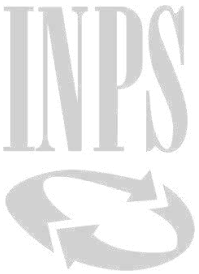



Between July and October 2023, I had the privilege of conducting research abroad at the Center for Marine Research, Ruđer Bošković Institute, under the guidance of Professor Daniel M. Lyons. During this period, I was involved in a series of experiments and investigations that significantly expanded the scope of my research, delving into various environmental scenarios.

I would like to express my heartfelt gratitude to Professor Daniel M. Lyons for hosting me during my stay and for providing invaluable support and collaboration throughout my research activities. The opportunity to work with the talented research team at the Center for Marine Research played a pivotal role in broadening my research horizons and deepening my understanding of the complex field of marine environmental science.

During my time abroad, I conducted toxicity tests on *Mytilus galloprovincialis*, as well as oxidative stress tests on lanthanum and cerium nanoparticles, going beyond the initial focus on levofloxacin removal. These experiments were instrumental in extending my studies to different environmental scenarios, shedding light on the potential effects of advanced oxidation processes with nanoparticles in a broader context.

The knowledge and experiences gained during my time abroad have significantly enriched my research, and I am truly thankful for the support and collaboration I received during my stay at the Center for Marine Research. This international experience has played a crucial role in enhancing the scope and depth of my research.

# CONTENTS

# *List of Figures*

# *List of Tables*

# *Publications*

The thesis is based on the following co-authored papers.

| ***Paper*** | ***IF*** | ***Citations*** |
|---|---|---|
| ***Saviano, L.,*** *Brouziotis, A. A., Suarez, E. G. P., Siciliano, A., Spampinato, M., Guida, M., Trifuoggi M., Del Bianco, D., Carotenuto, M., Spica, V.R., Lofrano, G., Libralato, G. Catalytic Activity of Rare Earth Elements (REEs) in Advanced Oxidation Processes of Wastewater Pollutants: A Review (**2023**) 28(17), 6185. DOI: 10.3390/molecules28176185* | ***4.927 (Q1)*** | **0** |
| *Lofrano, G., Serafini, S., **Saviano, L.,** Carotenuto, M., Guida, M., Spica, V. R., Cardito A., Libralato, G. A holistic picture of spatial distribution of river polluting loads in a highly anthropized area (**2023**) 887, 163784. DOI: 10.1016/j.scitotenv.2023.163784* | ***10.754 (Q1)*** | **0** |
| *Siciliano, A., Medici, A., Guida, M., Libralato, G., **Saviano, L.,** Previtera, L., Di Fabio, G., Zarrelli, A. Newly Discovered Irbesartan Disinfection By-products via Chlorination: Investigating Potential Environmental Toxicity (**2023**) 13(14), 8170. DOI: 10.3390/app13148170* | ***2.7 (Q2)*** | **0** |
| *Medici, A., **Saviano, L.**, Siciliano, A., Libralato, G., Guida, M., Previtera, L., Di Fabio, G., Zarrelli, A. Octocrylene: From Sunscreens to the Degradation Pathway during Chlorination Processes: Formation of By-products and Their Ecotoxicity Assessment (**2022**) 27(16), art. no. 5286. DOI: 10.3390/molecules27165286* | ***4.927 (Q1)*** | **1** |
| *Luongo, G., Siciliano, A., Libralato, G., Guida, M., **Saviano, L.**, Previtera, L., Di Fabio, G., Zarrelli, A. Complete characterization of degradation by-products of olmesartan acid, degradation pathway, and ecotoxicity assessment (**2021**) 11 (12), art. no. 5393. DOI: 10.3390/app11125393* | ***2.7 (Q2)*** | **0** |
| *Luongo, G., **Saviano, L.**, Libralato, G., Guida, M., Siciliano, A., Previtera, L., Di Fabio, G., Zarrelli, A. Secondary effects of hypochlorite treatment on the emerging pollutant candesartan: The formation of degradation by-products and their toxicological profiles. (**2021**) 26 (11), art. no. 3422. DOI: 10.3390/molecules26113422* | ***4.927 (Q1)*** | **1** |
| *Luongo, G., Siciliano, A., Libralato, G., Serafini, S., **Saviano, L.**, Previtera, L., Di Fabio, G., Zarrelli, A. LC and NMR studies for identification and characterization of degradation by-products of olmesartan acid, elucidation of their degradation pathway and ecotoxicity assessment (**2021**) 26 (6), art. no. 1769. DOI: 10.3390/molecules26061769* | ***4.927 (Q1)*** | **3** |
| *Siciliano, A., Guida, M., Libralato, G., **Saviano, L.**, Luongo, G., Previtera, L., Di Fabio, G., Zarrelli, A. Amoxicillin in water: Insights into relative reactivity, by-product formation, and toxicological interactions during chlorination. (**2021**) 11 (3), art. no. 1076, pp. 1-12. DOI: 10.3390/app11031076* | ***2.7 (Q2)*** | **5** |

| | | |
|---|---|---|
| *Luongo, G., Guida, M., Siciliano, A., Libralato, G., **Saviano, L.**, Amoresano, A., Previtera, L., Di Fabio, G., Zarrelli, A. Oxidation of diclofenac in water by sodium hypochlorite: Identification of new degradation by-products and their ecotoxicological evaluation (**2021**) 194, art. no. 113762.*<br>*DOI: 10.1016/j.jpba.2020.113762* | ***3.571 (Q2)*** | **14** |
| *Romanucci, V., Siciliano, A., Guida, M., Libralato, G., **Saviano, L.**, Luongo, G., Previtera, L., Di Fabio, G., Zarrelli, A. Disinfection by-products and ecotoxic risk associated with hypochlorite treatment of irbesartan (**2020**) 712, art. no. 135625.*<br>*DOI: 10.1016/j.scitotenv.2019.135625* | ***10.754 (Q1)*** | **20** |

## *Other Publications*

| | | |
|---|---|---|
| *Suarez, E. P., Pugliese, S., Galdiero, E., Guida, M., Libralato, G., **Saviano, L.,** Spampinato, M., Pappalardo, C., Siciliano, A. Multigenerational test on Daphnia spp.: A vision and new perspectives (**2023**) 122629.*<br>*DOI: 10.1016/j.envpol.2023.122629* | ***9.988 (Q1)*** | **0** |
| *Siciliano, A., Zorrilla, J. G., **Saviano, L.,** Cimmino, A., Guida, M., Masi, M., Meyer, S. Insights into the Ecotoxicology of Radicinin and (10 S, 11 S)-(—)-epi-Pyriculol, Fungal Metabolites with Potential Application for Buffelgrass (Cenchrus ciliaris) Biocontrol (**2023**) 15(6), 405.*<br>*DOI: 10.3390/toxins15060405* | ***5.075 (Q1)*** | **0** |
| *Siciliano, A., Sabatino, M., Paone, A., Padilla Suarez, E. G., Toscanesi, M., Brouziotis, A. A., Gambino, E., **Saviano, L.,** Trifuoggi, M., Guida, M., Libralato, G. A first attempt to evaluate the toxicity to Phaeodactylum tricornutum Bohlin exposed to rare earth elements (**2022**) 10, 957943.*<br>*DOI: 10.3389/fenvs.2022.957943* | ***5.411 (Q1)*** | **1** |
| *El Bouaidi, W., Libralato, G., Tazart, Z., Enaime, G., Douma, M., Ounas, A., **Saviano, L.**, ... & Loudiki, M. Nature-based coagulants for drinking water treatment: An ecotoxicological overview (**2022**) 94(8), art. no. e10782.*<br>*DOI: 10.1002/wer.10782* | ***3.306 (Q2)*** | **1** |

# INTRODUCTION

The world population growth has led to an increased demand for water in the production of food, supply industries, and sustenance of human populations. However, since the ocean constitutes the largest water reservoir (97.3%), the amount of fresh water available for human activities is only a small fraction [1]. Wastewater use is increasingly seen as an opportunity to meet these growing water needs. Currently, the agricultural sector is the largest user of water and wastewater globally, accounting for approximately 70% of water use on average [2].

However, the widespread use of wastewater in agriculture presents drastic public health risks that should be addressed. For this reason, organizations, including the WHO, have developed guidelines to ensure that contaminant levels in wastewater are below limits harmful to human health [3]. In many cities in developing regions, farmers in urban and peri-urban areas use untreated wastewater to irrigate their crops and accept these risks despite significant contamination that contributes to a wide burden of water-related disease [4]. The use of wastewater is also growing in response to climate change as it can guarantee a consistent source of water in variable or dry conditions [5]. Several parameters influence the type and gravity of health risks incurred, like the wastewater treatment extent, pollutant characteristics, human exposure, and local risk factors. Compounds normally present in irrigated wastewater that may pose risks to human health are the emerging contaminants (ECs). These include polycyclic aromatic hydrocarbons (PAHs), personal care products (PCPs), and endocrine disrupting chemicals (EDCs), creating potential health risks. Effluents from municipal wastewater treatment plants are a primary source of ECs, as conventional treatment processes are unable to effectively block the release of these compounds into the environment [6]. Furthermore, agriculture and farming are classified as additional EC sources, with the former contributing to diffuse pollution through pesticides and the latter through antibiotics [7].

Among the various ECs present in the environment, this study focus on pharmaceuticals and personal care products (PPCPs) due to their frequent use, detection in different environmental matrices in high concentrations and the potential risk for ecosystem [8], [9], [10].

The specific research areas include the analysis of the degradation pathways and ecotoxicity of sartans, which are widely used antihypertensive drugs worldwide, as well as non-steroidal anti-inflammatory drug as diclofenac, and well-known antibiotics as amoxicillin and levofloxacin. Additionally, the environmental fate and the impact on ecosystem of an important constituent of sunscreens, such as octocrylene, which has recently raised concerns regarding its potential adverse effects on the endocrine system [11], were investigated.

Furthermore, this work delves into the metabolic fate and adverse effects of some emerging contaminants on human and environmental health, and investigate also the potential removal processes. In particular, removal mechanism through advanced oxidation processes (AOPs) is emphasized because of their utmost importance in eliminating micropollutants. In detail, this thesis consists of **six chapters**.

**Chapter 1** is dedicated to the "Water Problem" which encompasses the depletion of this resource mainly due to increasing population densities and changing climatic conditions. The water deficit crisis has prompted a growing reliance on wastewater in the agricultural sector. Consequently, research has focused on the risks to human health and food safety, primarily associated with frequent exposure to a range of contaminants. This chapter provides a detailed overview of the primary pollutants and emerging pollutants found in water, with a specific focus on pharmaceuticals and the environmental and health risks associated with them.

**Chapter 2** describes the differences between conventional and non-conventional wastewater treatment systems, focusing on the potential of advanced treatments to reduce or even eliminate pollutants that are dangerous to human health. It presents classifications and fundamentals of advanced oxidation processes (AOPs) as a valid alternative to conventional water purification systems, due to their potential to completely mineralize pollutants or transform them into biodegradable molecules. The chapter also discusses the different types of AOPs for water treatment (Photolysis, Homogeneous phase AOPs, Heterogeneous photocatalysis, Process involving REEs catalysts), their catalytic mechanisms and their performance in addressing various targets, including pharmaceutical products.

**Chapter 3** addresses the environmental presence of pharmaceutical products, specifically sartans, a family of highly selective antihypertensive agents used to regulate blood pressure. It offers a comprehensive picture of sartans, including their chemical structure, chemical-physical properties, by-products in aqueous solutions,

low metabolic degradation, high environmental persistence, and their fate in wastewater treatment plants. The chapter focuses on irbesartan, candesartan, and olmesartan examining the degradation process following treatment with hypochlorite. It explains the mechanism of formation of the degradation by-products and their implications for ecotoxicological and environmental risk assessment in detail.

**Chapter 4** shifts the focus to another emerging micropollutant found in personal care products: octocrylene, an organic sunscreen primarily designed to absorb UVB radiation and short UVA wavelengths. It explores the behavior and fate of octocrylene in the environment, highlighting its potential to enter aquatic ecosystems through leaching from the skin or indirectly through wastewater. The study, conducted under similar chlorination conditions as for sartans, shows the potential generation of toxic degradation by-products, increasing the potential risk to the marine environment.

**Chapter 5**, following the approach used in Chapter 3 and 4, investigates the ecotoxicological effects of the degradation products of two drugs such as diclofenac and amoxicillin. It evaluates the environmental fate and toxicological interactions involving the degradation products of these contaminants, which emerge during simulated chlorination processes. Finally, the antibiotic activity of amoxicillin is measured by inhibition tests of microbial growth using 3 different bacterial strains, in order to determine the potential loss of antibacterial activity in the isolated degradation by-products.

**Chapter 6** introduces a new aspect related to the removal of emerging contaminants and especially unwanted by-products, given the high difficulty in their removal. In particular, a new frontier is represented by the use of Rare Earth Elements (REEs) as catalysts in AOPs, so much so that we can think about their implementation in wastewater treatment in the future. This chapter discusses how REE-based catalysts in heterogeneous AOPs can represent a promising technology in degrading contaminants such as pharmaceuticals. Specifically, the preliminary study on the drug Levofloxacin, a widely used antibiotic belonging to the quinolone family, is introduced. Simulated irradiation systems used in combination with different REE-based catalysts showed different degradation kinetics. The experimental activities have in fact made it possible to develop and compare kinetic models of advanced oxidation processes and to evaluate the best combination and performance of the process in terms of degradation capacity of the chosen target contaminant. In the

present study, the AOP process performance, under the same conditions, on the inactivation of a certified strain of *E. faecalis* selected on the basis of its resistance to Levofloxacin was also investigated.

In conclusion, I can say that this PhD thesis demonstrates that AOPs may be represent a new frontier of alternative eco-friendly treatments for the removal of emerging contaminants from wastewater effluents. Preliminary experimental results tend to demonstrate that AOPs coupling solar simulated radiation with REE-based catalysts have the potential to open up new viable remediation strategies for WWTPs effluent tertiary treatment before wastewater reuse, as in the case of irrigation. However, most investigations are done at lab-scale. For a practical view and commercial uses, it would be advisable to shift the working energies from batch work to a large scale work to discover the efficiency and ecotoxicity of the processes.

# CHAPTER 1

## 1.1 The “Water Problem” in the world – UN-SDGs

During the twentieth century, the world experienced a technological and industrial explosion which, along with economic development and population growth, led to a significant increase in the use of one of the most precious resources: water. Water plays a fundamental role in both human life and the environment, and despite its varied distribution, it remains the most widespread substance on our planet. Concerning humans, water represents the main component (73.2%) of our bodies and is essential for a good state of health. Furthermore, it serve as critical resource for various human activities, including agriculture, commerce, industry and domestic use [12].

The rise in water consumption has, as a direct consequence, increased water pollution, which either partially or totally precludes its intended use. In contrast to the excessive and thoughtless water use in industrialized countries, more than one billion people worldwide suffer from water shortages. Consider, for instance, that an African family uses less than 20 liters of water a day [13].

In 1977 the United Nations held the first World Conference on Water Resources in Argentina in which the unfavorable situation, relative to fresh water, of a third of the world located in areas with insufficient humidity was analysed. Furthermore, it was concluded that many of the same problems currently present in those areas would emerge in many other countries by the end of the century [1]. In the final resolution of this conference, the principle of the human right to water was introduced by stating that "everyone has the right to access drinking water in quantity and quality corresponding to their basic needs". In fact, among the Sustainable Development Goals (SDGs) of the UN Agenda 2030, we find Goal 6, which is "to ensure the availability and sustainable management of water and sanitation for all". Water connects us all. Water is embedded in almost all the other SDGs, particularly those dealing with food, energy and the environment. Water is the gossamer that links the web of the 17 SDGs and their 169 targets. No longer can water be addressed as a separate element in isolation from the other goals. But this interconnectedness has important implications. It means that the Water Goal will only be achieved if the other goals are attained, and in turn, that other SDGs will only be achieved if the

Water Goal is attained. Table 1 summarizes the targets of SDG6 to be achieved by 2030.

| **SDG6** | Ensure availability and sustainable management of water and sanitation for |
|---|---|
| ***6.1*** | By 2030, achieve universal and equitable access to safe and affordable drinking water for all |
| ***6.2*** | By 2030, achieve access to adequate and equitable sanitation and hygiene for all, and end open defecation, paying special attention to the needs of women and girls and those in vulnerable situations |
| ***6.3*** | By 2030, improve water quality by reducing pollution, eliminating dumping and minimizing release of hazardous chemicals and materials, halving the proportion of untreated wastewater, and at least doubling recycling and safe reuse globally |
| ***6.4*** | By 2030, substantially increase water-use efficiency across all sectors and ensure sustainable withdrawals and supply of fresh water to address water scarcity, and substantially reduce the number of people suffering from water scarcity |
| ***6.5*** | By 2030 implement integrated water resources management at all levels, including through transboundary co-operation as appropriate |
| ***6.6a*** | By 2030, expand international co-operation and capacity-building support to developing countries in water and sanitation-related activities and programmes, including water harvesting, desalination, water efficiency, wastewater treatment, recycling and reuse technologies |
| ***6.6b*** | Support and strengthen the participation of local communities for improving water and sanitation management |

**Table 1:** The Water Goal.

While progress is being made in many places, the overall speed of achieving the 2030 Agenda goals is not yet of the required scale. As a result, lack of access to safe drinking water and related problems remain a major concern [14]. Of all the activities that require water, agriculture is the most significant. According to the latest FAO data [15], water withdrawal for agricultural purposes represents 71.7% of total water consumption worldwide. This proportion is even higher in arid and semi-arid countries. The demand for water, related to agriculture, is destined to increase further due to population growth, which has led to an increase in the demand for food. Unfortunately, the overall amount of conventional water available in the world remains stable, therefore, additional non-conventional water resources are required. Currently less than 10% of irrigated land worldwide uses unconventional water. This percentage should be increased to meet growing water demand in the future [12]. One of the possible remedies for a more rational use of water resources is represented by the possibility of recovering waste water after an appropriate purification

treatment, to then allocate it to new uses. The choice of the type of process and the degree of treatment to be applied depends on the source of the water and the intended use of it. The purified water can be reused by industries for their internal processes, such as fire water, for washing roads and cars, for irrigation in agriculture, or by the civic network as drinking water. Unfortunately, developing countries begin from a disadvantaged position in the developing wastewater as a resource due to the lack of means and technologies that would enable them to set up purification plants and to divide wastewater into different treatment systems and destinations. In industrialized countries, on the other hand, there is the possibility of building two large pipeline networks: one for the supply of drinking water and the other for raw water.

### 1.1.1 Scarcity and importance of clean water

Clean water is a vital element for all living organisms. Population growth, economic development, and dietary shift (toward more animal products) have led to a rapid increase in the demand for water. In the Global Risks 2015 Report of the World Economic Forum, water supply crisis was recognized as the top 1 high-impact risk for our current times [16]. The contamination of present water resources, which can be chemical, physical and microbiological, however, has increased globally due to rapid industrialization and the massive population explosion [17]. Urbanization has created various challenges related to water use especially in low and middle income countries, in fact, it is estimated that 36% of the world's population already lives in regions with water scarcity [18]. The main regions experiencing water scarcity are Africa, Southeast Asia, India and China [14]. In agriculture, the demand for and consumption of clean water has increased on a wide scale. The consumption of fresh and clean water with a broad range of pollutants in industry, household sectors, and other forms of consumption is about 70%, 22%, and 8%, respectively [19]. Water scarcity can be mainly attributed to water shortages per se, lack of access, due to the inability of institutions to guarantee a regular supply, and global warming. However, understanding water scarcity is important to squeeze policies at global, regional, national, and local scales.

### 1.1.2 Challenges and concerns related to water resources

Nowadays, several regions in the world have no access to waters intended for human uses and the problem of water scarcity is expected to get worse in the coming decades. Hence, water scarcity is a serious problem to be addressed, involving urban, industrial and agricultural sectors, and that needs a rapid response.

A novel integrated approach considering that takes into account the main actors (urban, agriculture and industry) involved in the whole water cycle management (water supply, water use, and wastewater treatment and reuse/recycle) has to be established.

Furthermore, as a result of the increased water scarcity and drought due to climate change [20], widespread water use for irrigation is expected to occur in the context of growing competition between agriculture and other sectors of the economy. To address future estimates of water shortages, some measures aimed at rationalizing and optimizing the efficiency of water consumption in the agricultural sector are critical in view of the huge volumes of water required for the production of crops. Irrigation is used to compensate losses due to crop evapotranspiration and to achieve full production under the given growing environment [21]. Irrigation, however, is also applied to fight parasites through products diluted in the water, for frost protection of sensitive crops, to add nutrients dissolved in the water, to increase the physical properties of land, to remove excess salinity from the soil and to modify the soil pH.

The main challenge is to enable a sustainable approach to water resource management that can provide economic, environmental and social benefits to all the contributing sectors.

The sustainable water management concept refers to all strategies that improve crop yield and minimize non-beneficial water losses. Such strategies are mainly based on the possibility to use the effluents of Waste Water Treatment Plants (industrial and/or urban) as a potential, valuable resource for one or several other industries or that can be used for agricultural purposes.

However, the recovery of this resource from WWTPs requires before effective wastewater treatment at a sustainable cost. This will allow to meet the stringent regulations for both environmental discharge and water reuse and to address the problem of the increasing release of more toxic and non-biodegradable contaminants

(especially by industrial and agricultural activities) that damage or resist conventional biological wastewater treatments.

Conventional water and wastewater treatments have been long established in removing many chemical and microbial contaminants that pose threats to public health and the environment. However, the effectiveness of these processes has become limited in recent years due to the implementation of much stricter new regulations (expansion of regulated contaminants and lowered danger threshold levels) and the ever increasing number of new organic substances in very low concentrations (micropollutants) which have been detected, thanks to more powerful analytical tools, in wastewater, natural water and even ground water, demonstrating the ineffectiveness of conventional treatments.

Among these new organic substances there are Emerging Contaminants (ECs), a group of organic substances that may be subject to future regulations, depending on the results of investigation regarding their effects on human health, aquatic life forms and their persistence in the environment. Pharmaceutical products and its metabolites, personal care products, detergents, pesticides, drugs of abuse, surfactants, industrial additives, steroids and hormones, are classified as particularly relevant emerging contaminants.

The main characteristic of ECs is that they are hardly biodegradable or toxic and so they can resist or even alter conventional biological treatments, causing several possible ecological problems (microbiological resistance and the presence of antibiotic resistance genes (ARGs), acute and chronic toxicity, microbial community inhibition in sewage treatment plants, etc…).

Advanced Oxidation Processes (AOPs) seem to be a valid alternative for the treatment of such biologically persistent wastewaters [22] because they are based on the formation of highly reactive and non-selective free radicals (above all hydroxyl radical, HO•) that are capable to mineralize almost any organic contaminants. However, significant costs due to chemical and energy consumption have prevented the implementation of successful applications in wastewater treatment plants as they cannot yet compete with the cheaper and easier to manageable biological treatments. To improve the performance of the entire treatment plant in the future, a possible option could be to apply AOPs before (pre-treatment, to increase biodegradability) or after (post-treatment, to improve water quality) a biological treatment.

However, Oller *et al.* [22] discussed the need to develop more accurate economic models for the estimation of the cost of the combined systems in the AOPs field as well as the improvement in the degradation kinetics and reactor modelling.

The application of all these efficient water management strategies is a key element in increasing water productivity. Regarding the agricultural sector, in addition to the evaluation of optimal crop management strategies, the improvement of irrigation systems and schemes can lead to a more efficient and sustainable agricultural water management.

## 1.2 Water Pollutants and Emerging Contaminants

The waters resulting from civil waste, industrial processes and agricultural activities contain a multitude of polluting compounds, most of which are particularly dangerous for human health and for the survival of multiple living species. These compounds are divided into three main groups:

- Bacteria, viruses, protozoa, all agents that cause diseases (cholera, salmonellosis, etc.);
- Inorganic compounds soluble in water, such as acids, salts and toxic metals (cadmium, lead, mercury). Radioactive residues also belong to this group of compounds, *i.e.* unstable elements that decay by emitting ionizing radiation;
- Organic compounds, such as saturated, unsaturated and aromatic hydrocarbons. These compounds form oils, detergents, which contain surfactants and emulsifiers, plastics, pesticides.

Wastewater treatment has become essential nowadays due to the toxic effects of pathogens and the risks of wastewater pollution to humans, agriculture and animals. Wastewater treatment at the personal and government level must be considered to protect the environment from pollution. Wastewater treatment can involve physical, chemical, and biological procedures to purify water from various contaminants [23], [24].

According to the United States Environmental Protection Agency (EPA), water pollution can be divided in six main categories:

- Urban wastewater discharges, including domestic wastewater or the mixture of domestic wastewater with industrial wastewater and/or run-off rain water;

- Domestic wastewater, including wastewater from residential settlements which originates mainly from human metabolism and from household activities;
- Industrial discharges, including any wastewater discharged from premises used for carrying on any trade or industry, other than domestic wastewater and run-off rain water;
- Discharges from farms, manure and slurry providing suspended solids, organic matter, nitrogen and phosphorus;
- Agricultural wastewater discharges, waters carrying fertilizers, pesticides and salts;
- Others, such as mining which release destructive substances like copper, cadmium and lead, boats which release hydrocarbons.

However, the US EPA also establishes the importance of considering a new group of contaminants, Emerging Contaminants (ECs), including pharmaceuticals and personal care products (PPCPs).

In this regard, European commission, in the context of the Water Framework Directive, identified a list of priority substances (PS), including the priority hazardous substances (PHS), or rather "persistent, toxic and liable to bioaccumulate, or that give rise to an equivalent level of concern" and sates the importance of monitoring a new group of pollutants, the so-called Emerging Contaminants. The following sections present a more detailed description of this latest worrying source of water pollution.

### 1.2.1 Overview of Emerging Contaminants

Industries, agriculture and the general population using water on a daily basis play an essential role in the release of many pollutants in wastewater. These practices, in addition to generating various pollutants, have altered the water cycle, causing global concern related to their possible impact on wildlife and human health [25].

As previously mentioned, most of the conventional WWTPs are designed to control a wide range of substances and although these substances can be efficiently and consistently eliminated, the removal of micropollutants is often insufficient. These recalcitrant compounds that bypass the treatments in WWTPs are called emerging contaminants (ECs). ECs are defined as synthetic or naturally occurring chemicals that are not commonly monitored in the environment but have the potential to enter

the environment and cause known or suspected adverse ecological and (or) human health effects. Their continuous introduction into the environment cannot be compensated even by high rates of transformation and/or removal, so they do not need to be persistent to cause negative effects on the aquatic environment [26]. These substances may be included in future environmental regulations and (inter)national routine monitoring programs depending on the results of the investigations into their potential ecotoxicological effects. The main ECs are: pharmaceuticals, personal care products, synthetic musk fragrances, sunscreens, insect repellents, surfactants and metabolites, steroid hormones and endocrine-disrupting compounds (EDCs), fire retardants, industrial additives and agents, gasoline additives, disinfection by-products and pesticides (Figure 1).

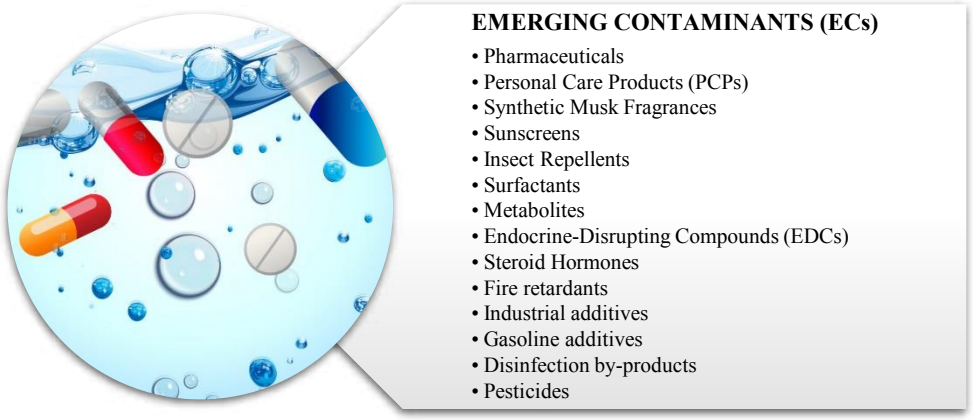


**Figure 1:** Classes of main Emerging Contaminants.

Current demographic projections, the rise of chronic diseases, the accessibility of inexpensive generic treatments, and the emergence of “lifestyle” drugs have been key to the abuse of pharmaceutical medicine worldwide. These pharmaceuticals are now the group of emerging contaminants with rising concern in the scientific world due to their presence in surface water, such as lake and river, groundwater, soil, and even drinking water and their associated impact on invertebrates, vertebrates and entire ecosystem. The two main routes of their spread in the environment are (1) when taken drugs are excreted in faeces and urine and (2) when unused drugs are thrown down. A study conducted in 2020 has found that 60-80% of these pharmaceutical medicines are flushed down the toilet or dumped as regular

household waste that ends up in sewage treatment plants, which are generally not designed to remove such pollutants from wastewater [27].

In the following section a more detailed description of the pharmaceuticals is presented because the present study addressed not only the assessment of the environmental risk deriving from the presence of disinfection by-products of different pharmaceuticals, but also the treatment of an antibiotic by using several Advanced Oxidation Processes (AOPs). Specifically, the antibiotic Levofloxacin was selected as the main model compound of the present work.

### 1.2.2 Pharmaceuticals as Emerging Contaminants

Potential sources of environmental pollution by pharmaceutical products include emissions during production, transport and storage, further intentional disposal of unused preparatives, and excretion of metabolites or non-metabolized residues via urine or feces. Another important source is the excreted manure, which contains the mixture of metabolite/unchanged pharmaceutical coming from the medicines administered to the farmed animals. The latter, being often used as fertilizer, allows the pharmaceuticals to reach the soil. Furthermore, the pharmaceuticals can also reach the environment through the sludge of the WWTPs, also often used as fertilizer. Finally, soil leaching and groundwater recharge due to heavy precipitation, are the main modes of transportation for pharmaceuticals through the soil and into the aquatic environment but also industrial spills and aquaculture play a major role.

Over the past decade, traces of pharmaceuticals, typically at range levels of nanograms to micrograms per liter, have been reported in water bodies, but advances in analytical technology have increased their detection. Even at these very low concentrations, scarce water has raised concerns among stakeholders, such as drinking water regulators, governments, water suppliers, and the public, regarding the potential risks to human health from exposure to traces of pharmaceuticals via drinking-water [28]. Pharmaceuticals include many very different substances regarding their chemical and physical properties and environmental behavior, although they may have potent biochemical activity. However, their presence in the aquatic environment and their impact on aquatic biota and human health have not been adequately studied. There is some experimental evidence that pharmaceuticals

can cause harmful effects such as morphological and metabolic alterations on aquatic species and induction of antibiotic resistance in aquatic pathogenic bacteria [29].

Pharmaceuticals are designed to have a specific mode of action, and many are persistent in the body. Furthermore, many pharmaceuticals transform in the human body, resulting in the release of their metabolites into the aquatic environment. They have been detected in low concentrations in many countries in many environmental samples, for example, sewage-treatment-plant effluents, surface water, seawater, and groundwater [30]. Prolonged exposure over time of these substances, at low concentrations, can cause:

- Allergies;
- Development of antibiotic resistance (antibiotics);
- Effects of the endocrine system (hormone-acting drugs);
- Cytolytic or cytostatic effects (antitumoral drugs).

The main categories of human pharmaceuticals and the most commonly used products include non-steroidal anti-inflammatory drugs (NSAID), beta-blockers, cardiovascular and lipid regulators, steroids and related hormones, antibiotics, anticonvulsants and other compounds used in high doses, as well as diagnostic aids and disinfectants. The most important factor of environmental pollution by pharmaceuticals is that although the amounts released into the environment are quite small, they are released over a long period and continuously [31].

### 1.2.3 Environmental impact and risks associated with pharmaceuticals contaminants

The modes of entering the environment and fate of pharmaceuticals and their metabolites are similar to other environmental pollutants, and therefore their effects are also similar, in principle, to the effects of other contaminants. Pharmaceuticals have the ability to target specific metabolic and molecular pathways in humans and animals, but they often have significant side effects too. Their presence in the environment is compromising aquatic life forms, sometimes deeply, and is producing changes that threaten the sustainability of the ecosphere. They are often found to cause adverse ecological effects on aquatic and terrestrial organisms and may present a human health risk associated with lifetime consumption of contaminated drinking water. Pharmaceuticals are present in the environment at trace levels, however, even

in these infinitesimal concentrations, some of them have the potential to harmfully interfere with the normal development of aquatic life. Generally, the efficiency of pharmaceuticals removal during water treatment is determined by the disappearance of the parent compounds while little attention has been given to the identification, let alone quantification, of the transformation products following treatment. Persistent pharmaceutical metabolites require consideration for risk assessment because the effects resulting from exposure to a mixture of parent pharmaceutical and its metabolites may be very different from what might be observed based only on toxicity of the single compound [32]. Some of these formed metabolites show the potential to bind to proteins and other cellular constituents causing a blockade of cellular function, which may trigger toxic effect and immune response [33], [34], [35]. Assessing the individual and collective toxicities of metabolites and parent pharmaceutical can indeed be a significant challenge, primarily due to the large number of metabolites that can be generated during pharmaceutical metabolism and the limited understanding of their potential effects. Mompelat *et al.* reported that approximately 160 pharmaceuticals and only 30 by-products (biotic and abiotic) have been in environmental investigations dealing with their occurrence, fate and ecotoxicology [30]. Another important issue is the potential environmental effects of pharmaceutical mixtures from sewage treatment plant effluents. Several works have reported the increase of the toxicity of pharmaceutical mixtures, as well as the development of parasite-resistant strains and the change in the physiology of host organism, responding to the synergetic effect of pharmaceutical mixtures [36], [37]. It's not enough to only consider the parent pharmaceutical compounds when assessing environmental risks. Transformation products and metabolites can be more persistent and potentially more toxic than the parent compounds. Therefore, a comprehensive identification and toxicity evaluation of all compounds produced during water treatment and biodegradation processes is necessary. Consequently, it is critical to prioritize which metabolites are important for toxicity testing and risk assessment. This data is essential as a starting point for determining the target compounds to monitor, with the goal of making reasonable predictions regarding the potential ecotoxicity of these metabolites. The lack of these data on the potential long-term ecotoxicological effects of pharmaceutical metabolites in the environment makes it difficult to make the necessary refinements to improve the accuracy of existing models for risk assessment [38].

# CHAPTER 2

## 2.1 Global Water Pollution and Human Health

Many of humanity's biggest problems are water quantity and water quality issues in the twenty-first century. These problems will be further aggravated in the future by climate change, resulting in higher water temperatures, melting of glaciers, and an intensification of the water cycle, with potentially more floods and droughts. Regarding human health, the most direct and serious impact is the lack of improved sanitation and related to it is the scarcity of safe drinking water, which currently affects more than a third of people in the world. Additional threats include, for example, exposure to pathogens or chemical toxicants via the food chain (*e.g.*, the result of irrigating plants with contaminated water and bioaccumulation of toxic chemicals by aquatic organisms, including seafood and fish) or during recreational activities (*e.g.*, swimming in polluted surface waters) [39]. Indeed, global industrialization has contributed significantly to uncontrolled increase in water pollution due to the continuous spillage of harmful substances into water bodies. Water pollution is defined as "any direct or indirect alteration of the physical, thermal, chemical, biological, radioactive properties of any part of the environment by, discharge, emission or deposit of wastes to affect any beneficial use adversely or to cause a condition, which is dangerous to public health, safety or welfare of animals, birds, wildlife, aquatic life or to plants of every description" [40]. There are various causes of water pollution:

1. Industrial waste: industries and industrial sites worldwide significantly impact on water pollution. Many industrial sites produce waste in the form of toxic chemicals and pollutants, and though regulated, some still do not have proper waste management systems.
2. Marine Dumping: contrary to what you might think, garbage is still collected and dumped into the oceans by many countries worldwide.
3. Sewage and wastewater: dangerous chemicals, bacteria and pathogens can be found in sewage and wastewater even when it's been treated. Each household's sewage and wastewater are released into the sea through fresh water. The pathogens and bacteria found in that wastewater breed disease, and therefore are a cause of health-related issues in both humans and animals.

4. Oil leaks and spills: large oil spills and oil leaks, are a significant cause of water pollution although often accidental. Leaks and spills are usually caused by oil drilling operations in the ocean or ships transporting oil.
5. Agriculture: farmers use pesticides and agricultural chemicals to protect crops from harmful insects, plant diseases and weed infestations. When these substances are sprayed or applied to fields, they can seep into the soil and reach underground aquifers. They can thus harm animals, plants and humans. Additionally, when it rains, the chemicals mix with rainwater, which then flows into rivers and streams that filter into the ocean, causing further water pollution.
6. Global Warming: rising temperatures due to global warming are a significant concern for water pollution. Global warming causes water temperature to increase, which can directly alter the ecological balance of aquatic ecosystems. When large die-offs occur, it further pollutes the water supply, making the problem worse.
7. Radioactive waste: radioactive waste that arises primarily from the nuclear industry, including nuclear power plants, nuclear medicine and scientific research, can be highly hazardous to the environment and must be disposed of properly. This is because uranium, the element used to develop atomic energy, is highly toxic.

Wastewater, which in the past contained almost exclusively biodegradable substances, currently presents greater disposal problems, due to the increasingly large presence of chemical compounds of synthetic origin. The sea, rivers and lakes are not able to receive a quantity of polluting substances greater than their own self-purifying capacity (the aerobic bacteria present in the water tear down and metabolize the biodegradable pollutants) without compromising the quality of their waters and the normal ecosystem balance. All social and productive activities lead to the production of discharges which must necessarily be subjected to purification to be returned to the environment.

The conventional and non-conventional processes, with their differences, which are applied in wastewater treatment plants are presented in detail below.

## 2.2 Conventional Wastewater Treatment Systems

The composition of wastewater is a function of the uses to which the water was submitted. However, given their dangerousness, they cannot be discharged as such into the environment but must necessarily undergo a series of treatments aimed at their purification and clarification. The primary goal of wastewater treatment is to remove or significantly reduce contaminants in the water and convert them into an effluent that can be returned to the water cycle. Once returned to the water cycle, the effluent creates an acceptable impact on the environment or is reused for various purposes (called water reclamation) [41].

The treatment process takes place in a wastewater treatment plant (WWTP), often referred to as a Water Resource Recovery Facility (WRRF) or a Sewage Treatment Plant (STP). These facilities are designed to apply a combination of various processes, including physical, chemical, and biological methods, to effectively treat wastewater and remove pollutants from it [42]. Traditional wastewater treatment plants (WWTPs) are effective at removing many common pollutants such as particulate matter, organic substances, nutrients (like nitrogen and phosphorus), and pathogens. However, when it comes to micropollutants, often referred to as emerging contaminants or trace contaminants, these conventional treatment processes are often insufficient. Evaluating the fate and removal of micropollutants during wastewater treatment is imperative optimization of treatment to prevent the release of these potentially harmful micropollutants. Although there are different WWTPs, most will have the following steps: preliminary (physical and mechanical), primary (physicochemical and chemical), secondary (chemical and biological), rarely, tertiary (physical and chemical) treatments (Figure 2). Below is a more accurate and detailed overview of each of these phases:

- **Preliminary Treatment** - This is the first stage in wastewater treatment, where the focus is on removing large and easily separable solids and debris. Mechanical processes like screening, grit removal, and homogenization are used to achieve this. The objective is to protect downstream equipment and processes from damage or clogging.
- **Primary Treatment** - In this phase, wastewater goes through a physical process known as sedimentation or primary clarification. Here, larger and heavier solids settle to the bottom, forming a sludge layer. The partially clarified water is then transferred for further treatment. Primary treatment

reduces the biochemical oxygen demand (BOD) and removes a significant portion of suspended solids.

- **Secondary Treatment** - Secondary treatment primarily relies on biological processes to further break down the organic matter remaining in the wastewater after primary treatment. The most common biological method is the activated sludge process, where microorganisms, including bacteria and protozoa, consume and digest organic pollutants. Other methods, like trickling filters and sequencing batch reactors (SBRs), are also used. Secondary treatment significantly reduces BOD and suspended solids, improving water quality.
- **Tertiary Treatment** - Tertiary treatment is an optional but important step in wastewater treatment, particularly when the effluent must meet stringent quality standards or when additional pollutant removal is required. This phase may include processes like sand filtration, activated carbon adsorption, chemical coagulation, advanced oxidation, and disinfection. These processes target specific contaminants, including fine suspended solids, nutrients (like phosphorus and nitrogen), and trace contaminants (micropollutants).
- **Sludge Treatment** - As you mentioned, significant quantities of sludge are generated during primary and secondary treatment processes. This sludge contains organic matter and may also contain pathogens and trace contaminants. Sludge management involves processes like thickening, dewatering, digestion, and sometimes further treatment to reduce its volume, stabilize its organic content, and render it less harmful. Proper sludge management is essential to prevent environmental pollution and to utilize the resulting biosolids as a resource in agriculture or other applications.

Overall, these wastewater treatment processes play a critical role in safeguarding public health, protecting the environment, and ensuring the responsible management of water resources. The specific methods and technologies used may vary depending on the characteristics of the wastewater and local regulatory requirements.

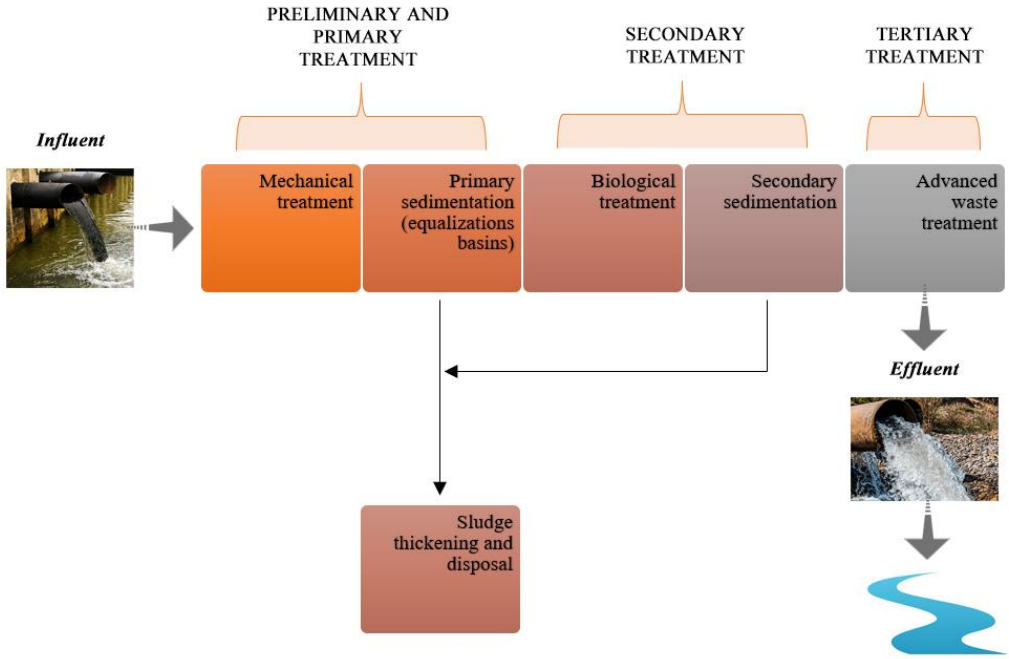


**Figure 2:** Typical composition of a wastewater treatment plant (WWTP).

### 2.2.1 Limitations and drawbacks of conventional treatments

Conventional WWTPs do not lead to the total degradation and removal of emerging contaminants like pharmaceuticals, personal care products, and industrial chemicals. As a result, these pollutants can persist in treated effluents and find their way into surface waters or groundwater, potentially impacting ecosystems and human health. These systems, in fact, are not destructive, as they transfer the pollutant from the contaminated aqueous phase to another phase, with the consequent need for subsequent treatment.

Another drawback is the production of polluting by-products caused by some traditional methods. The chlorination method, used to eliminate pathogens from treated water, leads to the formation of several halogenated hydrocarbons believed to be carcinogenic. Such compounds are normally removed with the use of activated carbon which, on the other hand, can lead to the production of chlorinated compounds, which can contribute to environmental issues like acid rain. This underscores the interconnectedness of various environmental concerns.

These are the reasons why in recent decades particular attention has been dedicated to the development and optimization of processes that allow the destruction of polluting molecules in an effective and eco-sustainable way. Advanced oxidation processes (AOPs) have proven to be particularly interesting, involving the formation

of highly reactive chemical species, which promote the degradation of organic substrates, including recalcitrant compounds.

| ***Benefits*** | ***Drawbacks*** |
|---|---|
| *Techniques already widely used, reliable and suitable for the automatic process* | *Systems that do not definitively eliminate water pollutants, but separate them into a solid matrix: this creates a risk for the environment* |
| *Possibility of reusing waste substances* | *Solid pollutants that are produced increase the costs of treatment* |
| *Waste in a wide concentration range can be treated* | *Economic drawback for all methods using chemical additives* |
| *Low costs* | *Chlorination can produce carcinogenic substances* |

**Table 2:** Main benefits and drawbacks of traditional treatments.

## 2.3 Water Treatment Technologies

To struggle contamination of water bodies and meet the regulations, different technologies are available. The selection of the most appropriate technologies will depend on the wastewaters to be treated. Usually, wastewaters are treated in Wastewater Treatment Plants (WWTPs), in which various treatment steps including physical, biological and eventually chemical processes, are carried out for the removal of physical, biological and chemical contaminants.

However, the concern regarding persistent and hardly biodegradable pollutants, such as PPCPs and others ECs has produced a great research effort in the development and implementation of Advanced Oxidation Processes (AOPs). With the aim of containing operational costs, the combination of conventional biological processes with AOPs has been proposed as an interesting potential alternative. AOPs could be used as pre-treatments, to convert persistent or toxic contaminants into more biodegradable substances or they could also be used as a post-treatment step following secondary treatment with the aim of achieving a higher quality level of treatment. For this reason, in the following sections, an overview of the AOPs is presented.

## 2.4 Advanced Oxidation Processes (AOPs) for Water Treatment

Advanced Oxidation Processes (AOPs) are considered today among the most promising treatments for the removal of toxic and refractory pollutants from water, as they potentially guarantee their complete mineralization while avoiding phase transfer. These processes can be broadly defined as aqueous phase oxidation methods based on the intermediacy of highly reactive species such as hydroxyl radicals ($HO^{\bullet}$) or sulphate radicals ($SO_4^{2-\bullet}$) in the mechanisms leading to the destruction of the target pollutant [43]. These radicals are very reactive, attack most organic molecules and are not highly selective [44]. A chemical wastewater treatment using AOPs completely mineralizes contaminants to $CO_2$, water, and inorganic compounds, or their transformation into more harmless products [45]. AOPs are classified based on how the radical species are generated: processes with chemical reagents, photolytic processes and finally photocatalytic processes. In the case of processes that use chemical reagents, radical compounds are generated starting from a reaction between some oxidants, without the use of physical promoting agents; instead, as regards photolytic processes, the production of radical agents is obtained by the combination of UV and visible radiation with chemical reagents. Finally, photocatalytic processes are another form of advanced oxidation that uses nano-semiconductors including $TiO_2$, ZnO, $SiO_2$, $Fe_2O_3$, CdS, ZnS or Rare Earth Elements (REEs) to remove pollutants from water. These processes take place in the heterogeneous phase, which means that they involve the reaction between the surface of the catalyst material and the contaminants present in the water.

AOPs are suited for effective degradation of dissolved organic contaminants such as halogenated hydrocarbons, aromatic compound, phenols, pesticides and several toxic pollutants, as well as inactivate pathogens in different environmental matrices (water, wastewater, soil, air). Therefore, AOPs appears as a promising technology for destruction of hazardous organic compounds in water without generating secondary pollutant commonly associated with conventional treatment technologies. Due to their potential as successful solution for environmental pollution problems, AOPs have been attracting the interest of researchers, practitioners and enterprises operating in the field of environmental remediation technologies.

### 2.4.1 Introduction to AOPs and their principles

As previously mentioned, AOPs in water treatment relies on the clean technologies that produce hydroxyl radicals ($HO^{\bullet}$) so as to attack organic contaminants and ideally yield $CO_2$, $H_2O$ and some inorganic ions as final products under mild conditions, or at least, transform the contaminants into not dangerous products [46], [47], [48]. $HO^{\bullet}$ is an unselective, strong oxidant that could be produced by many different ways [46]. In addition to $HO^{\bullet}$, in progress of time, the contribution of other radicals has often been established, by which the AOP concept is accepted in a widened sense rather than being limited by only $HO^{\bullet}$ based oxidation [49]. Typical AOPs include ultraviolet (UV) light, ozone ($O_3$), hydrogen peroxide ($H_2O_2$), and their combinations such as ($UV/H_2O_2$), ($O_3/H_2O_2$), ($O_3$/UV), and ($O_3/UV/H_2O_2$). When no UV source is used the technology can be termed as a dark oxidative process, such as: ozonation ($O_3$), Fenton's reagent, ultrasound, and microwave to name a few. In fact, Fenton's reagent ($Fe^{2+}/H_2O_2$), ($Fe^{3+}$/UV) and photocatalysis using titanium dioxide and UV ($TiO_2$/UV) are often used. In conventional WWTPs, UV radiation is used for final disinfection. Therefore, a UV-based AOP would fulfill dual objectives of disinfection and recalcitrant compound removal in the final wastewater effluent.

The main different possibilities given by AOPs [47] are listed below:

- **Fenton ($H_2O_2/Fe^{2+}$) and Fenton-like ($H_2O_2/Fe^{3+}$):** the production of $HO^{\bullet}$ radicals by Fenton reagent occurs by means of addition of $H_2O_2$ to $Fe^{2+}$ salts.
- **Photo assisted Fenton ($H_2O_2/Fe^{2+}$ - ($Fe^{3+}$)/UV):** it's an extension of the Fenton process. The use of a UV-VIS light irradiation at wavelength values higher than 300 nm allows the photolysis of $Fe^{3+}$ complexes and the consequent regeneration of $Fe^{2+}$ leading to an increase of the degradation rate of organic pollutants.
- **$H_2O_2/Fe^{3+}$ - oxalate:** it's an improvement of photo-assisted Fenton processes. The irradiation of ferrioxalate in acidic solution led to the generation of $CO_2$ and $Fe^{2+}$, free or complexed with oxalate, which can provide a continuous source of Fenton's reagent by reaction with $H_2O_2$.
- **Photocatalysis ($TiO_2/h\nu/O_2$):** the photocatalytic processes are based on the use of oxygen as oxidizing agent and of a semiconductor metal oxide as catalyst. The initiating event is the absorption of the radiation with the formation of electron-hole pairs ($TiO_2 h\nu \rightarrow e^- + h^+$). The formed electrons have a high reducing power which allows the generation of the superoxide

radical ion $O_2^{\bullet-}$ by reducing some metals and dissolved oxygen, whereas remaining holes can oxidize adsorbed $H_2O$ or $HO^-$ to reactive $HO^\bullet$ radicals.

- **Peroxozone ($O_3/H_2O_2$) and Peroxone combined with Ultraviolet light ($O_3$/UV; $O_3/H_2O_2$/U):** Hoigné and Bader [50] showed $OH^-$ ion has the role of initiator of the process of ozone decomposition in aqueous solution that develops through the formation of $HO^\bullet$ radicals. Moreover, the addition of hydrogen peroxide to the ozone aqueous solution can enhance the $O_3$ decomposition allowing the formation of $HO^\bullet$ radicals.
- **$Mn^{2+}$ catalysed ozonation of oxalic acid ($Mn^{2+}$/Oxalic acid/ozone):** this system can be used to enhance ozone decomposition for the production of $HO^\bullet$ radicals. The $Mn^{2+}$ catalysed ozonation of oxalic acid develops according to a radical mechanism at pH > 4.0 at which Mn(III)-dioxalate and Mn(III)-trioxalate are formed. Then the oxidation process proceeds presumably through the formation of $HO^\bullet$ radicals.
- **Peroxidation combined with Ultraviolet light ($H_2O_2$/UV):** the irradiation of the pollutant solution containing $H_2O_2$ with a UV light source with $\lambda < 280$ nm led to the homolytic cleavage of $H_2O_2$ ($H_2O_2 \xrightarrow{h\nu} 2HO^\bullet$).
- **Vacuum Ultraviolet VUV photo-induced oxidation:** is the process that led to the generation of hydroxyl radicals by photolysing the water through the use of higher energies of the Vacuum Ultraviolet or VUV ($\lambda < 190$nm).

The different AOPs are summarized below and can be broadly divided into photolytic processes in the homogeneous phase and photocatalytic processes in the heterogeneous phase. Heterogeneous photocatalysis, involving REE-based catalysts, will be addressed in more detail, as it has been used to evaluate the degradation of the drug Levofloxacin in preliminary experimental

### 2.4.2 Different AOPs for water treatment (Photolysis, Homogeneous phase AOPs, Heterogeneous photocatalysis, Process involving REEs catalysts)

The selection of the most appropriate AOPs used for treatment will depend on the type of wastewater to be treated and consequently the specific contaminants (chemical and biological) to be removed.

Photolysis (also called *photochemical reaction* or *photodissociation*) is a water treatment process that relies on the degradation of contaminants through direct exposure to ultraviolet (UV) or visible light. During photolysis, contaminants in water are broken down primarily by the energy from absorbed photons. When a molecule absorbs a photon, it may undergo a photodissociation reaction, leading to the cleavage of chemical bonds. This process can be particularly effective for breaking down organic contaminants. Photolysis can be used to degrade a wide range of contaminants, including organic compounds, dyes, and some pathogens. To increase the production rate of oxidative species, some additives are added, like adding oxidant $H_2O_2$ and $O_3$, adding a catalyst (Photo-Fenton) or photocatalysis ($TiO_2$). It is often employed in the treatment of wastewater and the purification of drinking water. The effectiveness of photolysis depends on the wavelength and intensity of the light source, as well as the nature of the contaminants. Some contaminants may not absorb light efficiently, limiting the applicability of photolysis. Some researchers have classified AOPs, both singles and combined, differentiating them as homogeneous or heterogeneous.

Homogeneous phase AOPs involve the use of chemical reactions in which both the reactants and the catalyst are in the same phase (typically liquid). An example is provided by the Fenton Reaction. In the Fenton reaction, ferrous ions ($Fe^{2+}$) and hydrogen peroxide ($H_2O_2$) are mixed in an aqueous solution. The reaction between $Fe^{2+}$ and $H_2O_2$ generates highly reactive hydroxyl radicals ($OH^{\bullet}$), which can oxidize and degrade various organic pollutants present in the water. Fenton-based AOPs are used for the treatment of industrial wastewater containing persistent organic pollutants, such as dyes, phenols, and pesticides.

Heterogeneous photocatalysis involves the use of a solid-phase photocatalyst, often semiconductors like titanium dioxide ($TiO_2$) or zinc oxide (ZnO), to facilitate the degradation of contaminants in water under the influence of UV or visible light. When exposed to light, these photocatalysts generate electron-hole pairs on their surface. The resulting highly reactive species, such as hydroxyl radicals ($OH^{\bullet}$), can then react with and break down organic contaminants adsorbed onto the catalyst's surface. Heterogeneous photocatalysis is applied to the removal of a wide range of organic contaminants from water, including dyes, pharmaceuticals, and volatile organic compounds. It is also used for disinfection and the inactivation of pathogens in water. This process is effective for the removal of persistent and complex organic

pollutants. It does not require the addition of chemicals, and the catalyst can be regenerated or replaced.

Recently, the application of Rare Earth Elements (REEs) in AOPs has gained growing interest [51]. Heterogeneous catalysts doped with REEs are a class of catalysts that incorporate these elements into a solid support or substrate, typically a metal oxide, to enhance their catalytic activity for various chemical reactions. REE ions have a particular electronic structure compared to transition metal ions and are gaining great importance as Lewis acids in Green Chemistry because they can be used in aqueous solvents or water without any de-activation; they can be easily recovered from the reaction medium by extraction and can be used several times without loss of activity [51], [52]. The redox properties of REEs depend on the arrangement of the surfaces and the shape and size of their crystals, and for this reason they can be improved by checking the nanostructure [53]. REEs exhibit unique physicochemical properties, such as high surface area, reactivity, and redox potential [54]. These properties make REEs suitable to be used in AOPs, where they can enhance the performance of the processes [55], [56]. REEs can be used as catalysts: to promote the generation of reactive oxygen species (ROS) when exposed to UV radiation in photocatalysis processes [57]; to catalyze Fenton-like processes [58]; to enhance the efficiency of ozonation by increasing the production of hydroxyl radicals [59].

To date, most applications are still at lab scale and an increasing number of studies are being performed to fill the existing gaps in the usage of REEs for polluted water treatment. The main limitations to full scale applications deal with high energy and capital cost.

Each of these AOPs offers unique advantages and limitations, making them suitable for different water treatment scenarios. The choice of the appropriate AOP depends on the specific contaminants present, water quality, and treatment goals.

### 2.4.3 Efficiency and limitations of AOPs in degrading pharmaceutical pollutants

Among the various treatment technologies established to remove efficiently persistent emerging molecules, AOPs offer interesting assets for effective remediation of emerging pollutants, including proven flexible application and high removal efficiency of pharmaceuticals. These kind of treatment techniques such as

ozonation, photodegradation, electro-Fenton etc. are get in the way by high energy cost, high operating costs, formation of by-products which requires extra cost for treatment. Nowadays, the available data relating to the removal efficacies of pharmaceuticals in WWTPs allow us to conclude that substantial part of these exits secondary wastewater treatment unchanged and therefore conventional wastewater treatment is not a safe primary barrier against the spread of pharmaceuticals. Furthermore, it is clear that the presence and transformation of pharmaceuticals in wastewater has become an issue of growing environmental concern. In fact, the attention of the scientific community is now also focusing on the transformation by-products deriving from natural photolysis, photodegradation and advanced oxidation processes. These processes can lead to the formation of a wide range of transformation compounds from the original pharmaceutical compounds. Biological processes can induce the formation of only a limited degree of transformation due to the biopersistence of many organic compounds. The same holds true often for the number transformation by-products resulting from incomplete biodegradation. On the contrary, photoprocesses, such as AOPs, can generate myriads of reaction products due to non-selectivity of radical species that may trigger complex reaction pathways different from those of normal biochemical reactions [60]. Abiotic environmental factors on the other hand, can make a significant contribution to the transformation of such substances in the environment. Abiotic factors are chemical and physical factors such as temperature, soil composition, amount, intensity and wavelength of sunlight, salinity and pH. Biotic factors are the other living parts of the ecosystem with which an organism may interact; the organisms present and their diversity in number, type and function. Further to the abiotic and biotic processes that can induce a great variety of transformation by-products for the pharmaceutical compounds in the environment, the same processes can have the same effect on these compounds during the treatment processes applied at the sewage and drinking water treatment plants. Hence, biologically and chemically transformed by-products may result during treatment. These products formed during transformation processes can retain the mode of action of the parent compound. This means they can have similar or even more potent biological effects than the parent compound [61], [62]. Furthermore, in the cases where AOPs are combined with the biological treatment, by-products formed could be more bioresistant and/or induce adverse effects on the activity of microbial population present in the activated sludge system. Identifying

transformed by-products is a complex challenge, but is essential to fully understand the environmental effects. The use of modern analytical methods such as LC–MS/MS or $MS^n$ (*e.g.* by ion-trap) or Orbitrap and/or addressing the photoproducts' mixture biological activity without identifying them, *i.e.* to combine photochemical studies with biological assays, is crucial to analyze and characterize transformed by-products in detail. For a complete risk assessment study on the transformed by-products of pharmaceuticals formed during photolytic natural processes and treatment of water and wastewater, determination of their toxicity and ecotoxicity is fundamental and a prerequisite for comprehensive protection of the environment.

Next chapters will focus on this topic in order to also understand and assess the possible hazards related to the biotransformation products released in the environment.

# CHAPTER 3

In this chapter, the results based on original contributions published in [63], [64], [65], [66], [67] and submitted in ELSEVIER (*Science of The Total Environment*) and MDPI (*applied sciences, molecules*) are presented.

## 3.1 Overview of Sartans and Their Environmental Presence

Most of the medicines sold every year worldwide end up in the environment. The causes of this phenomenon are manifold and range from the incorrect disposal of expired products to the industrial discharge of production processes; however, patients may be the biggest cause of this type of pollution. In fact, when a drug is taken, it is absorbed by the body and enters the body's circulation to be distributed and sent to the target site, where it performs its function. Many of the medicines taken, however, are partially expelled without being metabolized [30]. A worrying fact is that the release of drugs into the environment has a higher frequency than the inactivation times of the compounds, which renders them pseudo-persistent. In most cases, the environmental concentrations of pharmaceuticals are too low to directly affect human lives; however, the presence of any drug in superficial waters can affect the local fauna continuously exposed to the drug through contact with the water, leading to the propagation of bioaccumulation problems along the food chain [68]. Pharmaceutical waste, together with sewage, reaches wastewater treatment plants, where the organic loads are degraded and the water is cleaned, but the fate of pharmaceuticals depends on their structural composition and reactivity towards the process used to treat the waste, which can lead to more toxic compounds. Hundreds of tons of pharmaceutical substances flow to WWTPs every year, hence the need to implement WWTPs with advanced treatments, tertiary wastewater treatments, capable of improving removal efficiencies. Advanced wastewater treatment processes are the subject of numerous studies. Technologies such as ozonation [69], [70], [71], membrane filtration [72], adsorption [73] and above all advanced oxidation [74], are configured as systems capable of improving the removal of emerging contaminants from wastewater.

One class of ECs is sartans (olmesartan, valsartan, irbesartan and candesartan), which are antihypertensive agents that act on the renin–angiotensin system with a different

mechanism than ACE inhibitors; the latter reduces the plasma and tissue levels of angiotensin II, while sartans antagonize its action on AT1 receptors [75]. The attention of the scientific community has focused on this category of drugs, which have been detected in the aquatic environment [76]. Irbesartan (IRB) has been found in samples of surface water of Africa and Europe up to 0.76 μg/L and 0.65 μg/L concentrations, respectively [77], and not infrequently, irbesartan has been detected even in drinking water, at up to 3.0 ng/L concentrations [78]. Due to AOPs, 21% of irbesartan resists normal wastewater purification treatments and is thus released into the environment, while 79% is partially mineralized or transformed into degradation by-products [19]. According to Minguez *et al.* [79], the predicted environmental concentration (PEC) and the predicted no effect concentration (PNEC) of irbesartan are of 0.6 μg/L, and 100 μg/L, respectively. Another ECs is olmesartan acid (OLM) [80], a hypertensive that is estimated to have an average daily consumption of almost 12 DDD per 1000 inhabitants (it was 3.7 in 2007), with a defined daily dose (DDD) value of 20 mg. In Italy alone, an expenditure of about EUR 150 million per year is estimated, almost five times more than the EUR 31 million in 2011 (it is among the top thirty active ingredients agreed upon for expenditure agreed by the national health system). It is marketed as olmesartan medoximil, the prodrug from which the active pharmaceutical is derived [81]. An excretion of 90% and a percentage of removal in wastewater treatment plants (WWTPs) not exceeding 20% are estimated for this drug. In recent studies, carried out in some European countries, it was found that the concentration of olmesartan acid in wastewater reaches up to 1200 ng/L [82], but in surface waters ranges from 150 ng/L to 800 ng/L, with peaks above 2 μg/L in some German rivers [80]. However, the concentrations are lower in groundwater [83]. Finally, cardiovascular drug candesartan (CAN) was found in Bavarian WWTP effluents at concentrations as high as 1712 ng/L [84]. Moreover, it is ubiquitous in England, where it was discovered at a concentration of 140 ng/L, and has been detected in surface waters at concentrations of up to 46 ng/L in Switzerland and up to 6.3 μg/L in Spain [80].

In the next paragraphs, the formation pathways of the degradation by-products of these cardiovascular drugs will be presented in detail, obtained through a simulated chlorination process that mimics the same one normally present in WWTPs to reduce similar emerging pollutants. Once by-products have been identified, it is important

to evaluate their toxicity and ecotoxicity to determine whether they may pose a concern to human health or the environment.

## 3.2 Materials and Methods

### 3.2.1 Reagents and chemicals

Irbesartan, Candesartan and Olmesartan (99.5%) were purchased from Sigma Aldrich (Milan, Italy). All the other chemicals and solvents were purchased from Fluka (Saint- Quentin Fallavier, France) and were of HPLC grade and used as received. For the toxicity assessment, the reference toxicant (potassium dichromate) and salts used for the preparation of artificial freshwater ($CaCl_2 \times 2H_2O$, $MgSO_4 \times 7H_2O$, KCl, $NaHCO_3$) were used. Double distilled water (Microtech) was used to prepare the dilution water and treatments.

### 3.2.2 Toxicity tests

Toxicity tests with *R. subcapitata* followed the ISO 8692:2012 protocol [85], adapted to a microplate format. The initial cell densities of *R. subcapitata* were correlated with optical density (OD) at 670 nm, according to the specification of the algae supplier, using a DR5000 spectrophotometer (Hach Lange, Weinheim, Germany). Percentages of growth inhibition were calculated according to time of exposure and concentrations compounds with respect to the controls. This assay was carried out in triplicate.

The acute ecotoxicity test with the bioluminescent bacterium *A. fischeri* was performed on a Microtox® 500 analyzer (New Castle, DE, USA) according to ISO 11348-3 [86]. The bacteria used belong to the NRRL line B-11177 supplied by Microbiotests, Gent, Belgium. The diluent used was 2% saline water solution (NaCl) to osmotically adjust the salinity of the sample. The toxicity of the samples was evaluated by the bioluminescence inhibition percentage. In particular, the % inhibition was evaluated after 5, 15, and 30 min of exposure of the bacteria to serial dilutions of the compounds.

Methods for acute ecotoxicity tests with *D. magna* conformed to guidelines set by the ISO 6341 [87]. For these tests, five neonates of *D. magna* (<24 h old) were carefully pipetted into glass beakers with 10 mL of ISO medium. During acute ecotoxicity tests, the organisms were not fed. For each treatment, 20 neonates (4

beakers) were exposed to the control and to each compound. The complete immobilization of the organisms was considered to be indicative of the toxic effect and was recorded using a stereomicroscope (LEICA EZ4-HD).

### 3.2.3 Chlorination Reaction

### 3.2.4 Apparatus and Equipment

Column chromatography (CC) was carried out with Kieselgel 60 (230–400 mesh, Merck, Darmstadt, Germany). HPLC was performed on a Shimadzu LC-8A system using a Shimadzu SPD-10A VP UV-VIS detector (Shimadzu, Milan, Italy). Preparative HPLC was performed using an RP Gemini C18-110A preparative column (10 μm particle size, 250 x 21.2 mm i.d., Phenomenex, Bologna, Italy) with a flow rate of 7.0 mL/min. The $^{1}$Hand $^{13}$C-NMR spectra were recorded with an NMR spectrometer operated at 400 MHz and at 25 °C (Bruker DRX, Bruker Avance, Billica, MA, USA) and referenced in ppm to the residual solvent signals ($CDCl_3$, at $\delta_H$ 7.27 and $\delta_C$ 77.0). The proton-detected heteronuclear correlations were measured using a gradient heteronuclear single-quantum coherence (HSQC) experiment, optimized for $^{1}J_{HC}$ = 155 Hz, and a gradient heteronuclear multiple bond coherence (HMBC) experiment, optimized for $^{n}J_{HC}$ = 8 Hz. The MALDI TOF mass spectrometric analyses were performed on a Voyager-De Pro MALDI mass-spectrometer (PerSeptive Biosystems, Framingham, MA, USA). The UV/Vis spectra were recorded with a PerkinElmer Lambda 7 spectrophotometer. The IR spectra were run on a Jasco FT/IR-430 instrument equipped with a single reflection ATR accessory. pH was recorded on a WTW pH 7110 pH-meter (Xylem Analytics, Weilheim, Germany) equipped with a WTW SenTix41 electrode with temperature sensor.

## 3.3 Chlorination Procedure and Product Isolation: Irbesartan

Irbesartan (1g, 2.34 mmol) dissolved in milliQ water (2 L) was treated for 2 h with 10% hypochlorite (molar ratio irbesartan hypochlorite 1:6 concentration, spectroscopically determined at a $\lambda_{max}$ of 292 nm, ε = 350 $dm^3$/mol cm) at room temperature [88]. The pH of the solution, measured by a pHmeter at five-minute intervals, increased after 5 min from the initial pH of 8.0 to 10.5, and the pH remained at this value during the reaction. After 2 h, the solution was quenched by excess

sodium sulphite, concentrated by lyophilisation (up to ~50 mL) and extracted with ethyl acetate. The ethyl acetate fraction (EA, 835 mg) was chromatographed with the silica gel CC using a gradient ofmethylene chloride-methanol (100:0 to 30:70, v/v) to yield 17 fractions. The fraction EA5 (105 mg), eluted with methylene chloride, was re-chromatographed on the silica gel CC by eluting with a gradient of petrol ether-acetone (100:0 to 70:30, v/v) to yield 13 subfractions. The subfraction EA5.10 (31 mg), eluted with petrol ether-acetone (50:50, v/v), was analysed by HPLC using a reversed phase column and eluting with a gradient of $CH_3COONH_4$ (pH 4.0; 10 mM) and methanol (30:70 to 0:100, v/v) to yield 7 subfractions. The subfractions EA5.10.6 and EA5.10.7 contained DP3 and DP5 (10 and 18 mg, respectively). The fraction EA8 (101 mg), eluted with methylene chloride-methanol (90:10, v/v), was re-chromatographed with the silica gel CC by eluting with a gradient of petroleum ether-acetone (90:10 to 70:30, v/v) to yield 9 subfractions.

The subfraction EA8.4 (14 mg), eluted with petrol ether-acetone (75:25, v/v), and DP2 (12 mg) were purified by HPLC using a reversed phase column and eluting with a gradient of $CH_3COONH_4$ (pH 4.0; 10 mM) and methanol (25:75 to 10:90, v/v). The fraction EA9 (17 mg), eluted with methylene chloride-methanol (85:15, v/v), was analysed by HPLC using a reversed phase column and eluting with a gradient of $CH_3COONH_4$ (pH 4.0; 10 mM) and methanol (20:80 to 10:90, v/v) to yield 2 subfractions, and the first subfraction contained DP4 (15 mg). The fraction EA14 (205 mg), eluted with methylene chloride-methanol (80:20, v/v), was re-chromatographed with the silica gel CC by eluting with a gradient of methylene chloride-acetone (100:0 to 65:35, v/v) to yield 7 subfractions. The subfraction EA14.1 (63mg), eluted with methylene chloride-acetone (97:3, v/v), contained DP1 (43 mg) and DP6 (4 mg), which were purified by HPLC using a reversed phase column and eluting with a gradient of $CH_3COONH4$ (pH 4.0; 10 mM) and methanol (35:65 to 5:95, v/v). (Figure 3).

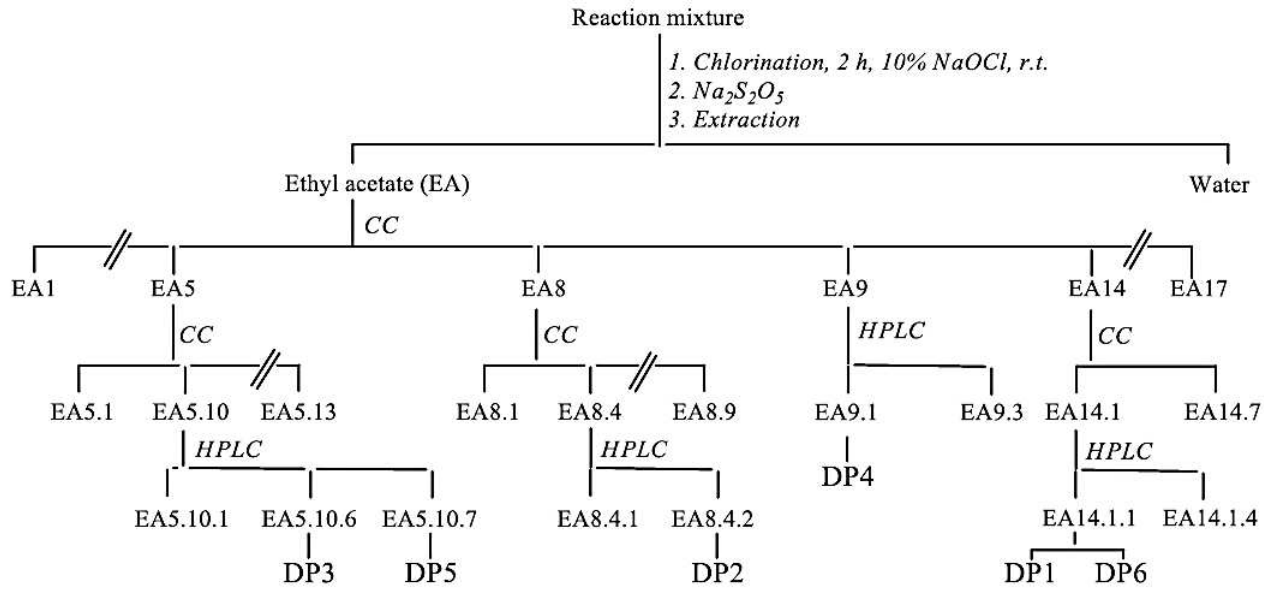


**Figure 3:** Isolation of six identified disinfection by-products.

The fraction EA7 (138 mg), namely, eluted methylene chloride–methanol (95:5, v/v), was re-chromatographed through silica gel CC via elution with a gradient of petrol ether–acetone (90:10 to 70:30, v/v), yielding 20 subfractions. The subfraction EA7.3 (30 mg), eluted with petrol ether–acetone (90:10, v/v), was separated in two subtractions using preparative HPLC column elution with a gradient of $CH_3COONH_4$ (pH 3.8; 20 mM) and methanol (30:70 to 0:100, v/v). The subfractions EA7.3.1 contained DBP7 (1 mg). The fraction EA8 (101 mg), eluted with methylene chloride/ methanol (90:10, v/v), was re-chromatographed with silica gel CC via elution with a gradient of petroleum ether-acetone (90:10 to 70:30, v/v), yielding 9 subfractions. The subfraction EA8.1 (30 mg), eluted with petrol ether–acetone (90:10, v/v), was purified via HPLC using a reversed phase column and elution with a gradient of $CH_3COONH_4$ (pH 4.0; 10 mM) and methanol (25:75 to 0:100, v/v), yielding 3 subfractions containing DBP10, DBP15, and DBP9 (10, 3, and 2 mg, respectively). The fraction EA13 (37 mg), eluted with methylene chloride–methanol (70:30, v/v), was separated into 5 subfractions under the same HPLC conditions as EA7.3, yielding DBP12, DBP18, and DBP11 (4, 3, and 16 mg, respectively). The fraction EA14 (205 mg), eluted with methylene chloride–methanol (60:40, v/v), was re-chromatographed with silica gel CC via elution with a gradient of methylene chloride–acetone (100:0 to 65:35, v/v), yielding 5 subfractions. The subfractions

EA14.3 (23 mg) and EA14.4 (9 mg), eluted with methylene chloride–acetone (80:20, v/v), contained DBP8 and DBP17 (3 and 2 mg, respectively), which were purified via HPLC using a reversed phase column and elution with a gradient of $CH_3COONH_4$ (pH 4.0; 10 mM) and methanol (35:65 to 5:95, v/v). The fraction EA16 (37 mg), eluted with methylene chloride–methanol (50:50, v/v), was purified via preparative HPLC under the same conditions as EA7.3, yielding four subfractions, of which the first of the two contained DBP14 and the second contained DBP13 (5 and 8 mg, respectively). The fraction EA16.3 (15 mg), containing DBP16 (3 mg), was purified via preparative HPLC under the same conditions as EA7.3. (Figure 4).

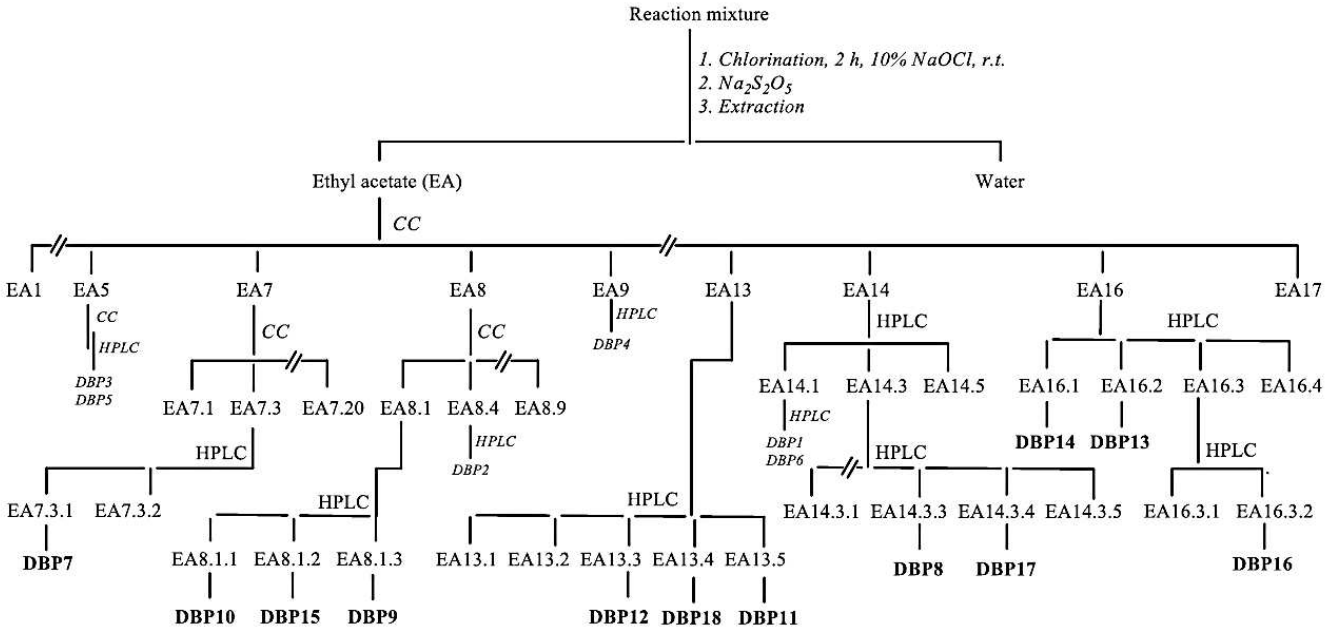


**Figure 4:** Isolation of twelve identified disinfection by-products.

# 3.4 Results and discussion

## 3.4.1 Chlorination Experiments

The chlorination experiments of irbesartan were performed by mimicking the conditions of a typical WWTP, in which a $10^{-5}$ M solution of the drug was treated for 30 min with 10% hypochlorite (irbesartan-hypochlorite molar ratio of 1:1; concn.) at room temperature [89], [90]. The changes of the drug were monitored by HPLC, and its main disinfection by-products (DP1–DP6/DBP7-DBP18) were identified by comparing their retention times with those of the standard compounds; these

irbesartan disinfection by-products were isolated for the first time by column chromatography and HPLC and were fully characterized by employing NMR and MS analyses by performing preparative experiments ($1.17 \times 10^{-3}$ M drug treated for 2 h, with 10% hypochlorite, irbesartan-hypochlorite molar ratio of 1:6, at room temperature). The concentrations of DP1–DP6 were at a maximum after 2 h and with a percentage of 4.5, 0.56, 0.25, 0.59 and 0.1, respectively. The concentrations of DBP7–DBP18 reached a maximum after 2 h, with percentages of 0.1, 0.3, 0.2, 1.0, 1.6, 0.4, 0.8, 0.5, 0.3, 0.3, 0.2, and 0.3% w/w, which could reflect the real percentages.

### 3.4.2 Structural Elucidation

All the by-products described below have been obtained with a degree of purity greater than 95% in order to be able to describe them by means of accurate NMR and mass spectrometry analyses. Compounds DBP7–DBP13 and DBP15–DBP16 are new compounds, which have been isolated for the first time.

I. Structure elucidation of DP1

The MS-TOF analysis showed a molecular ion peak at m/z 447.24 $[M + H]^+$ corresponding to the molecular formula $C_{25}H_{30}N_6O_2$. The $^1H$ NMR spectrum of DP1 showed the protons of the methylene $CH_2$–11 at 4.28 ppm. In the HMBC spectrum, these protons were correlated with the signals at 138.29 and 127.68 ppm, which were identified as the carbons C-12 and C-13/C-17, and with the signals at 174.75 and 174.43 ppm, which were identified as the imine carbon C-7 and the carbonyl carbon C-9, respectively. The imine carbon was correlated with the signals at 2.16 and 1.49 ppm, which were identified as the protons H-29 and H-30 of the alkyl side chain, while the carbonyl carbon was correlated with the signals at 1.97 and 2.22 ppm, which were identified as the protons H-3/H-5 of the cyclopentane group, respectively. These correlations support the hydrolysis of the bound C7-N8 [91], [92]. The plausible mechanism of the DP1-DP6 formation from irbesartan is shown in Figure 5.

II. Structure elucidation of DP2

The MS-TOF analysis showed a peak of molecular ions at m/z 458.23 $[M+ H]^+$ corresponding to the molecular formula $C_{26}H_{27}N_5O_3$. The $^1H$ NMR spectrum showed the presence of only seven aromatic protons, of which the three at 8.44, 8.49, 7.57 ppm were related to a 1,2,4-trisubstituted system. In particular, in the HMBC spectrum, the protons at 8.44 and 7.57 ppm were correlated to carbon C-11 at 45.73 ppm, while the protons at 5.48 ppm, which were bound to the C-11, were correlated with the carbons at 115.01 and 126.28 ppm, that in the HSQC spectrum were just correlated to the aromatic protons considered, allowing these protons to be assigned as protons H-13 and H-17, respectively. The doublet signal at 8.49 ppm, which was correlated with the H- 17 proton in the $^1H$—$^1H$ COSY spectrum, was then identified as being related to the H-16 proton and, in the HMBC spectrum, was correlated to the quaternary carbons C-12, C-14 and C-18 at 139.75, 129.56 and 129.75 ppm, respectively. The data suggest that a nucleophilic aromatic substitution reaction occurred by the tetrazole ring [93], resulting in the fusion of a new six-membered ring. Moreover, the protons H-3/H-5 were correlated with the signal at 186.65 ppm in the HMBC spectrum, which was identified as the carbonyl carbon C-9, to which the protons H-11 were also correlated. The H-11 protons, however, were also correlated with a second carbonyl carbon at 157.93 ppm, as well as with the protons at 2.68 ppm, which were identified as H-30 protons. The $^1H$—$^1H$ COSY spectrum also allowed for the protons H-31 and H-32 to be identified at 1.86 and 1.09 ppm, respectively. In the HMBC spectrum, the protons H-30 and H-31 were correlated to a signal at 83.02 ppm, which was identified as the quaternary carbon C-29.

III. Structure elucidation of DP3

The MS-TOF analysis showed a molecular ion peak at m/z 475.22 $[M + H]^+$ corresponding to the molecular formula $C_{25}H_{26}N_6O_4$. The NMR signals of the aromatic part of the molecule of DP3 were very similar to those of DP2 and to the presence of seven aromatic protons, of which three were part of a 1,2,4-trisubstituted system. Moreover, the $^1H$ NMR spectrum showed the presence of four signals at 2.51, 1.58, 1.26 and 0.82 ppm, which were identified as being related to protons H-29, H-30, H-31 and H-32, respectively, as indicated by their correlations in the $^1H$—$^1H$ COSY spectrum and the H—C correlations in the HMBC spectrum. In particular, the latter spectrum also showed the correlation of protons H-29 and H-30 with the

signal at 175.01 ppm, which was identified as the carbonyl carbon C-7, to which the protons H-11 at 5.31 ppm were also correlated. The H-29 and H-30 abovementioned protons and the H-3/H-5 protons at 2.68 ppm were also correlated to a second carbonyl carbon at 169.31 ppm, which was identified as C-9. The mass data and the IR spectrum that showed the presence of two bands centered at 1535 $cm^{-1}$ and 1328 $cm^{-1}$ agreed with the presence of a nitro group bound to a C-4 carbon.

IV. Structure elucidation of DP4

The MS-TOF analysis showed a molecular ion peak at m/z 391.14 $[M + H]^+$ corresponding to the molecular formula $C_{20}H_{18}N_6O_3$. The NMR and mass data related to this product were very similar to those of DP3 but without the C5 chain linked to N-8. In fact, in the $^1H$ NMR spectrum, there were no signals related to protons H-29, H- 30, H-31 and H-32 corresponding to the carbons in the $^{13}C$ NMR spectrum nor to the methyl and three methylene groups in the DEPT spectrum. Only the signals of the cyclopentane group were present, whose protons H-3/H-5 were related to the only carbonyl carbon at 172.01 ppm, to which the protons H-11 at 4.66 ppm were also correlated. Furthermore, the proton spectrum again showed the presence of only seven signals, of which three were related to an 1,2,4-trisubstituted ring.

V. Structure elucidation of DP5

The MS-TOF analysis showed a molecular ion peak at m/z 459.23 $[M + H]^+$ corresponding to the molecular formula $C_{25}H_{26}N_6O_3$. DP5 had NMR data very similar to the DP1 NMR data, in which the C5 chain was bound to N-6 as well as to the cyclopentane group, but consisted of only seven aromatic protons and a third carbonyl carbon identified as carbon C-11. In a strongly basic aqueous solution, it is conceivable to hypothesize the hydrolysis of the imine bond C7-N8 to yield DP1, which then, by nucleophilic aromatic substitution and the relative closure of a new six-membered ring and by the oxidation at carbon C-11 would yield DP5.

VI. Structure elucidation of DP6

The NMR data of DP6 were very different from those of the previous disinfection by-products, in which DP6 was missing the signals related to the cyclopentane group, the C5 alkyl side chain and the H-11 protons. The MS-TOF analysis showed a

molecular ion peak 270.10 $[M+H]^+$ corresponding to the molecular formula $C_{13}H_{11}N_5O_2$, which, in agreement with the NMR data, indicates the presence of an aromatic ring, a tetrazole ring bound to the aromatic ring and a 1,4-cyclohexadiene. The latter, in particular, showed 4 protons at 6.06, 6.95, 7.52 and 6.23 ppm, which were identified as the protons H-2, H-3, H-5 and H-6, respectively, and bound to the carbons at 131.03, 129.91, 123.06 and 136.63 ppm. The HMBC spectrum highlighted the correlations of the protons identified as H-3 and H-5 to the carbons C-1 and C-7 at 164.08 and 146.82 ppm, and, in addition, to carbon C-4 at 66.11 ppm. At carbon C-4, the proton H-12 at 7.34 ppm as well as the protons H-2 and H-6 were correlated.

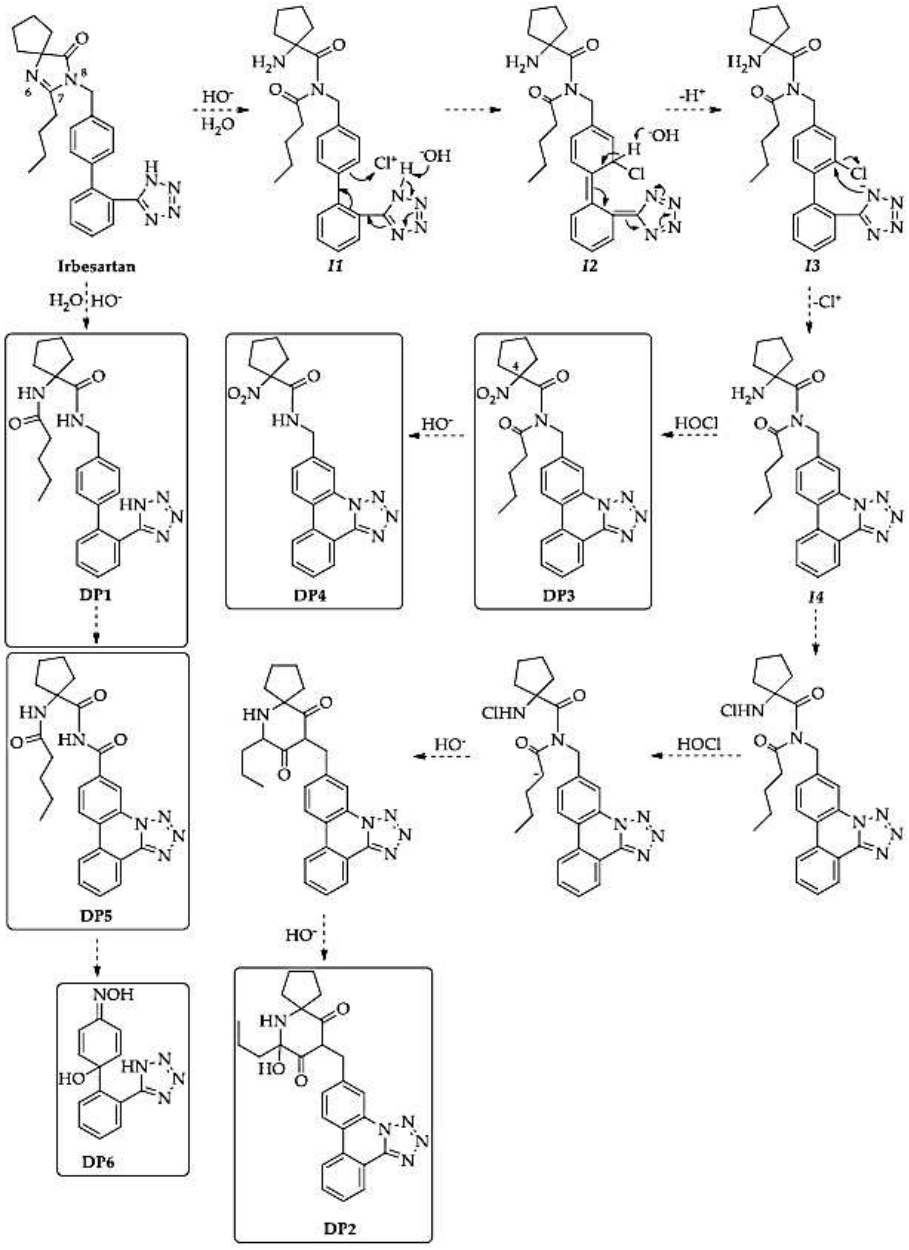


**Figure 5:** Plausible mechanism for the formation of DP1–DP6.

VII. Structure elucidation of DBP7

The MS-TOF analysis showed a molecular ion peak at m/z 249.11 $[M + H]^+$ corresponding to the compound with the molecular formula $C_{14}H_8N_4O$. The $^1H$ NMR spectrum did not show the presence of an n-butyl side chain, an A ring, or the proton H-11, just as the $^{13}C$ NMR spectrum did not show the corresponding carbons nor the signals of carbons C-7 and C-9 (the B ring). In the $^1H$ NMR spectrum, only aromatic signals were present, specifically only seven protons at 9.19, 8.73, 8.28, 8.61, 7.98, 7.92, and 8.86 ppm, as well as the signal of an aldehyde proton at 10.30 ppm. The HSQC spectrum allowed for the correlation of the aforementioned signals with the carbons at 127.19, 126.57, 125.41 120.18, 125.09, 130.95, 124.03, and 190.01 ppm. Based on the $^1H$—$^1H$ COSY and the HMBC spectra, the first three signals were attributed to the protons H-13, H-16, and H-17 of 1,2,4-trisubstituted benzene (the C ring). The next four were attributed to the protons H-19, H-20, H-21, and H-22 of 1,2-disubstituted benzene (the D ring), while the last one was attributed to the aldehyde proton H-11. Evidently, the starting product has undergone hydrolysis of the C-7/N-8 and N-8/C-9 bonds, along with the partial oxidation of carbon C-11 and the concomitant closure of a new six-term ring. The latter could result from an aromatic nucleophilic substitution reaction on the C-14 carbon of the previously chlorinated aromatic B-ring via the adjacent N-28 nitrogen of the tetrazole ring. The plausible mechanism of DBP7 formation from irbesartan is shown in Figure 6.

VIII. Structure elucidation of DBP8

In the $^1H$ NMR spectrum, the compound DBP8, like DBP7, showed the presence of only seven aromatic protons, indicating the formation of a new six-term ring. The 1D and 2D NMR data also show the presence of an A ring and the proton H-11. In the HMBC spectrum, these features (at 5.16 and 4.94 ppm) were correlated with the two carbons at 186.43 and 159.43 ppm, which were identified as carbonyls C-9 and C-7, respectively. In fact, if C-9 was correlated with the protons H-3 and H-5 at 1.91 ppm, carbon C-7 was correlated with the protons at 4.34 and 1.27 ppm. These last protons were identified as H-29 and H-30, respectively, indicating the presence of the n-butyl side chain, which, however, was oxidized to carbon C-29 in alpha to carbonyl C-7.

IX. Structure elucidation of DBP9

The NMR data regarding the compound DBP9 show the presence of the A, C, and D rings; the protons H-11 (at 5.25 and 46.84 ppm); and carbons identified as C-9 and C-7 at 187.48 and 158.02 ppm, respectively. In the HMBC spectrum, both carbonyls were correlated with protons H-11, but only the first of which was correlated with protons H-3 and H-5, and only the second of which was correlated with the protons at 2.67 ppm, identified as proton H-30. The 1D and 2D NMR data show the n-butyl side chain but with a quaternary carbon at position C-29. In fact, the $^{13}C$ NMR spectrum showed the presence of a carbon at 83.09 ppm, which was identified as an oxygenated quaternary carbon engaged in the closure of a six-term cycle with the amino function at carbon C-4. The compound DBP9 was, therefore, very similar to the compound DBP2 reported in a previous article on the degradation products of irbesartan [63], for which the formation of a new bond between the positions N-28 and C-14 did not occur.

X. Structure elucidation of DBP10

Compound DBP10 was very similar to compound DBP8, but it did not have the bond between the positions N-28 and C-14. Indeed, the $^{1}H$ NMR spectrum showed the presence of eight aromatic protons, attributed to two 1,4-disubstituted rings.

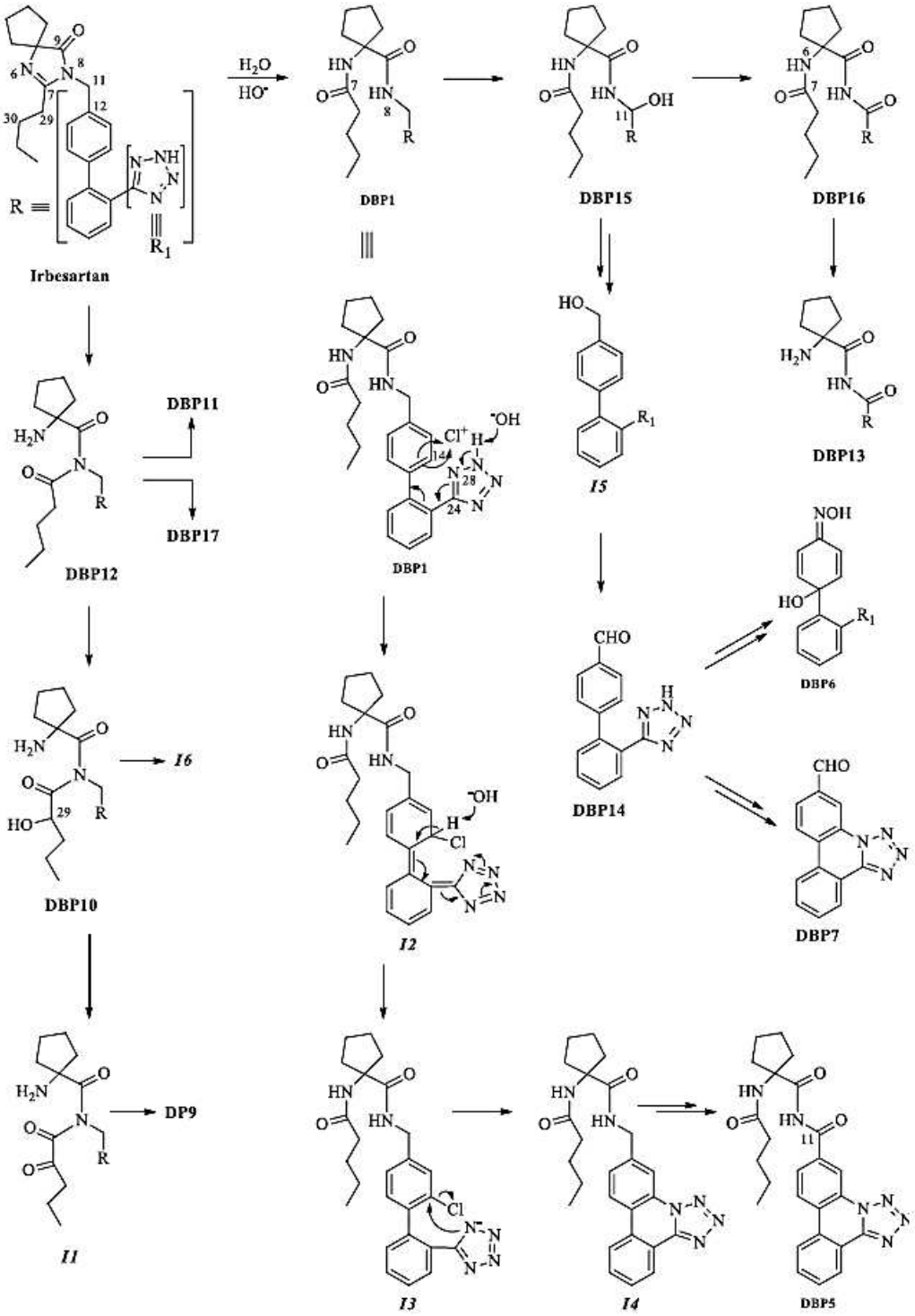


**Figure 6:** Plausible mechanism for the formation of DBP1, DBP5–DBP7, DBP10, and DBP12–DBP16.

XI. Structure elucidation of DBP11

The 1D and 2D NMR data indicate the opening of the B ring via the hydrolysis of the bond C-7/N-6. Indeed, in the HMBC spectrum, carbonyl C-7 at 176.01 ppm was correlated with the signals at 2.49 and 1.54 ppm, which were identified as protons H-29 and H-30 of the n-butyl side chain, while carbonyl C-9 at 180.05 ppm was correlated with the signals at 2.12 and 1.96 ppm, which were identified as protons H-3 and H-5 of the cyclopentane group. MS-TOF analysis showed a molecular ion peak at m/z 495.88 $[M+ H]^+$ in addition to the signals atm/z 494.13, 496.15, and 498.13, corresponding to the molecular formula $C_{25}H_{29}Cl_3N_2O_2$ and to the presence of three chlorine atoms. Indeed, in the HMBC spectrum, proton H-22 at 8.24 ppm was correlated with the carbons at 134.75 and 141.89 ppm, which were identified as carbons C-20 and C-18, respectively, and with carbon C-24 at 97.40 ppm, which, evidently, was obtained from the degradation of the tetrazole ring. The plausible mechanism behind the formation of DBP11 from irbesartan is shown in Figure 7.

XII. Structure elucidation of DBP12

The nuclear magnetic resonance (NMR) spectra obtained were consistent with those previously documented in the literature [94].

XIII. Structure elucidation of DBP13

The MALDI-TOF analysis of DBP13 showed a molecular ion peak at m/z 377.18 $[M+ H]^+$ corresponding to the compound with the molecular formula $C_{20}H_{20}N_6O_2$. The NMR and mass spectra data are like those of DBP12 but without the C5 chain bound to the nitrogen N-8 and with carbon C-11 oxidized at the carbonyl group. This last one at 166.70 ppm was correlated in the HMBC spectrum with protons identified as H-13/H-17 at 7.84 ppm.

XIV. Structural Elucidation of DBP14

The NMR data regarding compound DBP14 are very similar to those of compound DBP7 but without the bond between the positions N-28 and C-14. Evidently, the starting product was only hydrolyzed to the bonds C-7/N-8 and N-8/C-9 and partially oxidized at carbon C-11 [95].

XV. Structural Elucidation of DBP15

The MS-TOF analysis showed a molecular ion peak atm/z 463.26 $[M+H]^+$ corresponding to the compound with the molecular formula $C_{25}H_{30}N_6O_3$. The NMR data regarding DBP15 are very similar to those for DBP1 reported in the study by Romanucci *et al.* [63]. The difference is due to carbon C-11, present as methylene in compound DBP1 and as partially oxidized methine in DBP15. In fact, the $^1H$ NMR spectrum shows a singlet signal of a proton at 6.66 ppm, bound in the HSQC spectrum to the carbon at 83.04 ppm and correlated in the HMBC spectrum with carbonyl carbon C-9, as well as with carbons C-12 and C-13/C-17 at 169.00, 135.15, and 127.53 ppm, respectively.

XVI. Structural Elucidation of DBP16

Compound DBP16 was the corresponding oxidized product of DBP15. In fact, in the $^{13}C$ NMR spectrum, the signals of three carbonyl carbons appeared at 176.73, 168.48, and 168.42 ppm. In particular, in the HMBC spectrum, the third carbonyl carbon, identified as carbon C-11, was correlated with protons H-13 and H-17 of the 1,4-disubstituted aromatic C ring at 7.60 ppm. Compound DBP16 also corresponded to DBP5 reported by Romanucci *et al.* [63] but without presenting the bond between the positions N-28 and C-14.

XVII. Structural Elucidation of DBP17

The nuclear magnetic resonance (NMR) spectra obtained were consistent with those previously documented in the literature [94].

XVIII. Structural Elucidation of DBP18

Compound DBP18 was very similar to irbesartan but with the tetrazole ring partially degraded to the point of performing an amide function. In fact, proton H-22 at 7.78 ppm, which, according to the HSQC spectrum, was bonded to the carbon at 130.73 ppm, was correlated in the HMBC spectrum with a carbonyl at 170.51 ppm, which was identified as carbon C-24. The MS-TOF analysis showed a molecular ion peak at m/z 404.54 $[M + H]^+$ corresponding to the molecular formula $C_{25}H_{29}N_3O_2$ [96].

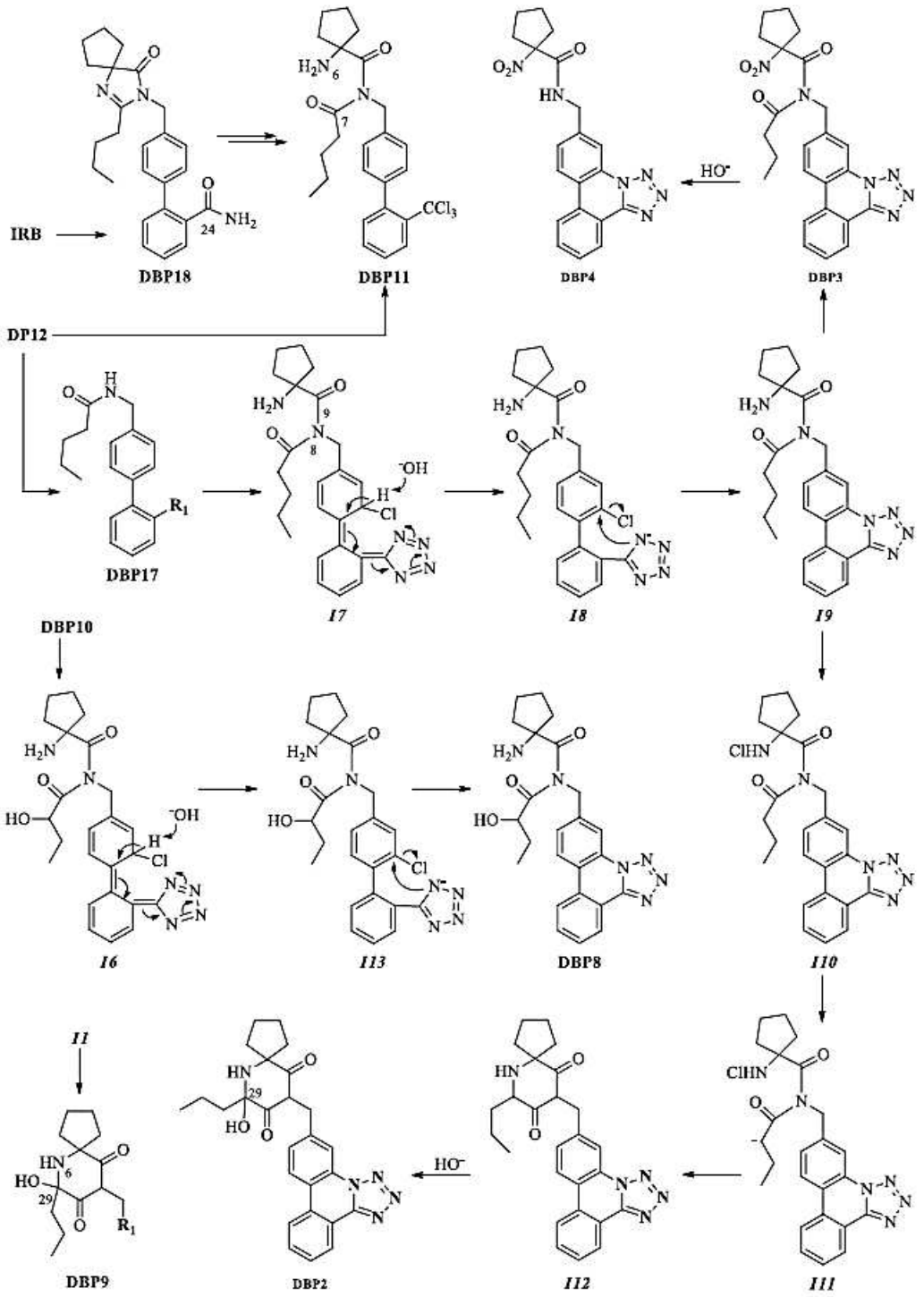


**Figure 7:** Plausible mechanism behind the formation of DBP2–DBP4, DBP8–DBP9, DBP11, and DBP17–DBP18.

### 3.4.3 Proposed Mechanism for the Formation of Disinfection By-products

The challenge was to hypothesize a plausible mechanism of action that leads to the formation of the tetracyclic aromatic nucleus of the four DP2–DP5, which is shown in Figure 5. In the authors' opinion, it could be hypothesized that, in the used strongly oxidizing reaction conditions, a neutral intermediate *I2* can be formed by the addition of chlorine on the aromatic ring (*I1*) and the consequential loss of a proton from the tetrazole ring. The loss of the proton geminal to the chlorine atom would allow the aromaticity of the ring to be restored and would yield intermediate *I3* with a negative charge on the nitrogen of the tetrazole ring. This intermediate, by nucleophilic attack, would then yield intermediate *I4*. From intermediate *I4*, it would then be relatively simple and reasonable to explain the formation of DP2–DP4. Specifically, DP2 could be obtained by the nucleophilic attack of the carbon C-29, which is adjacent to the carbonyl carbon C-7 and therefore weakly acidic, to yield the chloro amine-derivative function of the carbon C-4. DP3 could be obtained by the oxidation of the same amino function of intermediate *I4*, and finally, DP4 could be obtained from the hydrolysis of the amidic bond C7-N8 of DP3.

It is possible to propose a mechanism that explains the acquisition of all 18 compounds isolated to date from the chlorination of irbesartan, including compounds DBP2–DBP5 and DBP7–DBP8 with a tetracyclic aromatic nucleus (Figure 6 and Figure 7). With the hydrolysis of the C-7/N-8 bond of irbesartan, compound DBP1 was obtained, which, via oxidation of the C-11 carbon, led first to the formation of the corresponding carbinol DBP15 and then to the corresponding oxidized compound DBP16. The hydrolysis of the N-6/C-7 bond of DBP16 led to the production of compound DBP13. From compound DBP15, through intermediate *I5*, product DBP14 was obtained, and from this, the DBP6 oxime and compound DBP7 were obtained.

In the authors' opinion, it can be hypothesized that under the strongly oxidizing reaction conditions employed, a neutral intermediate, *I2*, can be formed via the addition of chlorine to the aromatic C ring of compound DBP1 and the consequential loss of a proton from the tetrazole ring. The loss of the proton geminal to the chlorine atom would allow for the aromaticity of the ring to be restored and would yield intermediate *I3* with a negative charge on the nitrogen of the tetrazole ring. This intermediate would evolve into intermediate *I4* via an intramolecular nucleophilic

attack, and from the latter, DBP5 would then be obtained by the oxidation of the benzyl carbon C-11.

Conversely, the hydrolysis of the C-7/N-6 bond of irbesartan leads to the formation of the by-product DBP12, and from this, it is possible to obtain by-product DBP10 via the oxidation of the n-butyl side chain at carbon C-29. The subsequent oxidation of carbon C-29 of the by-product DBP10 would lead to intermediate *I1*, and from this, with an intramolecular nucleophilic attack, by-product DBP9 would be obtained.

By-product DBP12 could yield DBP17 via the hydrolysis of the N-8/C-9 bond. In turn, by-product DBP17 would lead to by-product DBP3 through intermediates *I7-I9* and to by-product DBP2 through intermediates *I7-I12*. Finally, it can be hypothesized that by-product DBP18 could be obtained via the oxidation of the tetrazole ring of the starting irbesartan. By-product DBP4 could be obtained from the corresponding DBP3 for the hydrolysis of the C-7/N-8 bond, and by-product DBP8 could be obtained from DBP10 by incorporating the *I6* and *I13* intermediates.

### 3.4.4 Ecotoxicity results

The acute toxicity of irbesartan (IRB) and its chlorinated derivatives (DP1-DP6) towards *Daphnia magna* was showed in Figure 8. After both 24 h and 48 h of exposure, daphnids immobilization percentage at 100 mg $L^{-1}$ was <10% (*i.e.* 5%) confirming Minguez *et al.* [79] results, stating that EC50 of irbesartan is >100 mg $L^{-1}$, similarly to microalgae *Raphidocelis subcapitata* and (72 h EC50) and *Artemia salina* (48 h EC50). Thus, this compound is not toxic per se and can be considered as relatively nontoxic according to Persoone *et al.* [97] ranking (*i.e.* very toxic to aquatic organisms, percentage of effect (PE) >80%; toxic to aquatic organisms, PE > 50%; harmful to aquatic organisms, PE 20%–50%; and non-toxic to aquatic organisms, PE > 20%). The 24 h immobilization induced by the mixture and by-products ranged from 0% to 35%, indicating that only a slight acute toxicity was achieved only in DP2 (significantly different from the background level, $p < 0.05$).

After 48 h, the toxicity increased in daphnids exposed to DPs up to values significantly different from background level (5%, irbesartan). DP5 (60% effect) was the most toxic compound (*i.e.* 12-times more toxic than irbesartan), followed by DP1 and DP2 (30% < PE < 40%), and DP3, DP4 and DP6 (20% < PE < 30%). In-silico

evaluations (ECOSAR software) obtained by Carpinteiro *et al.* [91] about the toxicity of organic derivatives from irbesartan chlorination were confuted by our results. The predicted toxicity is not "lower", but increased after chlorination due to chlorinated by-products.

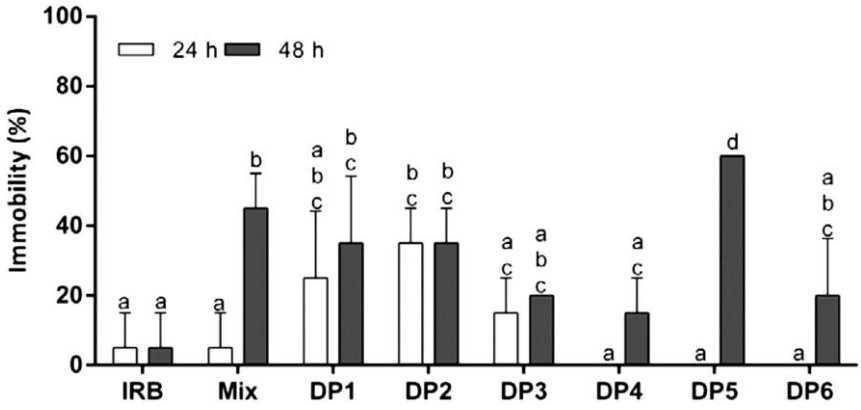


**Figure 8:** 24 h and 48 h immobility of *D. magna* exposed to irbesartan and oxidation by-products. Data with different letters (a–d) are significantly different ($p < 0.05$).

The original irbesartan compound was proven to be relatively non-toxic through the *D. magna*, *A. fischeri*, and *R. subcapitata* screening tests, with EC50 > 100mg/L. In the first part of this study it was observed that several by-products (DPs 1-6 and MIX) derived from the chlorination of irbesartan increase toxicity [63]. The second part shows that the chlorination of irbesartan involves more complex DBPs. Ecotoxicological tests on the by-products from DBP7 to DBP18, in fact, presented a dynamic and variable toxicity of irbesartan and its by-products (Figure 9). The lowest toxicity level occurred at an around -32% (indicating stimulation) concentration of DBP7 in the algal test, while the highest toxicity was at 84% of the mixture in the bacteria test.

Among the tested organisms, *A. fischeri* was the most sensitive to the DBPs, followed by *R. subcapitata* and, finally, *D. magna*, showing significant species-specific toxicity. According to a previous study, the sensitivity to DBP effects increases with decreasing trophic levels [98]. In contrast to species specific toxicity differences, only DBP10 showed the same range of toxicity in all the tested organisms, but no unique physicochemical characteristics have been associated with contributing to the observed effects.

The observed sensitivity and, consequently, toxicity changes can be attributed to the new smaller molecules present following the cleavage of functional groups that renders them more or less reactive against non-target organisms [98], [99]. This also aligns with previous studies that stated the introduction of a chlorine atom into a molecule or the formation of a chlorinated compound led to an increase in acute toxicity [100].

To further evaluate and interpret the toxicological relationships among the tested DBPs, the obtained results were compared to those reported in the study by Romanucci *et al.* [63] on *D. magna*. As mentioned previously, compounds DBP9, DBP15, and DBP16 were found to be very similar to DBP2, DBP1, and DBP5 [63], respectively. Although the toxicity of the new DBPs was lower than that of the DBPs previously reported [63], differences in the structures of the newly identified compounds compared to those previously reported could have led to different toxic effects. Even slight structural differences can significantly alter the physicochemical and biological properties of a compound, including its toxicity. Therefore, a comprehensive analysis of the ecotoxicity of all the identified DBPs, including the newly identified ones, is necessary to fully understand the potential health risks of irbesartan and its by-products in the aquatic environment.

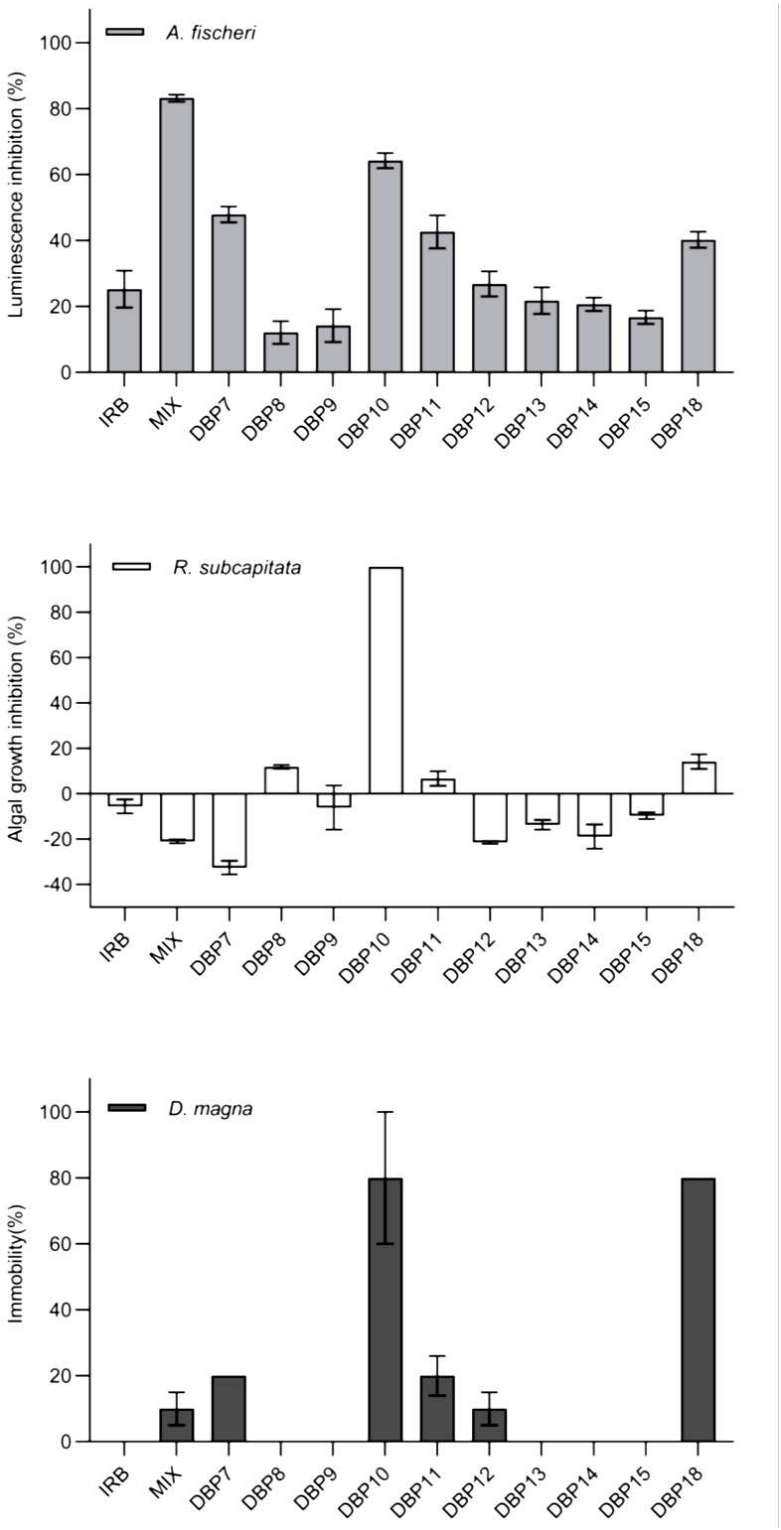


**Figure 9:** Toxicity results after exposure to irbesartan and its oxidation by-products.

## 3.5 Chlorination Procedure and Product Isolation: Candesartan

Candesartan (0.5 g, 1.14 mmol) was dissolved in phosphate buffer ($KH_2PO_4/K_2HPO_4$ 0.1 M, 500 mL), and 5% hypochlorite was added drop by drop (molar ratio CAN/HClO 1:20; concentration spectroscopically determined at $\lambda_{max}$ = 292 nm, ε = 350 $dm^3$/mol cm) at room temperature [89]. The pH of the solution, monitored with a pH meter, was adjusted by adding a 10% $H_3PO_4$ solution, and it remained stable at 6.5 for the entire duration of the experiment. The solution was quenched after 2 h with an excess of sodium thiosulfate, concentrated by lyophilization and extracted with ethyl acetate (EA) and water (W). The crude EA fraction (446 mg) was chromatographed on silica gel CC, eluting with a gradient of methylene chloride:methanol:acetic acid (100:0:0.5 to 70:30:0.5, *v/v/v*) to yield 18 fractions.

Fraction EA2 (9 mg), eluted with methylene chloride:methanol:acetic acid (100:0:0.5, *v/v/v*), was analysed by HPLC using a reversed-phase column (Luna 5 µm 100 Å C18(2); 150 x 4.6 mm) and eluting with water:methanol (20:80, *v/v*) at a solvent flow rate of 1 mL/min to yield **DP9** ($t_R$ 7.2 min, 2.1 mg) (Figure 10).

Fraction EA3 (47 mg), eluted with methylene chloride:methanol:acetic acid (98:2:0.5, *v/v/v*), was re-chromatographed on silica gel CC by eluting with a gradient of petrol ether:acetone (100:0 to 50:50, *v/v*) to yield 6 subfractions. Subfraction EA3.4 (13 mg), eluted with petrol ether:acetone (50:50, *v/v*), was analysed by HPLC using a reversed-phase column (Kromasil 10 µm 100 Å C18; 250 x 10 mm) and eluting with a gradient of $CH_3COONH_4$ (A, pH 4.0; 10 mM) and methanol (B), starting with 70% B for 1 min and establishing a gradient to obtain 100% B over 20 min at a solvent flow rate of 4 mL/min, in order to yield **DP2** ($t_R$ 17.9 min, 4.2 mg).

Fraction EA5 (57 mg), eluted with methylene chloride:methanol:acetic acid (90:10:0.5, *v/v/v*), was separated by semipreparative HPLC using a reversed-phase column (Kromasil 10 µm 100 Å C18; 250 x 10 mm) and eluting with a gradient of $CH_3COONH_4$ (A, pH 4.0; 10 mM) and methanol (B), starting with 60% B for 1 min and establishing a gradient to obtain 100% B over 30 min at a solvent flow rate of 4 mL/min, in order to yield 4 subfractions. Subfractions EA5.1 (8 mg) and EA5.2 (5 mg) were re-chromatographed by HPLC using a reversed-phase column (Kinetex 2.6 µm 100 Å C18; 100 x 4.6 mm) and eluting with a gradient of acetic acid:methanol (A, 1:99, *v/v*) and acetic acid:water (B, 1:99, *v/v*), starting with 60% B for 5 min and

establishing a gradient to obtain 100% A over 35 min and returning to 60% B for 10 min at a solvent flow rate of 0.8 mL/min. They contained **DP3** ($t_R$ 9.8 min, 3.2 mg) and **DP4** ($t_R$ 17.3 min, 3.1 mg), respectively.

Fraction EA6 (11 mg), eluted with methylene chloride:methanol:acetic acid (85:15:0.5, *v/v/v*), was analysed by HPLC using a reversed-phase column (Luna 5 µm 100 Å C18(2); 150 x 4.6 mm) and eluting with a gradient of $CH_3COONH_4$ (A, pH 4.0; 10 mM) and methanol (B), starting with 40% B for 1 min and establishing a gradient to obtain 100% B over 20 min at a solvent flow rate of 1 mL/min, in order to yield **DP5** ($t_R$ 11.5 min, 8.1 mg). Fraction EA8 (38 mg), eluted with methylene chloride:methanol:acetic acid (80:20:0.5, *v/v/v*), was analysed by HPLC using a reversed phase column and eluting with a gradient of $CH_3COONH_4$ (A, pH 4.0; 10 mM) and acetonitrile (B), starting with 20% B for 1 min and establishing a gradient to obtain 90% B over 25 min at a solvent flow rate of 3.5 mL/min, in order to yield **DP6** ($t_R$ 11.3 min, 5.3 mg) and **DP11** ($t_R$ 15.0 min, 3.1 mg).

Fraction EA9 (19 mg), eluted with methylene chloride:methanol:acetic acid (75:25:0.5, *v/v/v*), was analysed by HPLC using a reversed-phase column (Kromasil 10 µm 100 Å C18; 250 x 10 mm) and eluting with a gradient of water (A) and MeOH (B), starting with 10% A for 1 min and establishing a gradient to obtain 10% A over 30 min at a solvent flow rate of 1 mL/min, in order to yield **DP8** ($t_R$ 5.3 min, 4.0 mg) and **DP12** ($t_R$ 7.1 min, 4.3 mg).

Fraction EA10 (203 mg), eluted with methylene chloride:methanol:acetic acid (70:30:0.5, *v/v/v*), was re-chromatographed on silica gel CC by eluting with a gradient of chloroform: acetone (100:0 to 60:40, *v/v*) to yield 21 subfractions. Subfraction EA10.9 (73 mg), eluted with chloroform:acetone (70:30, *v/v*), was analysed by preparative HPLC using a reversed-phase column (Gemini 10 _m C18 110 Å; 250 _ 21 mm) and eluting with a gradient of $CH_3COONH_4$ (A, pH 4.0; 10 mM) and methanol (B), starting with 0% B for 1 min and establishing a gradient to obtain 100% B over 20 min at a solvent flow rate of 7.5 mL/min, in order to yield **DP1** ($t_R$ 18.4 min, 12.0 mg).

The aqueous fraction (W, 3.5 g) was dried by lyophilization, re-dissolved in water and filtered on an RP-18 reversed-phase silica gel for column chromatography (CC) using a gradient of water:methanol (100:0 to 0:100, *v/v*) to yield 12 fractions. The last fraction, eluted with methanol (165 mg), was dried by a rotary evaporator, re-

dissolved in methanol and separated with silica gel CC using a gradient of methylene chloride:methanol (100:0 to 0:100, *v/v*) to yield 15 fractions.

Fraction W12.13 (29 mg), eluted with methylene chloride:methanol (70:30, v/v), was dried, dissolved in an appropriate volume of methylene chloride (100 µL) and analysed using a Shimadzu 2010 series GC FID (Shimadzu, Milano, Italy). The gas chromatograph was equipped with an EquityTM-5 capillary column (30 m x 0.25 mm I.D. x 0.5 µm film thickness). The following parameters were set during the experiments: a detector temperature of 325 °C, helium as the carrier gas (25 cm/s) and an injected sample volume of 1.0 µL, introduced into the injector using an AOC-20i autosampler (Shimadzu, Milano, Italy) heated to 280 °C with a split ratio of 100:1. The initial temperature was 40 °C (2 min), which was increased at 50 °C/min to 100 °C, 10 °C/min to 200 °C and 30 °C/min to 325 °C (7.5 min). **DP7** ($t_R$ 15.9 min, 7.6 mg) and **DP10** ($t_R$ 21.2 min, 6.7 mg) were identified by comparing the results with data on standard compounds and their relative calibration lines.

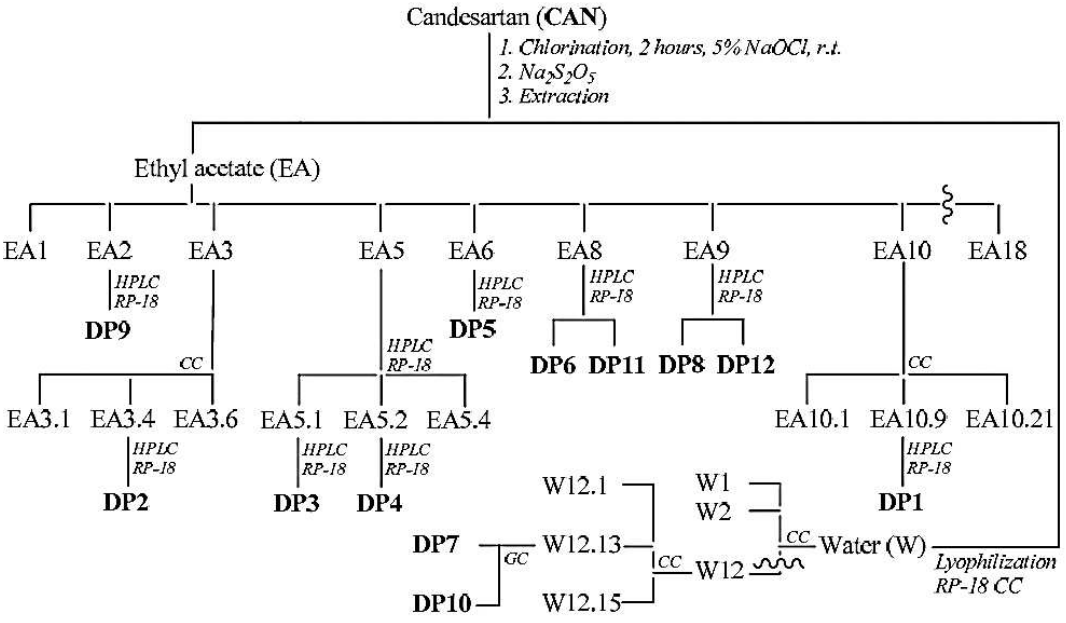


**Figure 10:** Isolation of twelve identified disinfection by-products.

## 3.6 Results and discussion

### 3.6.1 Chlorination Experiments

The Candesartan (CAN) chlorination experiments were performed by mimicking the conditions of a typical WWTP. A $10^{-5}$ M solution of the drug was treated for 1 h with 10% hypochlorite (CAN:hypochlorite molar ratio of 1:1; concn.) at room temperature [88], [89], [101], [102]. Then, the tests were repeated with the contaminant at concentrations $>10^{-3}$ M, with a much lower ratio of the CAN:oxidizing agent (1:5 or 1:6) so as to ensure the degradation of the studied contaminant and to isolate sufficient quantities of DPs for their subsequent structural identification. The DPs obtained were isolated by column chromatography and HPLC and completely characterized using NMR and MS analyses.

DP1–DP12 were isolated in relative percentages of 2.4, 0.84, 0.64, 0.62, 1.62, 1.06, 1.55, 0.80, 0.42, 1.34, 0.62 and 0.86, respectively. The proposed mechanism of their formation from CAN is shown in Figure 11. DP1, DP2, DP4 and DP5 were isolated for the first time. The quantity of CAN recovered after chromatography of the initial extract of the chlorinated solution and its identification by comparison with an authentic commercial sample allowed us to evaluate a percentage of mineralization that is around 35% under the specified conditions, which is doubled with a CAN:hypochlorite molar ratio of 1:2 applied for longer times (3 h), while the formation of DPs is around 13%. The data reported in the literature for other ECs generally foresee longer reaction times, even in the order of hours, and oxidant concentrations are often double that of the pollutant to ensure the complete mineralization of the latter, frequently after a double or triple treatment [89], [102], [103], [104].

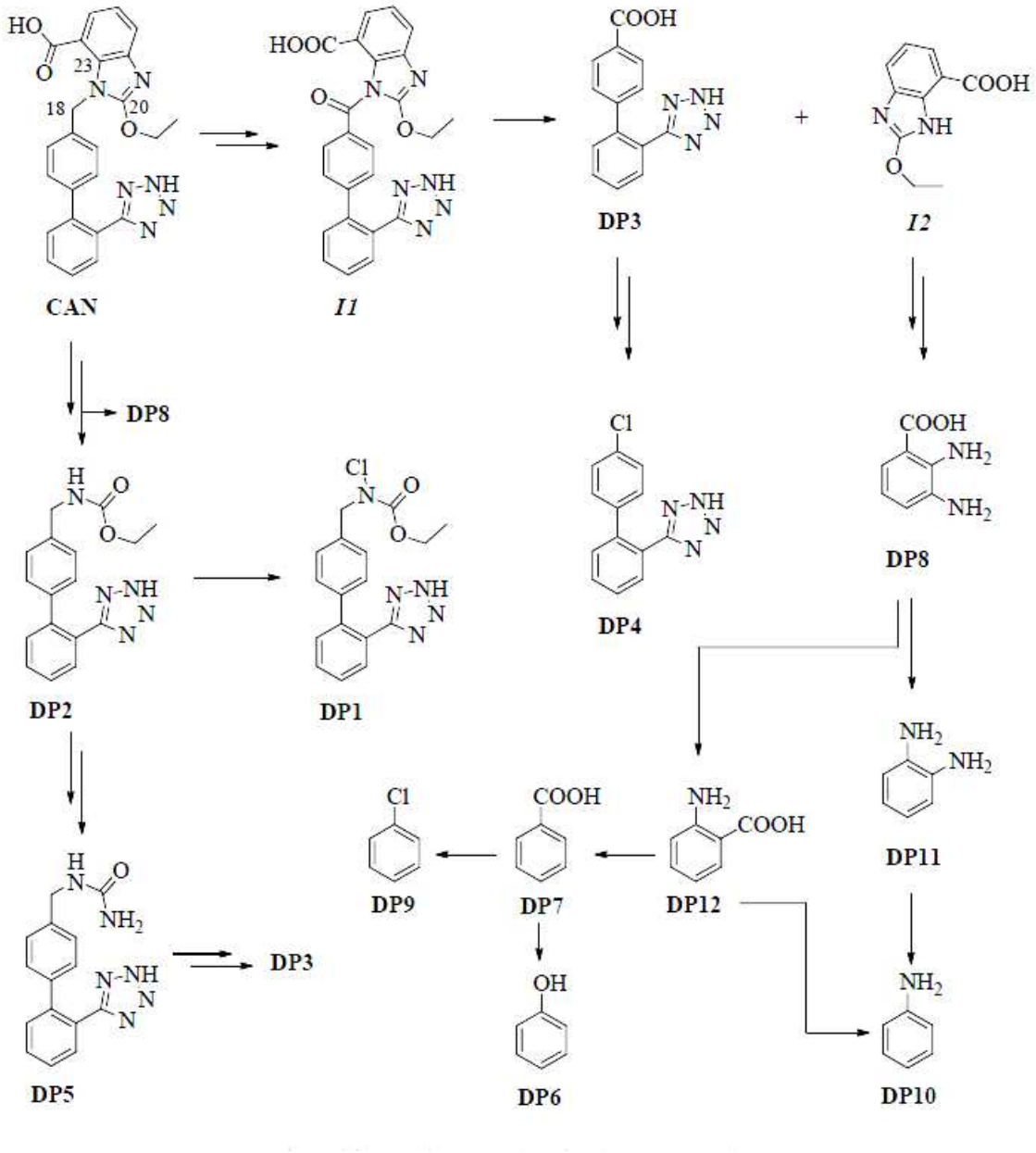


**Figure 11:** Plausible mechanism for the formation of DP1-DP12.

### 3.6.2 Structural Elucidation

In CAN treatment at buffered pH, the changes of the drug were monitored by HPLC. The concentration of DP1–DP12 was at a maximum after 2 h and ranged in the range of 2.40 to 0.42%. They were isolated by chromatographic processes (Figure 10) and identified by comparing their retention times with those of the standard compounds and by employing NMR and MS analyses. The plausible mechanism of the DPs formation from CAN is shown in Figure 11.

DP1–DP5 derive from the loss of the benzo[d]imidazole ring, with the chain linked to carbon C10 chlorinated on N19 (DP1), non-chlorinated (DP2), oxidized to carboxyl (DP3), replaced by a chlorine (DP4) or engaged in the formation of a urethane derivative (DP5). DP6–DP12 probably derive just from the degradation of the benzo[d]imidazole ring; in particular, we have three benzoic acids (DP7, DP8 and DP12), aniline (DP10) and its derivative DP11, phenol (DP6) and chlorobenzene (DP9).

Under the conditions used, in accordance with the data reported in the literature [63], [64] [105], [106], it is possible to hypothesize that CAN undergoes a first oxidation at carbon C18 to obtain the intermediate *I1*. The latter could undergo the hydrolysis of the C18-N19 bond and release the product DP3 and the intermediate *I2*. DP3 could first undergo a decarboxylation and then a subsequent chlorination to give DP4. Intermediate *I2* could undergo the hydrolysis of the N19-C20 and C20-N21 bonds to give DP8, from which DP11 could then be obtained by decarboxylation and DP12 by deamination. DP10 could be obtained by deamination of DP11 or decarboxylation of DP12. DP12 by deamination could provide DP7 and from the latter, by decarboxylation and subsequent oxidation, it could have DP6 or, by decarboxylation and subsequent chlorination, DP9. The starting product for hydrolysis of the N19-C23 and C20-N21 bonds could release DP2, together with DP8, and from this one, obtain DP1 by chlorination on N19. From DP2 by reaction with ammonia, the final product of the complete degradation of the drug, it could produce urethane DP5 and from this, by hydrolysis and subsequent oxidation, the product DP3.

### 3.6.3 Ecotoxicity results

Toxicity data were obtained using bioluminescent bacteria (*A. fischeri*), green algae (*R. subcapitata*) and crustaceans (*D. magna*). The results in Figure 12A reveal that both unicellular organisms were less sensitive than the multicellular species (*D. magna*), which unexpectedly proved to be the least resistant to the target compounds. The acute toxicity measured with aquatic organisms was expressed in toxic units (TU), where TU = 1/EC50. A class weight score (CWS) was calculated for each toxicity class in order to indicate the quantitative importance (weight) of the toxicity in that class [97]. Scores from the battery of toxicity tests performed on

pharmaceutical samples were transformed into percentage values and assigned to surface water hazard categories (Figure 12B).

The results indicate that approximately 21.4% of samples (CAN, **DP8** and a mixture) are not a significant acute hazard (class I), while 42.9% of samples (**DP1**, **DP2**, **DP6**, **DP7**, **DP9** and **DP12**) are classified as a slight acute hazard (class II) according to the classification system. Of the remaining samples (**DP3**, **DP4**, **DP5**, **DP10** and **DP11**), 35.7% belong to the acute hazard category (class III) and can definitely pose serious risks to ecosystem integrity. Biostimulation was observed only in three samples (**DP7**, **DP8** and **DP9**), and the highest contribution was from the bacteria *A. fischeri*.

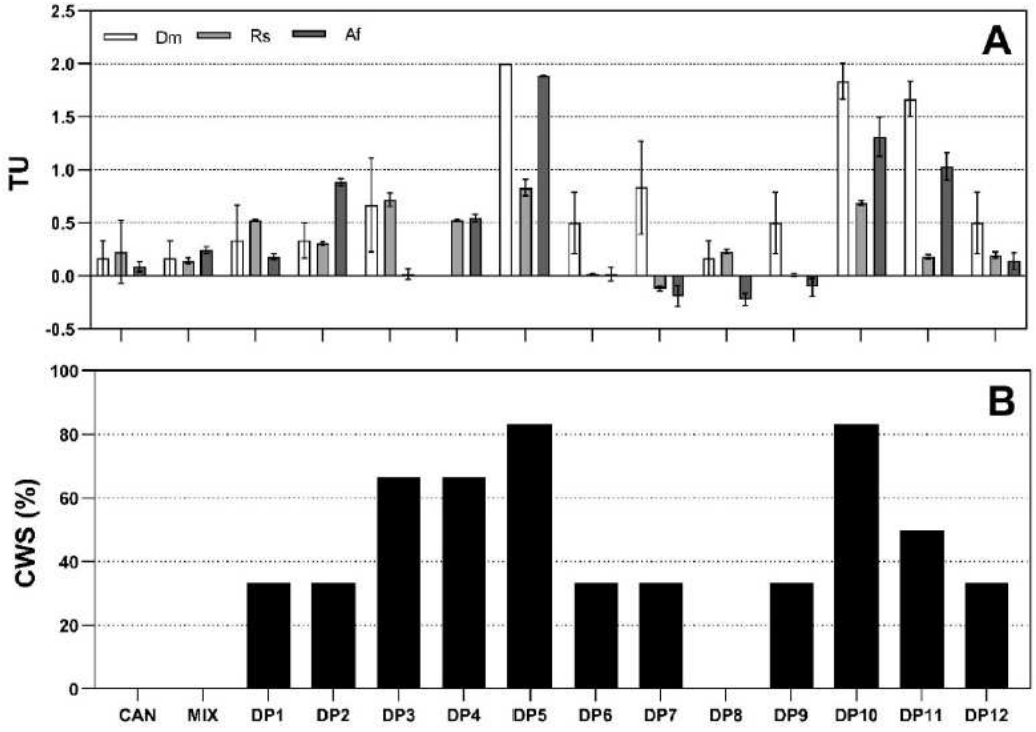


**Figure 12:** Toxic units (TU) for *D. magna* (Dm), *R. subcapitata* (Rs) and *A. fischeri* (Af) exposed to CAN and their DPs (**A**). Class weight scores (CWS %) for the selected battery tests (**B**).

## 3.7 Chlorination Procedure and Product Isolation: Olmesartan

Olmesartan acid (1 g, 2.24 mmol) was solubilized in 1.0 L of phosphate buffer ($KH_2PO_4/K_2HPO_4$ 0.1 M) [91]. A sodium hypochlorite solution (about 6% active chlorine, molar ratio OLM/HClO 1:20; concentration spectroscopically determined

at $\lambda_{max}$ of 292 nm, $\varepsilon = 350$ $dm^3$/mol cm) was added drop by drop to this solution under magnetic stirring at room temperature. The phosphate buffer pH was adjusted to 6.50 by adding a 10% $H_3PO_4$ solution, checking with a pH-meter. Reaction was stopped after 2 h with an excess of sodium thiosulphate and concentrated by lyophilization. The residue was dissolved in water, pH is adjusted to 7.00, and this solution was extracted with ethyl acetate (EA). The aqueous solution was subsequently extracted with n-butanol (B).

The crude EA fraction (579 mg) was chromatographed on silica gel CC, eluting with gradient of methylene chloride:methanol:acetic acid (100:0:0.5 to 70:30:0.5, v/v/v) to yield 16 fractions.

The fraction EA3 (16 mg), eluted with methylene chloride/methanol/acetic acid (100:0:0.5, v/v/v), was analysed via HPLC using a reversed-phase column and eluting with water/acetonitrile (20:80, v/v) to yield DP6 (6.7 mg). The fraction EA4 (30 mg), eluted with methylene chloride:methanol:acetic acid (98:2:0.5, v/v/v), was separated by semipreparative HPLC using a reversed-phase column Kromasil 10 µm 100 Å C18 (250 × 10 mm) and elution with a gradient of $CH_3COONH_4$ (A, pH 4.0; 10 mM) and methanol (B), starting with 70% B for 1 min and installing a gradient to obtain 100% B over 20 min at a solvent flow rate of 4 mL/min to yield DP2 (7.8 mg).

The fraction EA6 (36 mg), eluted with methylene chloride:methanol:acetic acid (95:5:0.5, v/v/v), was analysed via preparative HPLC using a reversed-phase column Gemini 10 µm C18 110 Å (250 × 21 mm) and elution with a gradient of $CH_3COONH_4$ (A, pH 4.0; 10 mM) and methanol (B), starting with 60% B for 1 min and installing a gradient to obtain 100% B over 30 min at a solvent flow rate of 7.5 mL/min to yield 5 subfractions.

The subfraction EA6.3 (7 mg) was re-chromatographed via HPLC using a reversed-phase column Luna 5 µm 100 Å C18(2) (150 × 4.6 mm) and elution with a gradient of $CH_3COONH_4$ (A, pH 4.0; 10 mM) and acetonitrile (B), starting with 60% B for 1 min and installing a gradient to obtain 100% B over 30 min at a solvent flow rate of 1 mL/min to yield DP8 (1.3 mg).

The fraction EA9 (13 mg), eluted with methylene chloride:methanol:acetic acid (90:10:0.5, v/v/v) was separated via preparative HPLC using a reversed-phase column Gemini 10 µm C18 110 Å (250 × 21 mm) and elution with a gradient of $CH_3COONH_4$ (A, pH 4.0; 10 mM) and methanol (B), starting with 50% B for 1 min and installing a gradient to obtain 100% B over 30 min at a solvent flow rate of 7.5

mL/min to yield 3 subfractions. The subfraction EA9.1 (15 mg) was re-chromatographed via HPLC using a reversed-phase column Kinetex 2.6 µm 100 Å C18 (100 × 4.6 mm) and elution with a gradient of $CH_3COONH_4$ (A, pH 4.0; 10 mM) and acetonitrile (B), starting with 40% B for 1 min and installing a gradient to obtain 100% B over 30 min at a solvent flow rate of 0.8 mL/min to yield DP9 (0.9 mg).

The fraction EA10 (30 mg), eluted with methylene chloride:methanol:acetic acid (85:15:0.5, v/v/v), was analysed via semipreparative HPLC using a reversed-phase column Kromasil 10 µm 100 Å C18 (250 × 10 mm) and elution with a gradient of $CH_3COONH_4$ (A, pH 4.0; 10 mM) and methanol (B), starting with 35% B for 1 min and installing a gradient to obtain 100% B over 20 min at a solvent flow rate of 4 mL/min to yield 4 subfractions. The subfractions EA10.2 (7 mg) and EA10.3 (9 mg) were re-chromatographed by HPLC using a reversed-phase column Kinetex 2.6 µm 100 Å C18 (100 × 4.6 mm) and elution with a gradient of acetic acid/acetonitrile (A, 1:99, v/v) and acetic acid/water (B, 1:99, v/v), starting with 75% B for 3 min and installing a gradient to obtain 100% A over 35 min and returning to 75% B for 10 min, at a solvent flow rate of 0.8 mL/min. They contained DP7 (2.6 mg) and DP5 (5.9 mg), respectively.

The fraction EA11 (63 mg), eluted with methylene chloride:methanol:acetic acid (80:20:0.5, v/v/v), was analysed via preparative HPLC using a reversed-phase column Gemini 10 µm C18 110 Å (250 × 21 mm) and elution with a gradient of $CH_3COONH_4$ (A, pH 4.0; 10 mM) and acetonitrile (B), starting with 20% B for 1 min and installing a gradient to obtain 90% B over 25 min at a solvent flow rate of 8 mL/min to yield DP1 (7.1 mg).

The fraction EA14 (120 mg), eluted with methylene chloride:methanol:acetic acid (70:30:0.5, v/v/v), was re-chromatographed on silica gel CC by elution with a gradient of chloroform:acetone:acetic acid (100:0:0.5 to 60:40:0.5, v/v/v) to yield 10 subfractions. The subfraction EA14.7 (33 mg), eluted with chloroform:acetone:acetic acid (70:30:0.5, v/v/v), was separated by semipreparative HPLC using a reversed phase column Kromasil 10 µm 100 Å C18 (250 × 10 mm) and elution with a gradient of $CH_3COONH_4$ (A, pH 4.0; 10 mM) and methanol (B), starting with 0% B for 5 min and installing a gradient to obtain 100% B over 20 min at a solvent flow rate of 3.5 mL/min to yield DP3 (11.6 mg) and DP4 (6.6 mg).

The fraction EA1 (26 mg), eluted with methylene chloride:methanol:acetic acid (100:0:0.5, v/v/v), was separated by semipreparative HPLC using a reversed phase

column Kromasil 10 µm 100 Å C18 (250 × 10 mm) and eluting with a gradient of $CH_3COONH_4$ (A, pH 4.0; 10 mM) and methanol (B), starting with 85% B for 1 min and using a gradient up to 100% B in 25 min, at a solvent flow rate of 2 mL/min, to yield DP10 and DP11 (3.1 and 1.3 mg, respectively).

The fraction EA6 (76 mg), eluted with methylene chloride:methanol:acetic acid (95:5:0.5, v/v/v), was analysed via preparative HPLC using a reversed-phase Gemini column of 10 µm C18 110 Å (250 × 21 mm), eluting with a gradient of $CH_3COONH_4$ (A, pH 4.0; 10 mM) and methanol (B), starting with 60% B for 1 min and using a gradient up to 100% B in 30 min at a solvent flow rate of 7.5 mL/min to get five subfractions. The subfraction EA6.1 (33 mg) was re-chromatographed by HPLC using a reversed-phase Kinetex column of 2.6 µm 100 Å C18 (100 × 4.6 mm), eluting with a gradient of $CH_3COONH_4$ (A, pH 4.0; 10 mM) and acetonitrile (B), starting with 40% B for 1 min and using a gradient up to 100% B in 30 min, at a solvent flow rate of 0.8 mL/min, to yield DP12, DP14, and DP17 (1.4, 1.1, and 13.4 mg, respectively). The subfraction EA6.2 (5 mg) was re-chromatographed by HPLC using a reversed-phase Kinetex column of 2.6 µm 100 Å C18 (100 × 4.6 mm), eluting with a gradient of $CH_3COONH_4$ (A, pH 4.0; 10 mM) and acetonitrile (B), starting with 50% B for 1 min and using a gradient up to 100% B in 30 min, at a solvent flow rate of 0.8 mL/min, to get DP15 (2.1 mg).

The fraction EA10 (51 mg), eluted with methylene chloride:methanol:acetic acid (85:15:0.5, v/v/v), was analysed by semipreparative HPLC using a reversed-phase Kromasil column of 10 µm 100 Å C18 (250 × 10 mm) and eluting with a gradient of $CH_3COONH_4$ (A, pH 4.0; 10 mM) and methanol (B), starting with 35% B for 1 min and using a gradient up to 100% B in 20 min, at a solvent flow rate of 4 mL/min, to yield four subfractions. The subfractions EA10.1 (7 mg) was re-chromatographed by HPLC using a reversed-phase Kinetex column of 2.6 µm 100 Å C18 (100 × 4.6 mm) and eluting with a gradient of acetic acid:acetonitrile (A, 1:99, v/v) and acetic acid:water (B, 1:99, v/v), starting with 75% B for 3 min and installing a gradient to obtain 100% A over 35 min and returning to 75% B for 10 min, at a solvent flow rate of 0.8 mL/min. It contained DP13 (3.2 mg). The subfractions EA10.4 (16 mg) was re-chromatographed by HPLC using a reversed-phase Kinetex column of 2.6 µm 100 Å C18 (100 × 4.6 mm) and eluting with a gradient of acetic acid:acetonitrile (A, 1:99, v/v) and acetic acid:water (B, 1:99, v/v), starting with 60% B for 5 min and using a

gradient up to 100% A in 20 min and returning to 60% B for 10 min, at a solvent flow rate of 1.0 mL/min. It contained DP16 (12.2 mg).

The fraction obtained by extraction with n-butanol (B, 635 mg) was again fractioned by silica gel CC, using a gradient of ethyl acetate:methanol, to give six fractions. The B5 fraction (12 mg), eluted with ethyl acetate:methanol (50:50, v/v), was dried, solubilized in water:ethanol (50:50, v/v), and analysed using a Shimadzu 2010 series GC FID (Shimadzu, Milano, Italy). The gas chromatograph was equipped with Zebron ZB-5 column (30 m × 0.32 mm I. D., 1.00 μm; Phenomenex, Bologna, Italy). The following parameters were set during the experiments: helium as a carrier gas with constant flow of 1.2 mL/min, 1.0 μL injected into samples with a 20:1 split, and introduced into the injector at 250 °C using an AOC-20i auto sampler (Shimadzu, Milano, Italy). The initial temperature was 60 °C, then rose with a 4 °C/min ramp to 200 °C with a 5 min hold. The identification of DP18 and DP19 was fulfilled by comparison with available standard compound.

The aqueous fraction (W, 711 mg) was dried by lyophilization, re-dissolved in methanol and separated with CC silica gel by running an ethyl acetate:methanol gradient (100:0 to 0:100, v/v) to get eight fractions.

The fraction W2 (155 mg), eluted with ethyl acetate:methanol (60:40, v/v), was filtered on reversed phase silica gel CC with water, methanol, and acetonitrile. The fraction eluted with acetonitrile (6 mg) was analysed by NMR and contained DP20.

The fraction W7 (187 mg), eluted with ethyl acetate:methanol (50:50, v/v), was chromatographed on a reversed phase Sep-Pak RP-18 with a gradient of acetic acid 1%:acetonitrile (100:0 to 0:100 v/v). The fraction eluted with acetic acid 1% was concentrated by lyophilization (31 mg), analysed by HPLC using a reversed-phase Luna column of 5 μm C8(2) 100 Å (150 × 4.6 mm), and eluted with an isocratic solution of $KH_2PO_4$ (pH 2.6, 20 mM):acetonitrile (75:25 v/v) at a solvent flow rate of 1 mL/min. It contained DP21, as evidenced by the RT comparison with a standard compound and NMR spectra. The fraction eluted with acetonitrile was analysed by HPLC using a reversed-phase Luna column of 5 μm Phenyl-Hexyl 100 Å (150 × 4.6 mm) and eluting with water (A) and acetonitrile (B), starting with 40% B for 10 min and later obtaining 55% B over 10 min, at a solvent flow rate of 1.2 mL/min. It contained DP22, as evidenced by the RT comparison with a standard compound and NMR spectra (Figure 13).

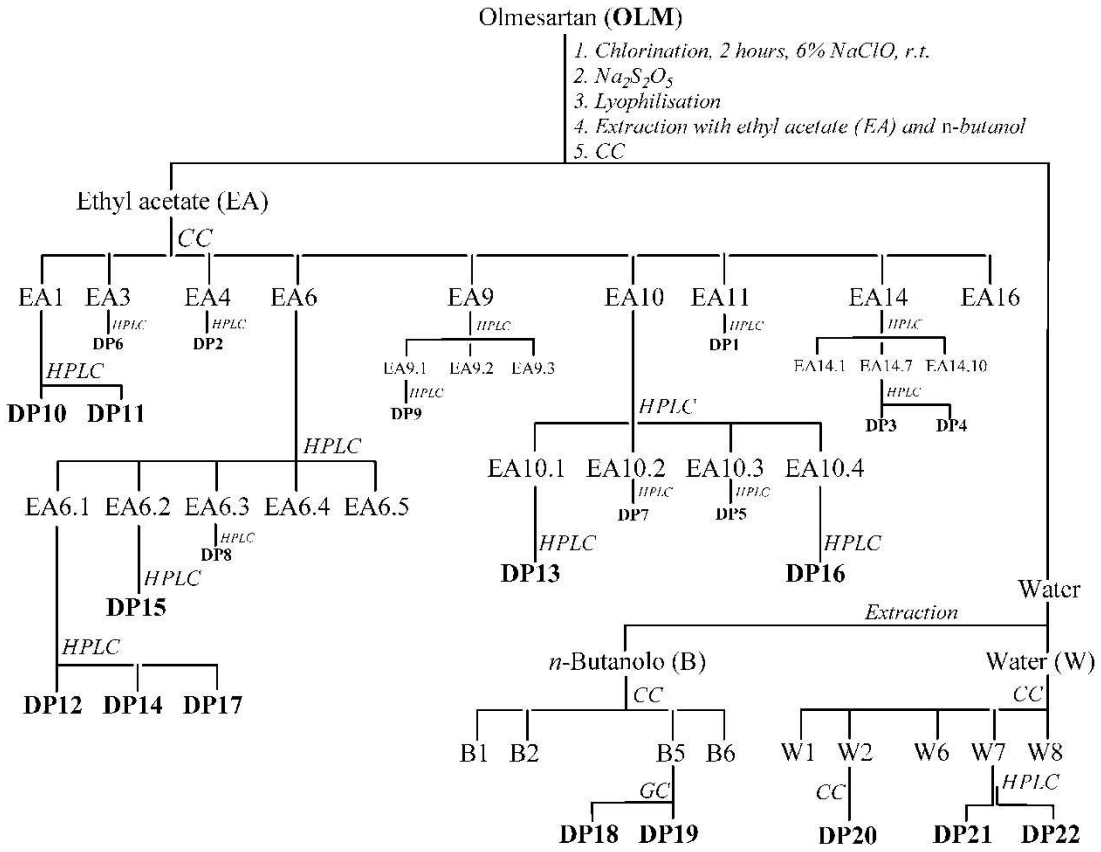


**Figure 13:** The isolation of all identified compounds (DP1–DP22).

# 3.8 Results and discussion

## 3.8.1 Chlorination Experiments

A $10^{-5}$ M OLM solution was treated for 10 min with 10% hypochlorite (molar ratio OLM/HClO 1:1 concentration, spectroscopically determined $\lambda_{max}$ 292 nm, ε 350 $dm^3$/mol cm) at room temperature [88], simulating the conditions used in a typical WWTP. The experiment was conducted at pH = 10.5. The presence of OLM was quantified using a Lambda 12 UV-Vis spectrophotometer (Perkin Elmer, Waltham, MA, USA). Absorbance peaks were determined at 230 nm. The absorbance values were converted into a concentration using a calibration curve prepared from standard solutions with known OLM concentrations. The pH of the solution, measured and recorded continuously using a pH-meter, increased immediately from the initial pH of 8.0 to 10.5, and pH remained at this value during the reaction. An aliquot of the solution was taken every 15 min, quenched by sodium thiosulphate excess, filtered,

dried by lyophilization, and the residue dissolved in a saturated sodium bicarbonate solution and extracted with ethyl acetate. The course of the reaction was monitored using HPLC.

DP1–DP9 were isolated from the ethyl acetate extract of the aqueous solution and identified by comparing their retention times with those of commercially available standard compounds.

DP10–DP17 for the EA fraction and DP18–DP22 for the aqueous fraction (W) were identified by comparing them with commercial reference compounds, or isolated through preparative experiments with an OLM solution at concentration above 10−3 M, using 6% hypochlorite at room temperature for 2 h.

The DPs obtained were isolated using column chromatography and HPLC and were completely characterized using NMR and MS analyses. The proposed mechanism of their formation and isolation from the OLM is shown in Figure 14.

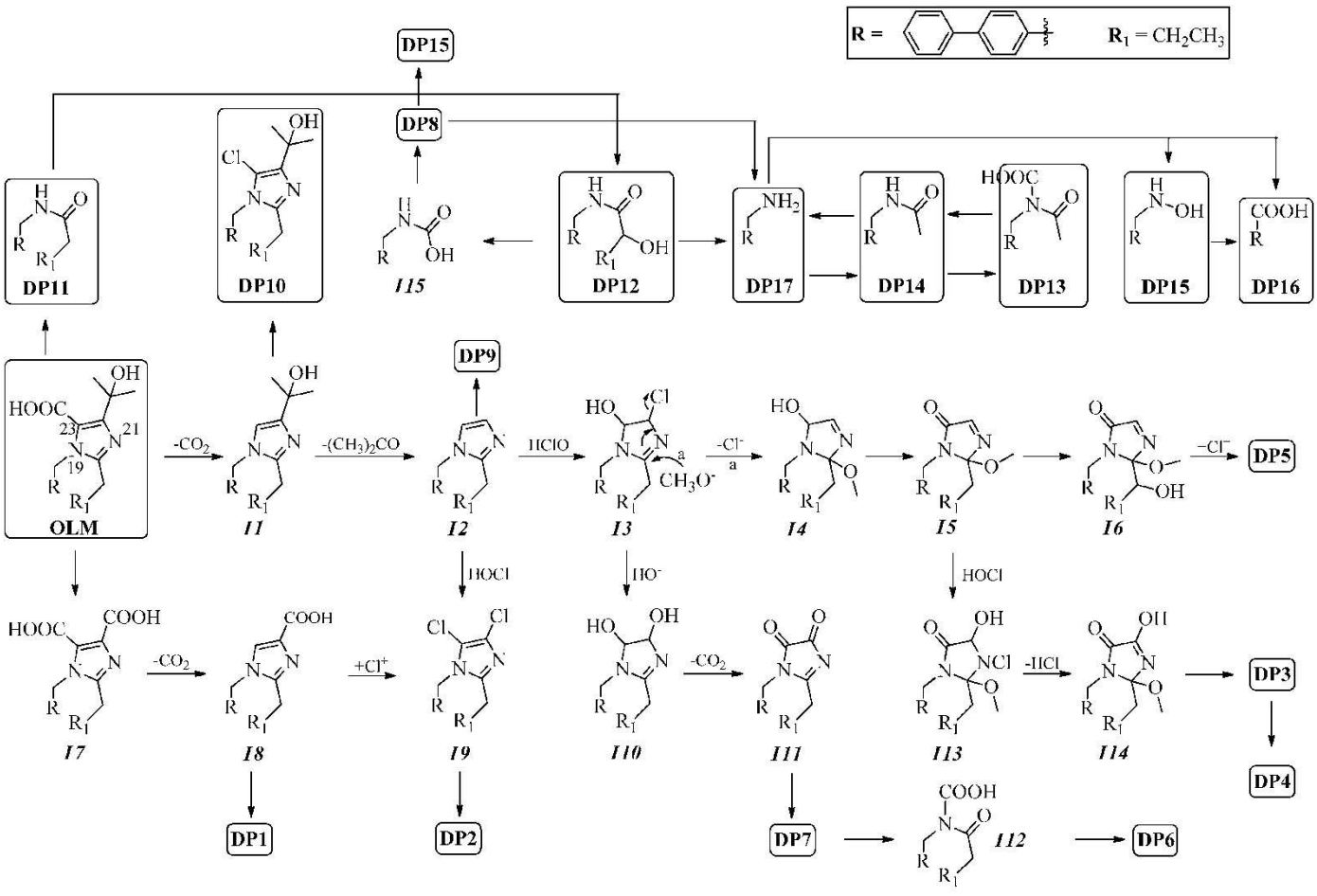


**Figure 14:** The plausible mechanism for the formation of DP11-DP1.

### 3.8.2 Structural Elucidation

In the OLM treatment at the buffered pH, the concentration of DP1–DP9 was at a maximum after 2 h and in the range of 2.01 to 0.15%. Olmesartan acid could undergo the oxidation of the side-chain at carbon C23 to obtain intermediate *I1*, whose subsequent decarboxylation at carbon C22 generates intermediate *I2*. The reaction of this with HClO could generate intermediate *I3* from which intermediate *I4* can be obtained via nucleophilic attack of the $CH_3O^-$ ion [107], [108], [109]. The oxidation at carbon C23 (intermediate *I5*) and C24 (intermediate *I6*) and the chlorination at carbon C22 could provide DP5. Intermediate *I6*, via its reaction with HClO, provides intermediate *I7*, which due to the loss of HCl would provide intermediate *I8*. From *I8*, the oxidation of DP4 could be obtained. Olmesartan acid could undergo the hydrolysis of the N19-C23 and C20-N21 bonds to release intermediate *I9*, from which intermediate *I10* could then be obtained via oxidation of the side-chain, precisely on the carbon adjacent to the carbonyl function. The complete oxidation of the *I10* side-chain would provide *I11*, and from the nitrogen oxidation of the latter, DP8 could be obtained. The partial oxidation of the C22 carbon of the starting product could provide intermediate *I12*, which via the decarboxylation at carbon C23 would provide intermediate *I13*. The chlorination of this could provide DP1. DP9 could be obtained from different precursors with the loss of all the substituents of the imidazole ring.

The intermediate *I2* could be chlorinated at carbons C22 and C23 to provide the intermediate *I14*, which could then provide DP2 via oxidation of the side-chain to carbon C24. Intermediate *I3*, by replacing the chlorine with $OH^-$, could provide the intermediate *I15* which then, via the oxidation and opening of the imidazole ring, could provide DP7 through intermediate *I16*. DP7 could then provide intermediate *I17* via oxidation of the adjacent carbon of the carbonyl function of the side-chain, and then lactone DP6 could be obtained via its intramolecular reaction.

Intermediate *I5* could provide the corresponding *I19* by reaction with HClO. The loss of HCl (intermediate *I20*) and subsequent oxidation at carbon C22 could yield DP3. The oxidation of the latter to the C-24 carbon of the side chain could provide DP4.

In the OLM treatment at the buffered pH, the concentration of DP10–DP17 was at a maximum after 1 h, in the range of 1.34 to 0.11%, while that of DP18–DP22 was at a maximum after 2.5 h. OLM can undergo the imidazole ring opening reaction with the cleavage of the N19-C23 and C20-N21 bonds, obtaining the DP11 product. This

could undergo an oxidation to the carbon of the side chain (which, in the starting product, was indicated as carbon C-24), producing the DP12 product. Luongo *et al.* [64] hypothesized that DP11 and DP12 could be two intermediates, which, through a third intermediate *I15*, would lead to the degradation of DP8 by-products. From this, then, by reductive decarboxylation, the obtaining of the DP15 product is justified, which would then provide DP16 by deamination of the side chain and oxidation of the C-18 carbon to a carboxyl group. From DP12, it is easy to justify the formation of DP17 by hydrolysis of the N19-C20 bond. The degradation of the DP17 by-product by oxidation would give DP15 by acetylation of DP14 and by subsequent oxidation of this, the DP13 product. Finally, the DP18–DP22 products are degradation products that can be justified in different ways and that constitute the step preceding the complete mineralization of the starting product.

### 3.8.3 Ecotoxicity results

The inhibition effects on the bioluminescence of *A. fischeri* and on the growth of *R. subcapitata* were measured in this section for characterizing the acute and chronic toxicity of OLM-DPs at concentrations of 5 mg/L.

The analysis of toxicity data on DP1-DP9 (Figure 15) evidenced the presence of three main groups of samples considering a threshold value for the effects statistically different from the control groups [110]: (I) no effect (−10% ≤ inhibition ≤ 10%); (II) biostimulation effect (inhibition < −10%); and (III) toxic effects (inhibition > 10%).

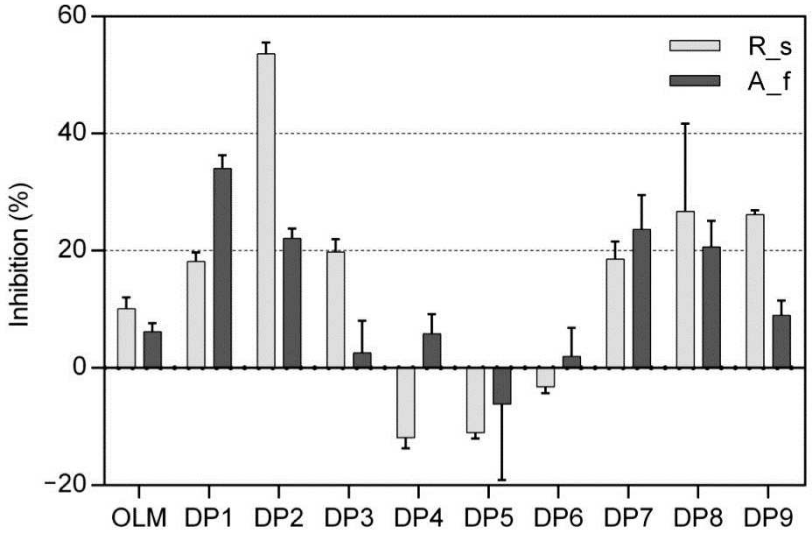


**Figure 15:** The toxicity data of olmesartan acid (OLM) and its by-products (DP1–DP9) with 72 h *R. subcapitata* (R_s) and *A. fischeri* (A_f).

After 72 h of exposure, OLM presented no effect on *R. subcapitata*. Comparing OLM and DPs results, only DP6 showed no toxicity. Several samples presented negative growth effects (DP1, DP2, DP3, DP7, DP8, DP9), and their toxicity values ranged from 18% to a maximum of 53%. DP4 and DP5 showed stimulatory effects. Toxicity data from *A. fischeri* confirmed that the parent compound OLM showed no toxic effect after 30 min of exposure. Five of nine isolated DPs (DP3, DP4, DP5, DP6 and DP9) showed no inhibitory effect. The other DPs presented acute toxicity like DP1, DP2, DP7, and DP8 showing inhibition effects from 20% to 34%. Comparing the results of the algal growth inhibition with bacteria luminescence inhibition, it was evident that the response of *A. fischeri* was less sensitive, but the toxicity trends were linearly correlated (Pearson correlation, r = 0.61, moderately high correlation).

The analysis of toxicity data was also carried out on the by-products from DP10 to DP22 (Figure 16) measuring, as previously, the inhibition effects on the bioluminescence of *A. fischeri* and on the growth of *R. subcapitata*.

Only in three DPs (DP14, DP20, and DP22) in *R. subcapitata* and two DPs in *A. fischeri* (DP14 and DP20) the stimulation was observed, showing no toxic effects. However, in 75% of the DPs investigated, the negative effects increased compared to the parent compound (OLM). In particular, the bioluminescence inhibition of the *A. fischeri* in DP16 exceeded 70%. The acute toxicity in each DPs followed the order of DP14 > DP20 > DP21 > DP15 > DP22 > DP11 > DP10 > DP12 > DP18 > DP19 > DP13 > DP16, while the chronic toxicity in each DPs followed the order of DP22 > DP20 > DP14 > DP13 > DP18 > DP15 > DP19 > DP12 > DP21 > DP11 > DP10 > DP16. Considering the overall toxicity, these results demonstrate that higher inhibitory values, especially for *A. fischeri*, were achieved for DP16, while lower inhibitory values were achieved for DP20. Thus, as a strong oxidant, sodium hypochlorite could decompose non-toxic OLM into small molecules, increasing the toxicity of the compound. Although the concentrations investigated and capable of exerting toxic effects may be higher than the environmental concentrations, the possible problems due to continued exposure, which can occur through contact with water and through the food chain, should not be underestimated.

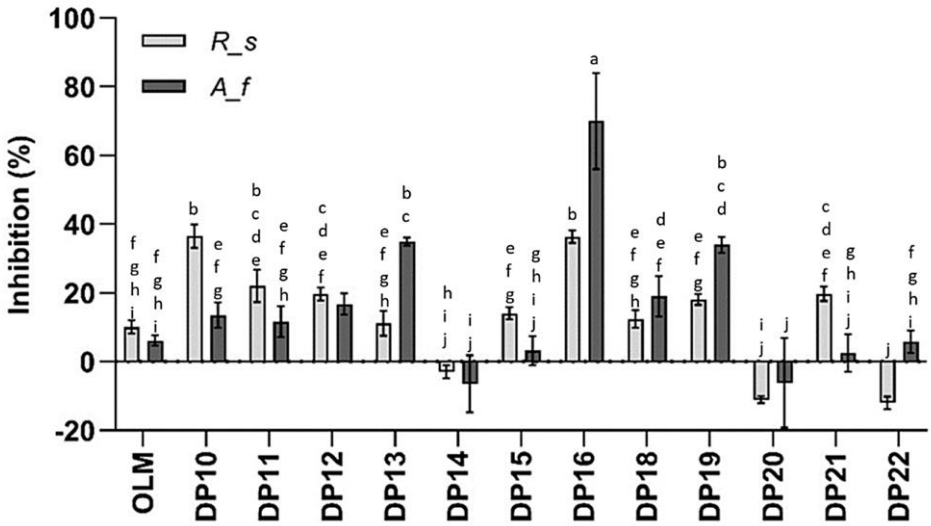


**Figure 16:** The comparison of the effects of DPs on the bioluminescence of *A. fischeri* (A_f) and on the inhibition of growth rates of *R. subcapitata* (R_s). Groups with the same letter were not significantly different (*Tukey post hoc, $p < 0.05$*).

## 3.9 Conclusions

This chapter provides a comprehensive picture of the transformation of cardiovascular drugs, known surface and wastewater pollutants, when subjected to chlorination processes, such as those carried out in WWTPs. The reaction was indeed carried out by simulating the conditions of a typical WWTP using excess sodium hypochlorite. After chlorination treatment, chromatographic techniques were used to isolate sartans degradation by-products and subsequently the structures were fully characterized by MS and NMR analyses and compared with the parental samples.

As regards irbesartan, following the chlorination treatment, 18 disinfection by-products were isolated and characterized. The first part of this research explains how just over 75% of irbesartan underwent a complete mineralization, while <15% was recovered and unchanged, and 6% was transformed into at least 6 new by-products (DPs 1-6). Four of the six by-products presented aromatic tetracyclic structures, probably due to an aromatic nucleophilic addition reaction of the tetrazole on the adjacent benzene ring through a neutral intermediate.

In the second part of the research 12 new disinfection by-products (DBPs 7-18) were isolated and identified using mono- and bidimensional NMR spectra and MALDI TOF experiments. In particular, 9 of these were isolated for the first time. Furthermore, by adding them to the library of previously compounds isolated, it was

possible to provide a complete overview of the by-products and hypothesize a formational mechanism for each of them. The products reported were derived from the hydrolysis of two different bonds of the imidazole-like ring or from the partial or complete oxidation of the C-11 carbon and/or the n-butyl side chain. Notably, the biphenyl nucleus did not undergo transformation apart from the formation of a new ring with the adjacent tetrazole, and, apart from one, no halogenated disinfection by-products were isolated. Regarding the detected toxicity via the biological assays, the by-products showed a dynamic trend, resulting in further transformation. The transformation pathway provided an overview of the fate of irbesartan and its by-products in the aquatic environment. Notably, a batch of by-products was detected, which showed higher toxicity than the parent compound. The by-products exhibited dynamic and variable toxicity, with different levels of toxicity observed in different organisms. *A. fischeri* was the most sensitive to the by-products, followed by *R. subcapitata* and *D. magna*, indicating species-specific toxicity. About two-thirds (64%) of the by-products exhibited a stimulating effect (hormesis) on the algal species *R. subcapitata*.

As regards candesartan, following the chlorination treatment, 12 disinfection by-products, 4 of which were isolated for the first time, were isolated and characterized. Some by-products retain the diphenyl base nucleus and the tetrazole ring of the side chain, but undergo the partial degradation (DP1–DP2 and DP5) or the loss (DP3 and DP4) of benzimidazole; others have a $C_6C_1$ (DP7, DP8 and DP12) or $C_6C_0$ (DP6, DP9–DP11) skeleton, obviously being the degradation products of the first five. About 35% of the initial quantity of candesartan is estimated to undergo complete mineralization, and about 13% is transformed into degradation by-products. The CWS approach confirmed that 78.6% of the total investigated pharmaceutical samples are able to have some adverse ecotoxicological effects on the aquatic environment and that effluents containing CAN degradation by-products with pollutant potential could generate negative impacts on water and/or soil equilibrium, as well as human health.

As regards olmesartan, following the chlorination treatment, 22 disinfection by-products, 6 of which were isolated for the first time, were isolated and characterized. The first analytical phase allowed 9 by-products to be obtained (DP1-DP9). In this phase OLM underwent complete mineralization in about 59% of cases, and in 21% of cases was recovered as is. OLM transformed into the corresponding by-products

in 20% of cases, and about 9% of these were identified. Half of the investigated DPs possessed anywhere from slightly to highly toxic effects on the target species *A. fischeri* and *R. subcapitata*; the remaining DPs presented no such effects. According to the selected battery of toxicity, the correlation of the results suggested that DPs acted very similarly in unicellular organisms. Moreover, due to the highlighted ecotoxicological effects, DPs acting on organisms of low levels of complexity could have negative effects also on the whole trophic chain (biomagnification). The second analytical phase allowed 13 by-products to be obtained (DP10-DP2). In this phase OLM transformed into the corresponding by-products in 20% of cases, and about 14% of these were identified. A total of 75% of the investigated DPs possessed anywhere from weak to high toxicity; the remaining DPs presented no such effects. Furthermore, the order of chronic and acute toxicity showed that the products disinfected with sodium hypochlorite showed the highest inhibition rates for algae.

These outcome raises concerns regarding the potential consequences of these by-products on organisms in water bodies that receive sewage, emphasizing the importance of further research and appropriate actions to safeguard water quality and the ecological equilibrium. Chlorine disinfection is not an optimal process for sartans removal because of its by-products generation, which possess greater toxicity compared to the original chemical. It is important to note that the primary goal of water chlorination is to ensure the safety of drinking water by disinfecting it and preventing the spread of waterborne diseases. The presence of by-products, including those derived from pharmaceutical compounds like sartans, highlights the need for comprehensive water treatment strategies that can address the removal of or reduction in both microbial contaminants and potentially harmful by-products.

It will also be important that environmental laws and regulations consider the formation of by-products and establish limits and regulations to ensure the safety of drinking water and the protection of the environment.

# CHAPTER 4

In this chapter, the results based on original contributions published in [111] and submitted in MDPI (*molecules*) are presented.

## 4.1 Octocrylene: From Sunscreen to Chlorination Process

Octocrylene (OCT) is a viscous, clear and colorless oil, introduced in commercial sunscreens and anti-aging creams about 15 years ago. It is the 2-ethylhexyl ester of 2-cyano-3,3-diphenylacrylic acid, with the extended conjugation of the acid portion that absorbs UVB and short-wave UVA (ultraviolet) rays, with wavelengths from 280 to 320 nm [112], which promote tanning but also contribute to the onset of sunburn and skin cancer. It is used in various body care products [113], [114], in concentrations up to 10%, in order to provide an adequate sun-protection factor or to protect the body care formulations themselves from UV radiation. This filter was recently indicted for the risk of inducing potential adverse effects on the endocrine system [11], as well as having an allergic and/or photoallergic potential [115]. In recent years, there has been an increase in the number of cases of photocontact allergic reactions to octocrylene, which has been referred to as an "emerging allergen". However, it has the advantage of working in synergy, allowing for wide and beneficial photoprotection; for example, it stabilizes avobenzone (butyl methoxydibenzoylmethane), a molecule present in the UVA filter. The European Chemicals Agency (ECHA) constantly evaluates the safety profile of this filter, like all chemicals used in cosmetics and registered under European legislation. Octocrylene has been found in various environments, not least those of swimming pools [116], where it is evidently released by consumers, to the point that it is now considered an emerging micropollutant similar to polyfluoroalkyl substances (PFAS) [117], blue-green algae [118], toxic fungal products [119], hormones [120], psychoactive drugs [121], [89], pesticides [122], cosmetics, and industrial additives and drugs [103], [123], [63], [124], [125]. These substances, unlike conventional and unconventional pollutants, are still largely unregulated by legislation and are not restricted by maximum permitted values. Furthermore, they are potentially dangerous for the environment and human health, even in an overall context of

insufficient data linked to their dangerousness [126], [127], [102], [84], [70]. Removal of emerging contaminants from wastewater can be accomplished by ozonation [71], membrane filtration [72], adsorption [69], and, above all, advanced oxidation [74], [94].

In this research, the degradation by-products (DPs) of OCT were investigated by mimicking the chlorination process normally used in swimming pools to sterilize and disinfect water and to reduce similar emerging pollutants [6,29]. In particular, two different experiments were carried out, one at concentrations of about $10^{-5}$ M, comparable to those at which OCT is present in wastewater, and one at concentrations at least 100 times higher in order to isolate and identify the DPs. The structures of 11 isolated DPs, 6 of which were isolated for the first time, were determined by crossing the data provided by nuclear magnetic resonance (NMR) and those obtained by mass spectrometry (MS), using matrix-assisted laser desorption/ionization as a source and a time-of-flight analyser (MALDI-TOF) for mass spectroscopy. It was also possible to propose a mechanism of formation to justify obtaining of the isolated products in a similar way to that used for sartans.

The spatial distribution of OCT is strictly connected to its presence in the marine aquatic environment; this presence is due to the anthropogenic activities responsible for its direct emission. For this reason, an ecotoxicological assessment was carried out with marine aquatic bioindicators such as *Aliivibrio fischeri*, *Phaeodactylum tricornutum* and *Brachionus plicatilis*. Emerging organic pollutants such as UV filters therefore require biological assays capable of detecting potential toxicity from a one-health perspective.

## 4.2 Materials and Methods

### 4.2.1 Reagents and chemicals

Octocrylene (99%) was purchased from Sigma Aldrich (Milan, Italy). All of the other chemicals and solvents were purchased from Sigma Aldrich (Milan, Italy) and were of HPLC grade and used as received. All of the chemicals were of analytical grade and supplied by Sigma Aldrich.

The toxicity tests were conducted with two combinations. In the first combination, osmotic adjustment solution (OAS) (22 g $L^{-1}$ NaCl) was used as a control for optimal conditions according to the ISO 11348-3 standard [86]. In the second

combination, synthetic sea water was used as the control solution according to the ISO 10253 standard [128] [129]. The synthetic sea water used for analytical procedures comprised the following salts: NaCl (22 g $L^{-1}$), $MgCl_2 \cdot 6H_2O$ (9.7 g $L^{-1}$), $Na_2SO_4$ (3.7 g $L^{-1}$), $CaCl_2$ (1.0 g $L^{-1}$), KCl (0.65 g $L^{-1}$), $NaHCO_3$ (0.2 g $L^{-1}$) and $H_3BO_3$ (0.023 g $L^{-1}$).

### 4.2.2 Toxicity tests

The toxicity of OCT and its degradation by-products was assessed regarding the following organisms: *A. fischeri*, *P. tricornutum* and *B. plicatilis*. A Microtox® acute ecotoxicity test was performed using the marine bioluminescent bacteria *A. fischeri* (NRRL-B-11177) to assess the toxicity of OCT and DPs. The bacteria were supplied in a freeze-dried form by Aqua Science LLC (Newark, Delaware, USA) and were stored at −20 °C to preserve their microbial activity. The acute toxicity endpoint was determined after 30 min of exposure according to ISO 11348-3 [86].

An algal growth-inhibition test was performed using benthic diatom *P. tricornutum*. The algal culture was kept at 20 ± 2 °C and 6000–10,000 Lux light, to obtain a cellular density of $10^6$ cells/mL. Inocula were taken from pre-cultures set up three days before the experiment to adjust the initial cell density to approximately $10^4$ cells/mL [129]. The test was carried out and miniaturized for 24-well sterile polystyrene micro-plates. The growth inhibition rate was calculated after 72 h exposure using a UV–Vis spectrophotometer (Hach Lange DR5000) and a 5 cm cuvette.

The acute toxicity test with estuarine rotifer *B. plicatilis* was performed according to the standard procedure of Rotoxkit M® using certified dehydrated cysts (MicroBioTests Inc.). The test was conducted in multiwell plates with 300 µL per well. Six wells with ten rotifers each were filled to assess the toxicity of the parent compound and of its 11 DPs. Incubation was carried out for 48 h, at 25 °C, in darkness. The number of dead rotifers after the exposure period was observed under a stereomicroscope (LEICA EZ4-HD). The significance of the differences between the mean values of the different tests and controls was verified using Addinsoft XLSTAT (2016.02.27444 Version) by analysis of variance (ANOVA) with a 0.05 significance level. In addition, the post-hoc analyses were carried out with Tukey's test.

## 4.3 Chlorination Reaction

### 4.3.1 Apparatus and Equipment

Column chromatography (CC) was carried out with Kieselgel 60 (230–400 mesh, Merck, Darmstadt, Germany). HPLC was performed on a Shimadzu LC-8A system using a Shimadzu SPD-10A VP UV-VIS detector (Shimadzu, Milan, Italy). Preparative HPLC was performed using an RP Gemini C18-110A preparative column (10 μm particle size, 250 mm × 21.20 mm i.d. Phenomenex, Bologna, Italy) with a flow rate of 8.0 mL/min. The $^{1}$H- and $^{13}$C-NMR spectra were recorded with an NMR spectrometer operated at 400 MHz and at 25 °C (Bruker DRX, Bruker Avance) and referenced in ppm to the residual solvent signals ($CDCl_3$, at $\delta_H$ 7.27 and $\delta_C$ 77.0; and $CD_3OD$, at $\delta_H$ 3.30 and $\delta_C$ 49.0). The proton-detected heteronuclear correlations were measured using a gradient heteronuclear single-quantum coherence (HSQC) experiment, optimized for $^{1}J_{HC}$ = 155 Hz, and a gradient heteronuclear multiple bond coherence (HMBC) experiment, optimized for $^{n}J_{HC}$ = 8 Hz. The MALDI-TOF mass spectrometric analyses were performed on a Voyager-De Pro MALDI mass-spectrometer (PerSeptive Biosystems, Framingham, MA, USA). The samples were lyophilized using a Lyovapor$^{TM}$-200 (Buchi, Cornaredo (MI), Italy), with a compressor with cooling capacity: 1.97 kW for 50 Hz and minimum condenser temperature: -55 °C.

## 4.4 Chlorination Procedure and Product Isolation

A $10^{-5}$ M OCT solution was treated for 10 min with 10% hypochlorite (molar ratio OCT/HClO 2:1 concentration, spectroscopically determined $\lambda_{max}$ 292 nm, ε 350 $dm^3$/mol cm) at room temperature [88]. The presence of OCT was quantified using a Lambda 12 UV-Vis spectrophotometer (Perkin Elmer, USA). Absorbance peaks were determined at 310 nm. The absorbance values were converted into a concentration using a calibration curve prepared from standard solutions with known OCT concentrations. **DP1**–**DP11** were isolated from the methylene chloride extract of the aqueous solution (Figure 17) and identified by comparing their retention times with those of commercially available standard compounds, or isolated by performing preparative experiments with a solution of OCT at a concentration higher than $10^{-3}$ M and treated with 6% hypochlorite at room temperature for 2 h. The pH of the solution, measured and recorded continuously using a pH-meter, increased

immediately from the initial pH of 8.0 to 10.8, and the pH remained at this value during the reaction. An aliquot of the solution was taken every 15 min, quenched by sodium thiosulphate excess, filtered, and dried by lyophilisation, and the residue was dissolved in a saturated sodium bicarbonate solution and extracted with ethyl acetate. The course of the reaction was monitored using HPLC. The DPs obtained were isolated using CC and HPLC and were completely characterized using NMR and MS analyses.

Octocrylene (607 mg, 1.68 mmol) was dissolved in 22 mL of acetonitrile, and the solution was diluted with water until a final volume of 0.9 L was reached. A sodium hypochlorite solution (approximately 6% active chlorine, molar ratio OCT/HClO 1:20; concentration spectroscopically determined at $\lambda_{max}$ of 292 nm, $\varepsilon = 350$ $dm^3$/mol cm) was added drop by drop to this solution under magnetic stirring at room temperature. The reaction was stopped after 2 h with an excess of sodium thiosulphate and concentrated by lyophilisation. The residue was dissolved in water and pH-adjusted to 5.0, and this solution was extracted using methylene chloride. The crude organic fraction (835 mg) was chromatographed on silica gel CC, eluted with a gradient of chloroform:methanol (99:1 to 10:90, v/v) to yield 9 fractions. The fraction Fr. 2 (62 mg), eluted with chloroform:methanol (97:3), was chromatographed on silica gel CC, eluted with a gradient of petroleum ether:acetone (98:2 to 90:10, v/v) to yield **DP1** (27 mg). The fraction Fr. 4 (49 mg), eluted with chloroform:methanol (90:10), was chromatographed on silica gel CC, eluted with a gradient of petroleum ether:acetone (90:10 to 50:50, v/v) to yield **DP2** (29 mg). The fraction Fr. 7 (58 mg), eluted with chloroform:methanol (60:40), was separated by semipreparative HPLC using a reversed-phase column Phenomenex Gemini 10 µm 110 Å C18 (250 × 21.20 mm) and eluted with a gradient of $CH_3COONH_4$ (A, pH 4.0; 10 mM) and methanol (B), starting with 30% B for 5 min and followed by the installation of a gradient to obtain 100% B over 30 min, at a solvent flow rate of 8 mL/min to yield **DP3** (7 mg) and **DP4** (3 mg). The fraction Fr. 8 (405 mg), eluted with chloroform:methanol (80:20), was chromatographed on silica gel CC, eluted with a gradient of methylene chloride:methanol (90:10 to 0:100, v/v) to yield 9 fractions.

The fraction Fr. 8.2 (61 mg), eluted with methylene chloride:methanol (90:10), was chromatographed on TLC, eluted with chloroform:methanol (80:20), to yield **DP5** (47 mg). The fraction Fr. 8.4 (131 mg), eluted with methylene chloride:methanol

(80:20), was chromatographed on TLC, eluted with chloroform:methanol (70:30), to yield **DP9** (89 mg). The fraction Fr. 8.6 (43 mg), eluted with methylene chloride:methanol (65:35), was separated by analytical HPLC using a reversed-phase column Phenomenex Gemini 10 µm 110 Å C18 (250 × 21.20 mm) and eluted with a gradient of $CH_3COONH_4$ (A, pH 4.0; 10 mM) and methanol (B), starting with 30% B for 5 min and followed by the installation of a gradient to obtain 100% B over 30 min, and eluted again with the same mixture for another 10 min, at a solvent flow rate of 8 mL/min to yield **DP8** (20 mg). The fraction Fr. 8.8 (53 mg), eluted with methylene chloride:methanol (60:40), was chromatographed on TLC and eluted with petroleum ether:acetone (65:35), to yield **DP7** (20 mg).

The fraction Fr. 9 (31 mg), eluted with chloroform:methanol (90:10), was separated by analytical HPLC using a reversed-phase column Phenomenex Kromasil 10 µm 100 Å C18 (250 × 10.00 mm) and eluted with a gradient of $CH_3COONH_4$ (A, pH 4.0; 10 mM) and acetonitrile (B), starting with 20% B for 5 min and followed by the installation of a gradient to obtain 100% B over 30 min, at a solvent flow rate of 4 mL/min to give 3 fractions. The fraction 9.1 was purified by HPLC using a column Discovery RP-amide C16 (150 × 4.6 mm), 5 µm, and eluted with 0.1% TFA in acetonitrile:water (25:75), at a solvent flow rate of 0.8 mL/min to give **DP11** (2 mg). The fractions Fr. 9.2 and Fr. 9.3 were identified as **DP6** (5 mg) and **DP10** (2 mg), respectively.

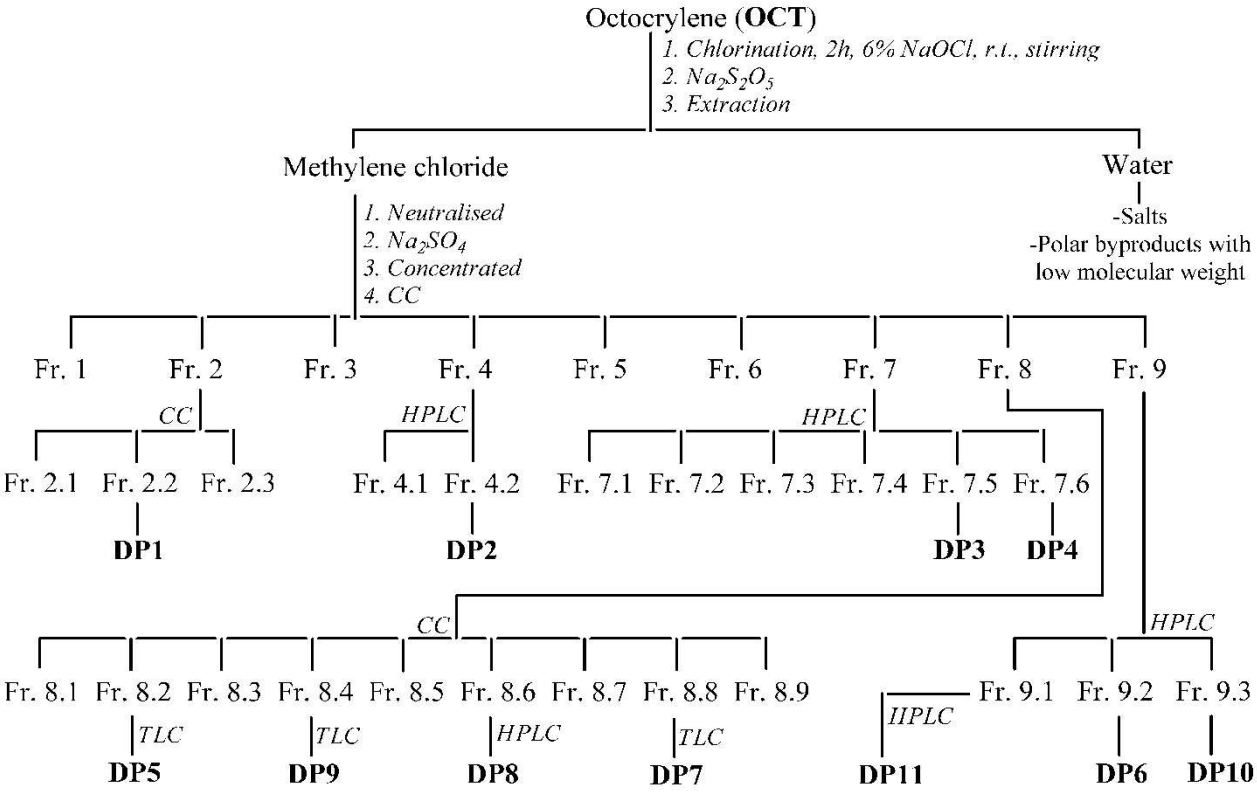


**Figure 17:** The isolation of all identified compounds (DP1–DP11).

## 4.5 Results and discussion

### 4.5.1 Chlorination Experiments

The OCT chlorination experiments were performed in the concentrations in which this micropollutant was detected in swimming pool water [116], of approximately $10^{-5}$ M. Specifically, the solutions of the sunscreen were treated for 10 min with 10% hypochlorite (OCT: hypochlorite molar ratio of 2:1; concn.), under magnetic stirring and at room temperature. Then, the tests were repeated at much higher concentrations of the contaminant (>$10^{-3}$ M), with a much lower ratio of OCT: oxidizing agent (1:20), in order to have sufficiently high quantities of by-products isolated to proceed with the structural identification.

The course of the reaction was monitored by HPLC, and the DPs obtained were isolated according to Figure 17, using column chromatography and HPLC and completely characterized using NMR and MS analyses. Finally, **DP1**–**DP11** were isolated at percentages of 1.12, 2.97, 0.89, 0.91, 1.15, 2.36, 1.08, 1.55, 6.39, 0.59,

and 1.19, respectively. The proposed mechanism of their formation from OCT is shown in Figure 18, and **DP3**–**DP5** and **DP7**–**DP9** were isolated for the first time.

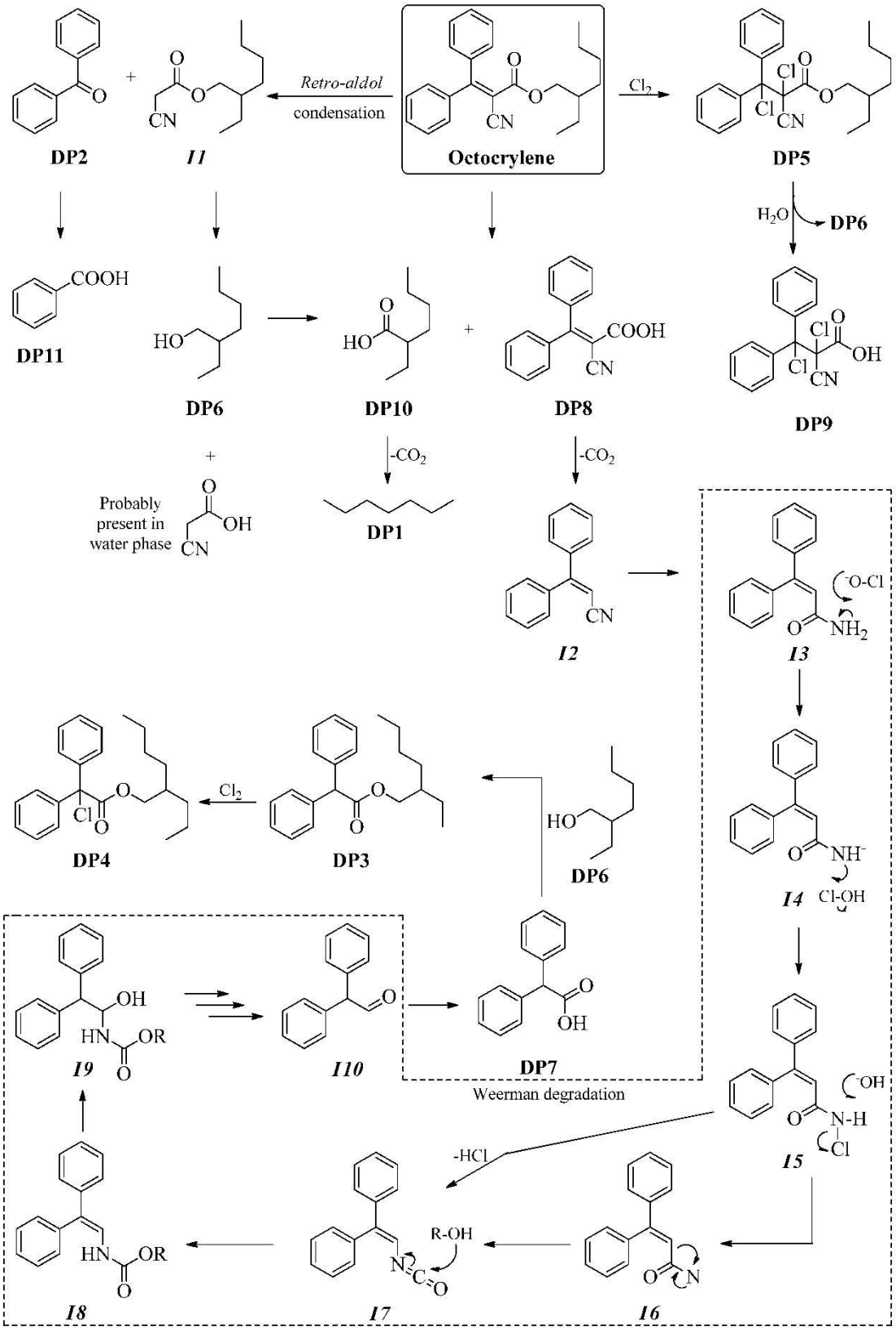


**Figure 18:** Plausible mechanism for the formation of DP1-DP11.

### 4.5.2 Structural Elucidation

In the OCT treatment, the concentration of **DP1**–**DP11** reached its maximum after about 2 h, with a degradation of 15% and a transformation of approximately 20%; percentages of by-products ranged from 0.59% for **DP10** to 6.39% for **DP9**. In a basic environment, OCT can undergo a retro-aldol condensation, which leads to the formation of intermediate *I1* and the by-product **DP2**. From this and other by-products, it is usually possible to obtain the by-product **DP11**; the intermediate *I1*, identifiable with 2-ethylhexyl cyanoacetate, can undergo hydrolysis of the ester bond and lead to the formation of the by-product **DP10** and α-cyanoacetic acid, probably contained in the aqueous phase rich in salts and low-molecular-weight compounds. Finally, the **DP10** could decarboxylate to the **DP1** by-product. The by-product **DP10** is also obtained from the hydrolysis of the ester bond of the starting product, together with the by-product **DP8**. The latter, by decarboxylation, could provide the intermediate *I2*, which, by the hydrolysis of the cyano group, provides the intermediate *I3*. Considering the degradation reaction of OCT in the presence of sodium hypochlorite, it can be assumed that a Weerman degradation takes place that leads to the formation of nitrene *I6*, through the deprotonation (*I4*) and chlorination (*I5*) of the amide nitrogen of the intermediate *I3*.

The transposition of nitrene *I6*, or more probably the elimination of HCl from the intermediate *I5* with the concomitant transposition of the residue bound to the carbonyl, allows for the obtainment of the isocyanate *I7*, from which alcoholises of the intermediate *I8* are obtained, from which, for the subsequent oxidation, the intermediate *I9* is obtained. The hydrolysis of the latter and the subsequent oxidation of the intermediate *I10* obtained provides the by-product **DP7**. This can react with the **DP6** present in the solution and provide the by-product **DP3** and, for subsequent chlorination, create the by-product **DP4**. The direct chlorination to the C-2/C-3 carbons of the starting product allows for and explains the obtainment of the by-product **DP5**, from which **DP9** and **DP6** are obtained by the hydrolysis of the ester bond.

### 4.5.3 Ecotoxicity results

Octocrylene has a relatively high environmental stability in aquatic environments and is hardly removed from wastewater treatment plants [130], [131]. Previous studies showed that OCT was poorly removed from wastewater treatment plants (0–10% degradation in aerobic conditions) [132].

Toxicity data were reported in Figure 19A–C for *P. tricornutum*, *B. plicatilis* and *A. fischeri*, in that order, considering the effect of OCT and its by-products.

Chronic toxicity with *P. tricornutum* was also identified, as 83% of DPs showed growth inhibition effects ranging between 20% and 50% (OCT, **DP1**, **DP3**, **DP4**, **DP6**, **DP7**, **DP8**, **DP9**, **DP10** and **DP11**). **DP5** has no toxicity, while **DP2** was the most toxic compound (Figure 19A).

The effects of this UV filter and its chlorinated derivates on the acute toxicity of *B. plicatilis* change, probably due to the lower sensibility of the bioindicator. The toxicity has been evaluated by observing the mortality rate of *B. plicatilis* after 24 h of exposure. As reported in Figure 19B, no significant effect on mortality was observed in rotifers exposed to OCT and its degradation by-products. In fact, all the investigated samples showed a toxicity ranging between 10% and 32%, with the exception of **DP3,** which had a residual toxicity of approximately 47%. In the latter case study, **DP2**, on the other hand, has a toxicity of only 20%, while **DP3** appears to be the most toxic degradation by-product for the aforementioned bioindicator.

The acute toxicity of OCT and its chlorinated derivatives towards *A. fischeri* was shown in Figure 19C. After 30 min of exposure, the bioluminescence inhibition swung between 14% and 90%, except for the parent compound OCT, which was the only compound to exhibit biostimulation behaviour. So, 16% of the tested samples did not exceed 20% of the effect (**DP1** and **DP3**), 33% of the degradation by-products are included in the range between 26% and 33% of the effect (**DP5**, **DP9**, **DP10** and **DP11**), while there was another 33% increase in toxicity up to 60% of the effect (**DP4**, **DP6**, **DP7** and **DP8**). **DP2** (90% of the effect), once again, appears to be the most toxic product. The toxicity trend observed in *A. fischeri* is in good agreement with our previous results on *P. tricornutum*.

The discharge into the marine environment of chlorinated sewage effluents containing these degradation by-products represents the worst-case scenario for environmental safety, indeed these by-products could have negatively influenced the physiology of single-celled organisms such as *A. fischeri* and *P. tricornutum*, but they

did not affect rotifers. This research highlighted the concerns and the potential risks from OCT by-products that may emerge and impact the quality of the marine ecosystem, especially concerning uncontrolled doses.

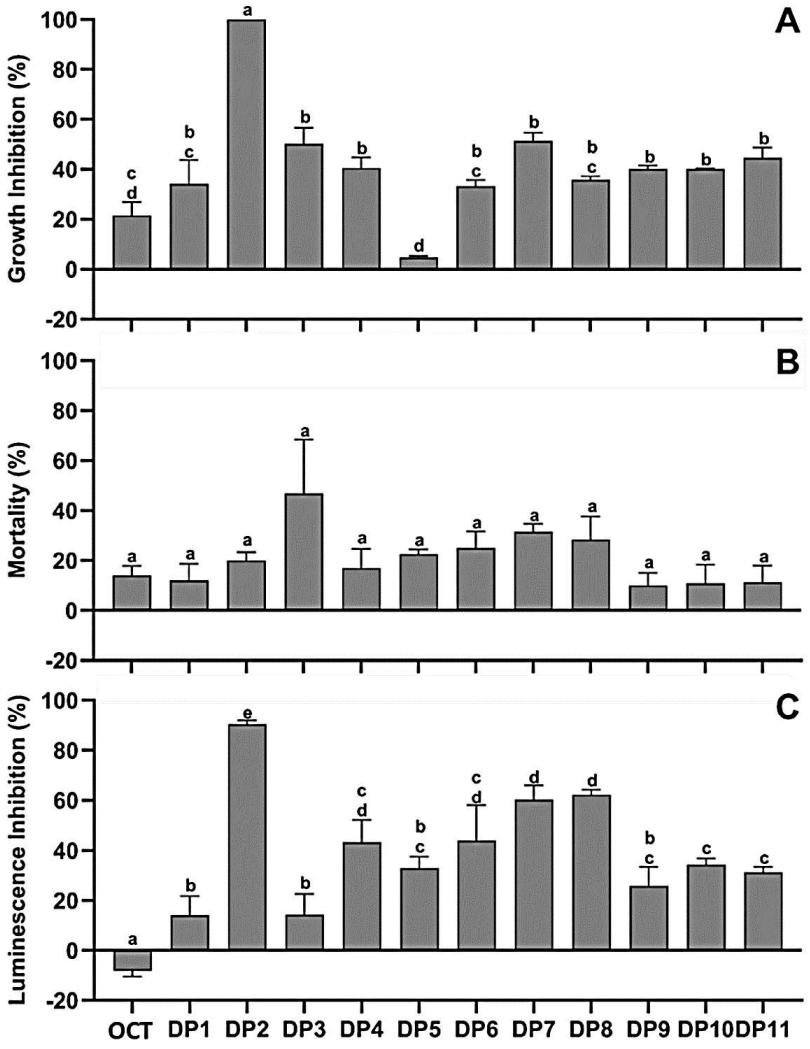


**Figure 19:** Toxicity data regarding exposure of *P. tricornutum* (**A**), B. *plicatilis* (**B**) and *A. fischeri* (**C**) to OCT and its by-products (**DP1**-**DP11**). Data with different letters (a–d) are significantly different (*Tukey post hoc, $p < 0.05$*).

## 4.6 Conclusions

This research investigated the fate, following degradation treatment by chlorination, of one of the most widely used sunscreens, namely, octocrylene, conventionally considered an emerging micropollutant. The reaction was carried out by simulating the disinfection treatment employed in swimming pool waters, using excess sodium hypochlorite. After the chlorination treatment, chromatographic techniques were used to isolate eleven degradation by-products, which were fully characterized by MS and NMR analyses and via comparison with a commercial standard. Four of them were isolated for the first time. Compared to the initial quantity considered, OCT was recovered unchanged for 45% and transformed into the corresponding by-products for 20%. A possible mechanism for the degradation of OCT and its degradation by-products has been hypothesized. Half of the investigated DPs possessed anywhere from slightly to highly toxic effects. Thus, acute toxicity evaluation demonstrated that the presence of OCT in the water distribution system might pose a more significant threat to safety and quality of the water and the environment. In fact, if on the one hand the disinfection process involves the partial degradation of OCT, it is also true, however, that it involves the formation of degradation by-products, which are in some cases even more toxic than the starting product.

# CHAPTER 5

In this chapter, the results based on original contributions published in [133], [105] and submitted in ELSEVIER (*Journal of Pharmaceutical and Biomedical Analysis*) and MDPI (*applied sciences*) are presented.

## 5.1 The issue of antibiotics in the environment

The presence of pharmaceutical compounds in natural water bodies, even at low concentrations, raises health concerns. Pharmaceutical substances, used to prevent and fight diseases, are produced to guarantee their maximum effectiveness and, at the same time, ensure their resistance to inactivation until they perform their intended functions. Thus, these compounds can be excreted through feces and urine in the form of metabolite mixtures and their unchanged product, which flow into wastewater treatment plants (WWTPs). The recent widespread detection of these compounds in such environments [26], [134], [135], [136], [80], [137] have led to their designation as emerging contaminants, as they are still unregulated. The environmental persistence and high biological activity that characterizes them make these substances harmful, even at low concentrations. These contaminants can, in fact, cause alterations to the endocrine system [126] and an increase in microbial resistance to drugs [138], [139], [140], [141]. They can also be adsorbed by plants [142] and bioaccumulated [125] in the food chain. Additional risks are associated with biodiversity loss [126], infertility, and cancer [143], [144].

One of the categories of drugs on which the attention of the scientific community is most focused is that of antibiotics present in the aquatic environment and in foods, which have the possibility of inducing the formation of antibiotic-resistant bacteria and the health risks that may derive from them [145], [146].

Kovalakova *et al.* [147] report that the most frequently used antibiotics were broad-spectrum penicillins (39% of total DDDs in 2015) [148]. In European countries is the consumption ranging from 36% (Germany) to 71% (Slovenia), followed by macrolides from 5% (Sweden) to 25% (Slovakia), β-lactams from 0.2% (Denmark) to 22% (Germany), and quinolones from 2% (United Kingdom) to 16% (Hungary) [149], [150]. Penicillins were also the most prescribed antibiotics in the USA in 2010

(38%), followed by β-lactams (16%), tetracyclines (15%), macrolides (12%), quinolones (9%), and trimethoprim (10%) [151]. However, in India, penicillins were the third most commonly prescribed antibiotics in 2008 (28%), after quinolones (34%) and cephalosporins (32%), followed by macrolides (14%) and tetracyclines (6%) [152]. A similar trend was also found in China and Thailand [151].

In this chapter, the environmental fate of two antibiotics and their disinfection by-products is discussed. These are commonly used pharmaceutical products which include Diclofenac, a non-steroidal anti-inflammatory drug (NSAID), and Amoxicillin, a penicillin-like antibiotic.

## 5.2 Materials and Methods

### 5.2.1 Reagents and chemicals

Diclofenac (99.3 %) and Amoxicillin (99.5%) were purchased from Sigma Aldrich (Milan, Italy). All the other chemicals and solvents were purchased from Fluka (Saint-Quentin Fallavier, France) at HPLC grade and were used as received. The reagents and other required test solutions (including dilution water and reconstitution water) for ecotoxicity assays were purchased from Ecotox LDS s.r.l. (Milan, Italy). For the antimicrobial assessment, Tryptic Soy Broth (TSB, Difco, Becton-Dickenson Labs) was used. Double distilled water (Microtech) was used to prepare the dilution water and treatments. The microbial growth was measured with automatic plate reader (Synergy HTX, BioTek Instruments, Winooski, VT, USA).

### 5.2.2 Toxicity tests

The acute bioluminescence assay was conducted in accordance with the standard protocol ISO 11348-3 [86]. The experiments used *Aliivibrio fischeri* (NRRLB-11177) bacteria that were liquid dried and frozen at -20 °C. Toxicity tests are carried out on *A. fischeri* being a consolidated biological model that in included in most regulation for wastewater assessment on an end-of-pipe basis. The battery of toxicity tests proposed in the paper is of widespread use also for drugs detection. *A. fischeri* bioluminescence inhibition observed in the presence of pharmaceuticals was measured after different treatment durations (5, 15 and 30 min). All tests were performed in triplicate. To provide the relevant osmotic pressure for test organisms, the salinity concentration of the stock solution was adjusted by 2 % for NaCl. The

temperature during exposure was 15 °C according to the Microtox standard procedure. For the final analysis, only the data from the 30 min exposure were reported due to the negligible difference in toxicity between results from different exposure durations. The toxic effect values reflect the ratio of the decrease in bacterial light production to the remaining light. An algal growth-inhibition test was performed according to the European standard EN ISO 8692 [85] using *Raphidocelis subcapitata*, formerly known as *Selenastrum capricornutum* or *Pseudokirchneriella subcapitata*. The following salts were used for the preparation of algal medium: $CaCl_2 \cdot 2H_2O$ (18 mg $L^{-1}$), $MgSO_4 \cdot 7H_2O$ (15 mg $L^{-1}$), $NH_4Cl$ (15 mg $L^{-1}$), $MgCl_2 \cdot 6H_2O$ (12 mg $L^{-1}$), $KH_2PO_4$ (1.6 mg $L^{-1}$), $FeCl_3 \cdot 6H_2O$ (0.08 mg $L^{-1}$), $Na_2EDTA \cdot 2H_2O$ (0.1 mg $L^{-1}$), $H_3BO_3$ (0.185 mg $L^{-1}$), $MnCl_2 \cdot 4H_2O$ (0.415 mg $L^{-1}$), $ZnCl_2$ (0.003 mg$L^{-1}$), $CoCl_2 \cdot 6H_2O$ (0.0015 mg $L^{-1}$), $Na_2MoO_4 \cdot 2H_2O$ (0.007 mg $L^{-1}$), $CuCl_2 \cdot 2H_2O$ (0.00001 mg $L^{-1}$). ISO artificial freshwater (ISO, 2012; ISO, 2013), containing $CaCl_2 \cdot 2H_2O$ (294 mg $L^{-1}$), $MgSO_4 \cdot 7H_2O$ (123.25 mg $L^{-1}$), $NaHCO_3$ (64.75 mg $L^{-1}$), and KCl (5.75 mg $L^{-1}$), was used for the preparation of cladoceran tests and for the control medium. The growth of algae exposed to the sample was compared with the growth of algae in a negative control. For each sample, six replicates were inoculated with $10^7$ algal cells $L^{-1}$ in well plates and incubated for 72 h at 23 ± 2 °C under continuous illumination (in an irradiance range of 120−60 µein $m^{-2}$ $s^{-1}$). The specific growth rate (µ) of *R. subcapitata* in each replicate was calculated from the logarithmic increase in cell density in the interval from 0 to 72 h as follows:

$$\mu = \frac{ln_{N_i} - ln_{N_0}}{t_i - t_0}$$

where $N_0$ and $N_i$ represent the cell concentration at times $t_0$ and $t_i$ respectively. The results were expressed as the mean (±standard deviation) of the percentage inhibition of cell growth compared to the negative control. *R. subcapitata* density was determined by an indirect procedure using a spectrophotometer (Hach Lange DR5000) and a 1 cm cuvette. The acute toxicity bioassay at 48 h with *D. magna* was conducted according to ISO 6341 [87]. *D. magna* was selected from laboratory stock cultures, were moved to 2.0 L glass beakers maintained at 24 ± 10 °C and were fed on *R. subcapitata*. Newly hatched neonates (less than 24 h old) obtained from the continuous laboratory culture were used (20 organisms for each tested concentration

and control). The total duration of the exposure was 48 h. Immobilized organisms were counted, and the results were expressed as the percentage of control. The test was considered valid if the immobilization in the control did not exceed 10 %. *D. magna* viability and mobility were observed with a stereomicroscope (LEICA EZ4-HD). Ecotoxicity data were expressed as the EC50 (median effect concentration) values, and its 95 % confidence intervals were calculated by non-linear regression. After verification of normality (Shapiro-Wilk test) and homogeneity of variance (F-test), the significance of differences between mean values of experimental treatments and controls was assessed by Student's t-test and analysis of variance (ANOVA) with a 0.05 significance level. When ANOVA revealed significant differences among treatments, post-hoc analyses were carried out with Dunnett's method and Tukey's test. Statistical analyses were performed using GraphPad Prism software. Toxicity data have been integrated according to Persoone *et al.* and Lofrano *et al.* [97], [153]. The hazard classification system based on the percentage of effect and the integrated class weight score (CWS) was determined by averaging the values corresponding to each biotest class.

### 5.2.3 Measurement of Antibiotic Activity

Microbial growth inhibition tests were performed on AMO and samples were isolated from NaOCl experiments at initial concentrations of 5 mg/L and used *E. coli* (ATCC 25922), *K. pneumoniae* (ATCC 20081), and *S. aureus* (ATCC 6538) as reference strains. A preculture of bacteria was grown in tris-buffered solution (TBS) overnight at 37 °C and then diluted with the same medium for a concentration of $10^3$ cell/mL. Bacteria were inoculated into 96 wells with samples and incubated at 37 °C for 24 h. The growth of bacteria was evaluated by the degree of turbidity of the culture measuring the absorbance at 600 nm. Negative and positive controls were included in each test. Negative tests were carried out on TBS, containing 0.001% of DMSO (used with the aim of dissolving AMO) per liter of solution.

## 5.3 Diclofenac: Identification of Degradation Products and Ecotoxicological Assessment

Diclofenac (DCF) is the most widely prescribed non-steroidal anti-inflammatory drug (NSAID) in the world [154], [155] and it is used in the treatment of both musculoskeletal and systemic inflammatory states. Since its introduction in 1973 [156], numerous new drugs containing DCF [157] have been approved and are available in numerous pharmaceutical formulations, suitable for different routes of administration and with analgesic, antipyretic and inflammatory actions.

It's used in the veterinary field too, but it was banned in several South Asian countries [158] because its traces in cattle carcasses are lethal to vultures and eagles that eat them [159], [160].

DCF ranks 13th among the best-selling generic drugs (Voltaren; Torsilax; Diclofenac). It is included in the list of emergency drugs in over 74 countries, had a total production of over 877 t in 2007 [161], and has a total estimated revenue of more than 1.60 billion dollars and an annual sales growth rate of more than 15 % [162]. Yearly DCF consumption has been reported to vary between 195 and 940 mg per inhabitant in different countries [163], [164], [165]. It was detected up to 10 ng $L^{-1}$ in drinking water [161], [166], while in surface waters ranged between 100 and 500 ng $L^{-1}$ with values up to 1200 ng $L^{-1}$ in some German rivers and up to 8500 ng $L^{-1}$ in some Pakistani rivers [167], [168]. In groundwater, the detected limits are considerably lower and are below the limits of instrumental detectability, although there are certainly exceptions such as 380 ng $L^{-1}$ measured in the underground waters of Barcelona or some German locations [169]. In municipal wastewaters, concentrations between 0.44 and 7.1 μg $L^{-1}$ were detected, with mean values between 0.11 and 2.3 μg $L^{-1}$. The highest concentrations were measured in hospital (6.88 μg $L^{-1}$) and pharmaceutical manufacturers (> 203 μg $L^{-1}$) wastewater. In municipal wastewater treatment plants (WWTP) effluents, DCF is among the most frequently detected drugs with concentrations between 800 and 1600 ng $L^{-1}$ [161]. Its percentage of removal oscillates between 0% is absorbed by the ecosystem and the rest ends up in the oceans.

In this research, the pathway of DCF was investigated after chlorination, one of the processes normally used in WWTP for disinfection [63], [89], [103], carrying out two different experiments, one at a concentration similar to that at which the DCF

was detected in the environment and one at least 100 times higher concentration in order to isolate and identify the degradation by-products (DPs).

Normally the disinfection processes both in laboratory-scale studies and in full-scale applications are studied only in relation to the abatement of the bacterial load and the amount of emerging pollutant considered. The risk is that the pollutant present is not mineralized but only transformed into a series of products that are in turn more recalcitrant to degradation and even more toxic than the pollutant from which they derive. In this frame, it is interesting identify the degradation by-products formed during the chlorination process and outline their ecotoxicological profile.

Indeed, the structures of 14 isolated DPs, of which nine are new, have been determined from combining mass spectrometry (MS) and nuclear magnetic resonance (NMR) data and justified by a proposed mechanism of formation starting from the parent drug. Ecotoxicological bioassays with *Daphnia magna* were used to provide information about the potential residual toxicity effects and to compare degradation by-products to the parent compound.

### 5.3.1 Chlorination reaction

### 5.3.2 Apparatus and Equipment

Column chromatography (CC) was carried out with Kieselgel 60 (230–400 mesh, Merck, Darmstadt, Germany). HPLC was performed on a Shimadzu LC-8A system using a Shimadzu SPD-10A VP UV-VIS detector (Shimadzu, Milan, Italy). Semipreparative HPLC was performed using an RP Gemini C18-110A preparative column (10 μm particle size, 250 mm × 21.2 mm i.d., Phenomenex, Bologna, Italy) with a flow rate of 7 mL $min^{-1}$. The $^{1}H$- and $^{13}C$ NMR spectra were recorded with a NMR spectrometer, operated at 400 MHz and at 25 °C (Bruker DRX, Bruker Avance) and referenced in ppm to the residual solvent signals ($CDCl_3$, at $\delta_H$ 7.27 and $\delta_C$ 77.0). The proton-detected heteronuclear correlations were measured using a gradient heteronuclear single-quantum coherence (HSQC) experiment, optimized for $^{1}J_{HC}$ = 155 Hz, and a gradient heteronuclear multiple bond coherence (HMBC) experiment, optimized for $^{n}J_{HC}$ = 8 Hz. The MALDI-TOF mass spectrometric analyses were performed on a Voyager-De Pro MALDI mass spectrometer (PerSeptive Biosystems, Framingham, MA, USA). The UV/Vis spectra were recorded with a Perkin Elmer

Lambda 7 spectrophotometer. The IR spectra were recorded with a Jasco FT/IR-430 instrument equipped with a single reflection ATR accessory.

## 5.4 Chlorination Procedure and Product Isolation: Diclofenac

The $10^{-3}$ M solution of DCF after chlorination was quenched with excess sodium sulfite, neutralized with HCl 0.5 N and extracted with ethyl acetate (Figure 20). The organic fraction (1067 mg) was fractionated into acidic and neutral fractions with aqueous NaOH 0.5 N. The organic alkaline layer was neutralized, dried with $Na_2SO_4$ and concentrated under vacuum. The crude neutral residue (750 mg) was chromatographed on silica gel with a gradient of dichloromethane:methanol (99:1 to 80:20), to give 11 fractions. The 3rd fraction (75 mg), eluted with dichloromethane:methanol (99:1), was purified by HPLC using a reversed phase column and eluting with a gradient of $CH_3COONH_4$, pH 4, 10 mM, and $CH_3OH$ (15:85 for 5 min; 15:85 to 0:100 in 15 min; 0:100 for 10 min) to give DP1 (5 mg), DP2 (13 mg), DP6 (3 mg) and DP7 (7 mg). The 4th fraction (83 mg), eluted with dichloromethane:methanol (99:1), was purified by HPLC using a reversed phase column and eluting with a gradient of $CH_3COONH_4$, pH 4, 10 mM, and $CH_3OH$ (15:85 for 5 min; 15:85 to 0:100 in 15 min; 0:100 for 10 min) to give DP3 (17 mg), DP9 (4 mg) and DP13 (5 mg).

The aqueous layer was neutralized with HCl 0.5 N and extracted with ethyl acetate. It was dried with $Na_2SO_4$, concentrated under vacuum (287 mg), and chromatographed on silica gel with a gradient of chloroform: methanol (99:1 to 80:20) to give 10 fractions. The 1st fraction (36 mg), eluted with chloroform:methanol (97:3), was purified by HPLC using a reversed phase column and eluting with a gradient of $CH_3COONH_4$, pH 4, 10 mM, and $CH_3OH$ (10:90 for 5 min; 10:90 to 0:100 in 20 min; 0:100 for 10 min) to give DP4 (17 mg) and DP5 (11 mg). The 2nd fraction (24 mg), eluted with dichloromethane:methanol (80:20), was purified by HPLC using a reversed phase column and eluting with a gradient of $CH_3COONH_4$, pH 4, 10 mM, and $CH_3OH$ (25:75 for 5 min; 25:75 to 0:100 in 30 min; 0:100 for 10 min) to give DP8 (10 mg) and DP10 (4 mg). The 4th fraction (41 mg), eluted with dichloromethane:methanol (80:20), was purified by HPLC using a reversed phase column and eluting with a gradient of $CH_3COONH_4$, pH 4, 10 mM,

and $CH_3OH$ (15:85 for 5 min; 15:85 to 0:100 in 15 min; 0:100 for 10 min) to give DP11 (5 mg), DP12 (7 mg) and DP14 (5 mg).

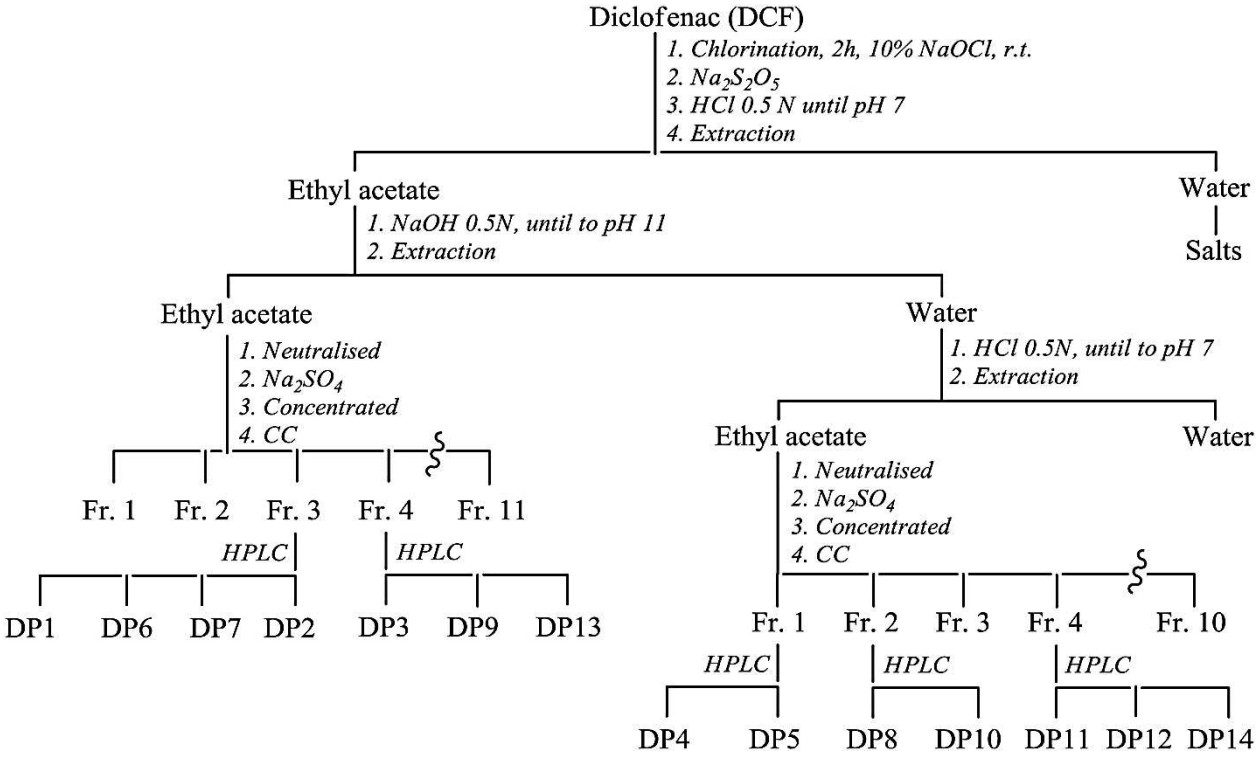


**Figure 20:** The isolation of all identified compounds (DP1–DP14).

## 5.5 Results and discussion

### 5.5.1 Chlorination Experiments

A $10^{-5}$ M solution of DCF was treated for 2 h with 10 % hypochlorite (molar ratio DCF:hypochlorite 1:1. The chlorine concentration was spectroscopically determined $\lambda_{max}$ 292 nm, ε 350 $dm^3$ $mol^{-1}$ cm) at room temperature [88, 102], simulating a chlorination process. The pH of the solution, measured by a pH meter at 10 min intervals, rose from the initial pH 8.5–9.0 after 10 min, and it remained at this value through the duration of the reaction. An aliquot of the solution was taken every 10 min, quenched by sodium sulfite excess: $Na_2SO_3 + Cl_2 \rightarrow 2NaCl + SO_3^{2-}$, filtered and fractionated into acidic and neutral fractions. The course of the reaction was monitored by HPLC. The main degradation by-products (DP1 – DP3, DP6 – DP7, DP9 and DP13 for the neutral fraction and DP4 – DP5, DP8, DP10 – DP12 and DP14 for the acidic fraction) were identified by comparing their retention times with those

of standard compounds commercially available or compounds isolated for the first time. The latter were obtained by performing preparative experiments with a solution of DCF at a concentration higher than $10^{-3}$ M treated with 12 % hypochlorite at room temperature. The degradation by-products obtained were isolated by column chromatography and HPLC and completely characterized using NMR and MS analysis. DP1 – DP14 were isolated in relative % of 1.68, 4.39, 5.74, 5.74, 3.71, 1.01, 3.38, 1.35, 2.36, 1.35, 1.68, 2.36, 1.68 and 2.36, respectively. The proposed mechanism of their formation and isolation from the DCF is shown in Figure 21 and Figure 22.

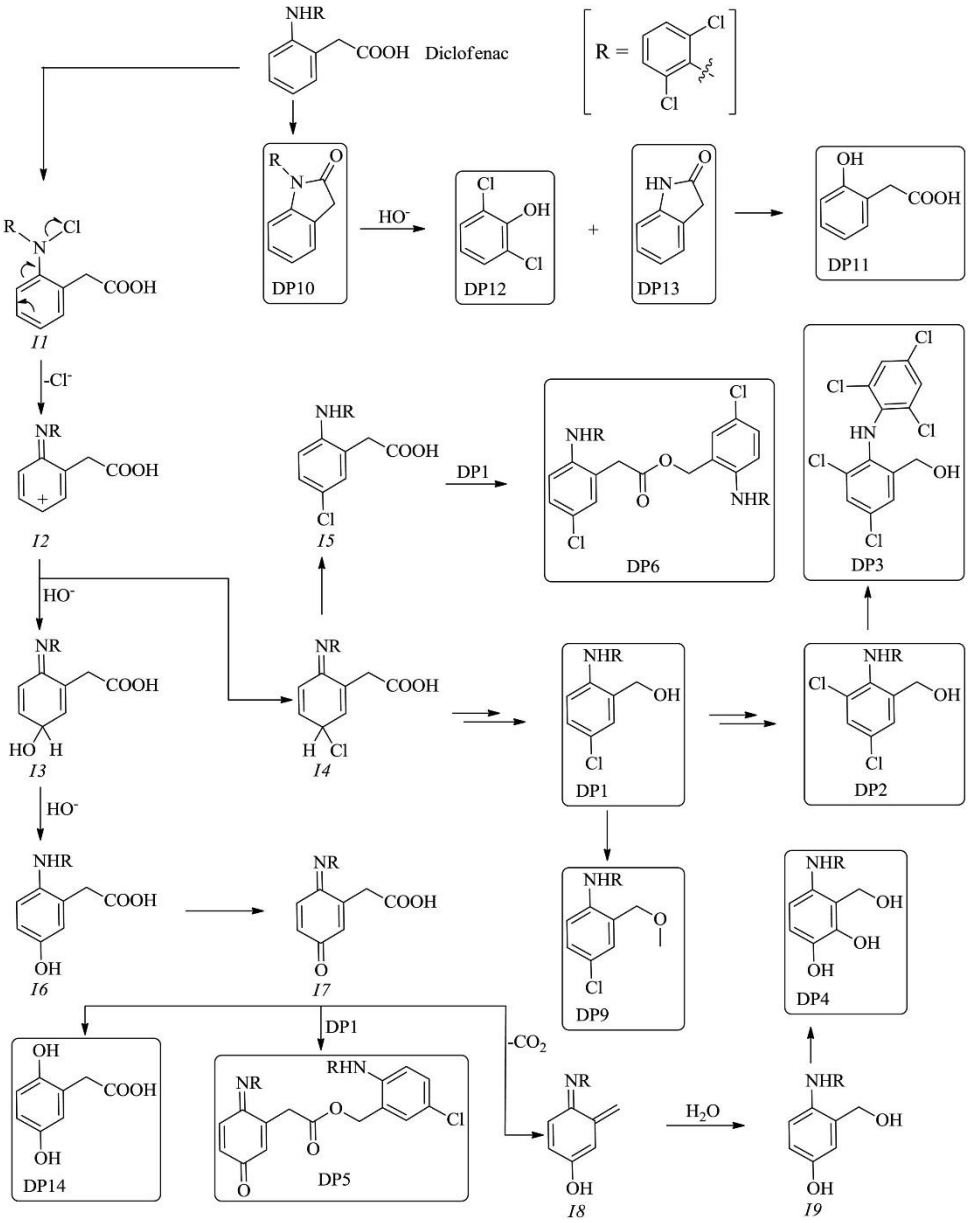


**Figure 21:** Plausible mechanism for the formation of DP1 – DP6 and DP9 – DP14. Boxed structures represent isolated by-products.

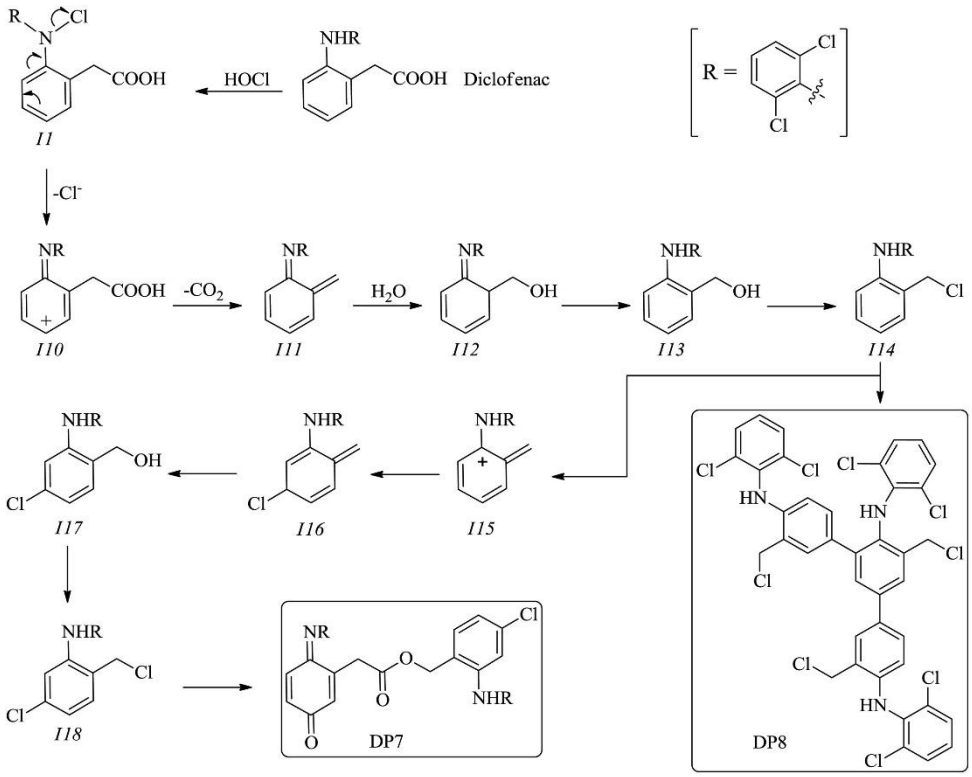


**Figure 22:** Plausible mechanism for the formation of DP7 and DP8. Boxed structures represent isolated by-products.

## 5.5.2 Structural Elucidation

The first four degradation by-products are DCF chloro-derivatives which have undergone oxidative decarboxylation of the side chain.

DP1/5-Chloro-2-[(2,6-dichlorophenyl)aminophenyl]methanol:

the MS-TOF analysis showed a molecular ion peak at *m/z* 301.98 corresponding to molecular formula $C_{13}H_{10}Cl_3NO$. In the $^1H$ NMR spectrum, six signals were present, of which five related to aromatic protons at 7.40, 7.22, 7.13, 7.09 and 6.39 ppm and one to the methylene $CH_2$-8 at 4.83 ppm. These signals correlated to the carbons in the HSQC spectrum at 128.91, 128.48, 128.59, 125.29, 116.63 and 64.18 ppm, respectively. In addition to the signals of protonated carbons, the $^{13}C$ NMR spectrum showed five quaternary carbon signals at 141.78, 128.80, 124.94, 136.53 and 130.92 ppm. HMBC experiments allowed the assignment of the first three signals to the carbons C-2, C-3 and C-5, respectively, of the ring A 1,2,4-trisubstituted, while the last two signals were attributed to the carbons C-1′ and C-2′/C-6′ of the ring B 1,2,3-trisubstituted.

DP2/3,5-Dichloro-2-[(2,6-dichlorophenyl)amino]phenyl)methanol:

the MS-TOF analysis showed a molecular ion peak at *m/z* 337.95 corresponding to molecular formula $C_{13}H_9Cl_4NO$. In the $^1H$ NMR spectrum, only five signals were present. Four were related to aromatic protons at 7.33, 7.30, 7.27 and 6.90 ppm and one to the methylene $CH_2$-8 at 4.64 ppm, and they correlated to the carbons in the HSQC spectrum at 129.05, 129.79, 128.67, 122.67 and 63.07 ppm, respectively.

In addition to the signals of the protonated carbons, the $^{13}C$ NMR spectrum showed six quaternary carbon signals at 136.85, 136.56, 126.49, 129.06, 137.56 and 126.81 ppm. HMBC experiments related the first four signals to the carbons C-2, C-3, C-5 and C-7, respectively, of the ring A 1,2,3,5-tetrasubstituted, while the last two signals were attributed to the carbons C-1′ and C-2′/C-6′ of the ring B 1,2,3-trisubstituted.

DP3/3,5-Dichloro-2-[(2,4,6-trichlorophenyl)amino)phenyl]methanol:

the MS-TOF analysis showed a molecular ion peak at *m/z* 371.91 corresponding to molecular formula $C_{13}H_8Cl_5NO$. In the $^1H$ NMR spectrum, only three signals were present. Two were related to aromatic protons at 7.32 and 7.29 ppm, and one to the methylene $CH_2$-8 at 4.66 ppm. The first signal in the HSQC spectrum was correlated to the carbon at 129.21 ppm, the second, of area three, was correlated to the carbons a 128.41 (x2) and 126.76 ppm, and the last one to the carbon a 63.23 ppm. In addition to the signals of the protonated carbons, the $^{13}C$ NMR spectrum showed seven quaternary carbon signals at 136.53, 136.32, 128.94, 128.96, 136.65, 126.93 and 126.76 ppm. HMBC experiments allowed the assignment of the first four signals to the carbons C-2, C-3, C-5 and C-7, respectively, of the ring A 1,2,3,5-tetrasubstituted, while the last three were attributed to the carbons C-1′, C-2′/C-6′ and C-4′ of the ring B 1,2,3,5-tetrasubstituted.

DP4/3-Hydroxymethyl-4-[(2,4,6-trichlorophenyl)amino]benzene-1,2-diol:

the MS-TOF analysis showed a molecular ion peak at *m/z* 334.96 corresponding to molecular formula $C_{13}H_{10}Cl_3NO_3$. Only four signals were present in the $^1H$ NMR spectrum; three of them were related to aromatic protons at 7.27, 6.79 and 6.51 ppm, and one at the methylene $CH_2$-8 at 5.09 ppm. They correlated to the carbons in the HSQC spectrum at 128.90, 115.60, 120.70 and 60.50 ppm, respectively. In addition to the signals of the protonated carbons, the $^{13}C$ NMR spectrum showed six quaternary carbon signals at 133.83, 116.74, 136.98, 152.43, 137.54 and 129.25 ppm. HMBC experiments allowed the assignment of the first four signals at ring A 1,2,3,4-tetrasubstituted which were respectively identified as the carbons C-2, C-3, C-4 and

C-5; the last two signals were attributed to the carbons C-1′ and C-2′/C-6′ of the ring B 1,2,3-trisubstituted.

DP5/(*E*)-5-chloro-2-((2,6-dichlorophenyl)amino)benzyl-2-(6-((2,6-dichlorophenyl)imino)-3-oxocyclo hexa-1,4-dien-1-yl)acetate:

the MS-TOF analysis showed a molecular ion peak at *m*/*z* 594.89 corresponding to molecular formula $C_{27}H_{17}Cl_5N_2O_3$. In the $^1$H NMR spectrum, 12 signals were present, 10 of which were related to aromatic protons at 7.31, 7.30, 7.22, 7.10, 7.01, 6.93, 6.72, 6.63, 6.49 and 6.28 ppm. The other two were related to methylenes $CH_2$-8 and $CH_2$-8″, of which the second linked to an oxygen at 3.82 and 5.28 ppm. These signals were correlated to the carbons in the HSQC spectrum at 128.92, 130.63, 128.18, 129.33, 125.36, 125.84, 133.80, 128.81, 133.49, 117.06, 37.80 and 65.48 ppm, respectively. In addition to the signals of the protonated carbons, the $^{13}$C NMR spectrum showed 11 quaternary carbon signals at 160.18, 144.45, 186.75, 143.55, 124.01 (x2), 141.98, 125.43, 124.36, 136.34, 129.33 (x2) and 169.63 ppm. HMBC experiments allowed for identification and definition of four aromatic rings, including two 1,2,3-trisubstituted and two 1,2,4-trisubstituted. One of the latter two was oxidized to *p*-quinone and an ester in which the acidic part was a residue of DCF oxidized at C-4 and the corresponding alcoholic part a residue of DCF chlorinated at C-4 and decarboxylated on the side chain.

DP6/5-chloro-2-((2,6-dichlorophenyl)amino)benzyl2-(5-chloro-2-((2,6-dichlorophenyl)amino)phenyl) acetate:

the MS-TOF analysis showed a molecular ion peak at *m*/*z* 615.61 corresponding to molecular formula $C_{27}H_{18}Cl_6N_2O_2$. In the $^1$H NMR spectrum, 12 signals were present, 10 of which related to aromatic protons at 7.37, 7.35, 7.33, 7.23, 7.15, 7.10, 7.07, 7.04, 6.48 and 6.41 ppm. The other two related to methylenes $CH_2$-8 and $CH_2$-8″, of which the second linked to an oxygen, at 3.87 and 5.32 ppm. These signals were correlated to the carbons in the HSQC spectrum at 128.96, 128.12, 128.89, 129.52, 130.53, 130.95, 117.91, 119.70, 124.42, 125.31, 38.38 and 53.41 ppm, respectively. In addition to the signals of the protonated carbons, the $^{13}$C NMR spectrum showed 11 quaternary carbon signals at 130.70, 126.94, 125.98, 136.38, 137.37, 141.49, 141.59, 125.55, 136.38, 137.37 and 170.01 ppm. HMBC experiments allowed for identification and definition of four aromatic rings, including two 1,2,3-trisubstituted and two 1,2,4-trisubstituted. There was also an ester function in which the acidic part was a residue of DCF chlorinated at C-4 and

the corresponding alcoholic part a residue of DCF which was always chlorinated at C-4 but decarboxylated on the side chain.

DP7/4-chloro-2-((2,6-dichlorophenyl)amino)benzyl-2-(5-chloro-2-((2,6-dichlorophenyl)amino)phenyl) acetate:

the MS-TOF analysis showed a molecular ion peak at *m/z* 615.48 corresponding to molecular formula $C_{27}H_{18}Cl_6N_2O_2$. In the $^1$H NMR spectrum, 12 signals were present, 10 of which were related to aromatic protons at 7.37, 7.33, 7.30, 7.19, 7.15, 7.09, 7.04, 6.76, 6.49 and 6.40 ppm. The other two were related to methylenes $CH_2$-8 and $CH_2$-8″, of which the second linked to an oxygen, at 3.88 and 5.28 ppm. These signals were correlated to the carbons in the HSQC spectrum at 129.12, 131.01, 130.59, 128.50, 129.55, 125.49, 125.51, 121.50, 119.70, 117.75, 39.06 and 64.79 ppm, respectively. In addition to the signals of the protonated carbons, the $^{13}$C NMR spectrum showed 11 quaternary carbon signals at 131.24, 125.82, 124.37, 171.51, 138.57, 136.33, 138.52, 141.57, 131.77, 136.33 and 137.65 ppm. HMBC experiments allowed for identification and definition of four aromatic rings, including two 1,2,3-trisubstituted and two 1,2,4-trisubstituted. There was also an ester function in which the acidic part was a residue of DCF chlorinated at C-5 and the corresponding alcoholic part a residue of DCF chlorinated at C-6 but decarboxylated on the side chain.

DP8/3,3″,5′-tris(chloromethyl)-N4,N4′,N4″-tris(2,6-dichlorophenyl)-[1,1′:3′,1″-terphenyl]-4,4′,4″-triamine:

the MS-TOF analysis showed a molecular ion peak at *m/z* 856.29 corresponding to molecular formula $C_{39}H_{26}Cl_9N_3$. The $^1$H NMR spectrum showed the presence of 14 signals, which, through the COSY spectra, were attributed to six different aromatic rings, including three 1,2,3-trisubstituted, two 1,3,4-trisubstituted and one 1,2,3,5-tetrasubstituted. The $^1$H NMR spectrum also shows the presence of three signals relating to three chloromethylene functions. The presence of the three 1,2,3-trisubstituted rings indicated the presence of three residues of DCF, which also underwent an oxidative decarboxylation of the side chain and subsequent chlorination of the hydroxymethyl function.

DP9/4-chloro-*N*-(2,6-dichlorophenyl)-2-(methoxymethyl)aniline:

the MS-TOF analysis showed a molecular ion peak at *m/z* 316.01 corresponding to molecular formula $C_{14}H_{12}Cl_3NO$. In the $^1$H NMR spectrum, seven signals were present, of which five were related to aromatic protons at 7.41, 7.20, 7.13, 7.08 and

6.73 ppm. These correlated to the carbons in the HSQC spectrum at 128.88, 129.62, 128.44, 125.25 and 115.99 ppm. The $^{1}$H NMR spectrum also revealed two signals related to a methoxyl and a methylene function at 3.44 e 4.62 ppm, which correlated to the carbons in the HSQC experiments at 57.55 and 73.31 ppm, respectively. In addition to the signals of the protonated carbons, the $^{13}$C NMR spectrum showed five quaternary carbon signals at 141.79, 125.73, 124.55, 136.45 and 130.94 ppm. HMBC experiments assigned the first three to the aromatic ring A 1,2,4-trisubstituted, which were identified as the C-2, C-3 and C-4 carbons, respectively. The last two were attributed to the carbons C-1′ and C-2′/C-6′ of the ring B 1,2,3-trisubstituted.

DP10-DP14 were identified by the comparison of their spectroscopic data (EI mass spectrum, $^{1}$H- and $^{13}$C NMR spectra) with those of authentic standards.

Miyamoto *et al.* [170] reported that oxidation of DCF by HOCl resulted in formation of the monochloroderivatives to the positions 5 and 7 of ring A and of a generic dichloroderivative. From the hypochlorination of DCF, the formation of a generic monochloroderivative of the decarboxy-DCF was reported [171]. The latter was obtained by oxidative decarboxylation [172], [173]. The structure of mono-, di- and tri-chloroderivatives of decarboxy-DCF as well as three ester derivatives that contain DCF, a carboxy-DCF derivative, and a product with three residues of DCF have been isolated and determined. Soufan *et al.* [174] reported the UV data and masses of a generic decarboxy-DCF monochloride. The latter, once isolated and structurally determined, could undergo an intramolecular cyclization with the formation of the DP10 lactone, which could then undergo saponification with the formation of the by-products DP12 and DP13 and the latter then lead to the by-product DP11. DCF could undergo chlorination on the amino function to obtain the intermediate *I1*, which through a carbocation intermediate could lead to the formation of its structural isomer *I4*, which by oxidative decarboxylation of the side chain would give the by-product DP1. The latter could evolve to its derivative DP9, or first undergo chlorination at ring A to obtain the derivative DP2 and then also to ring B to have its derivative DP3. The coupling reaction of the DP1 with the intermediate *I5* would explain the obtainment of the product DP6. The intermediate *I1*, first by loss of the chloride ion and then by oxidation, could lead to the formation of the intermediate *I7*. The latter could be hydrolyzed to DP14, react with DP1 to form DP5, or undergo an oxidative decarboxylation of the side chain and subsequent oxidation of the ring A to give DP4. The intermediate *I1* could also undergo decarboxylation and subsequent chlorination

to the side chain to obtain the intermediate *I14*, which could give its DP8 trimer or provide its derivative chlorine *I18*, which by reaction with *I7* leads to the formation of DP7.

### 5.5.3 Ecotoxicity Results

Although not entirely clear for most ecological models, DCF is considered a compound that negatively affects non-target organisms belonging to different biological levels [175]. The effects of DCF on *A. fischeri*, *R. subcapitata* and *D. magna* in terms of EC50 are reported in Table 3. Species presented a great range of sensitivities with the following order of magnitude: *D. magna* < *R. subcapitata* < *A. fischeri*. In particular, the EC50 of DCF was estimated as 14.09 mg $L^{-1}$ (10.94 mg $L^{-1}$ to 20.28 mg $L^{-1}$), 19.05 mg $L^{-1}$ (15.58 mg $L^{-1}$ to 23.30 mg $L^{-1}$) and 49.29 mg $L^{-1}$ (40.30 mg $L^{-1}$ to 57.86 mg $L^{-1}$) for *A. fischeri*, *R. subcapitata* and *D. magna*, respectively. Despite a slight discrepancy which was expected due to biological variation, our results generally correlate well with those previously reported. Luminescent bacteria were the most sensitive biological model, and the EC50 values, measured here, are very close to those stated by Ferrer *et al.* [176] (13.3 mg $L^{-1}$ and 13.7 mg $L^{-1}$) and Zhang *et al.* [161] (13.8 mg $L^{-1}$).

| **Species** | **EC50** **mg $L^{-1}$** | **95 % CI** **mg $L^{-1}$** |
|---|---|---|
| *A. fischeri* | 14.09 | 10.94–20.28 |
| *R. subcapitata* | 19.05 | 15.58–23.30 |
| *D. magna* | 49.29 | 40.30–57.86 |

**Table 3:** Toxicity effect of DCF on *A. fischeri*, *R. subcapitata* and *D. magna* presented as effective concentration able to promote 50 % effect (EC50) and its confidence interval (95 % CI).

DCF EC50 for *R. subcapitata* was similar to that reported by Ferrari *et al.* [177] (16 mg $L^{-1}$); DCF EC50 for *D. magna* was in accordance with that reported by Cleuvers [178] (68 mg $L^{-1}$) but was approximately two orders of magnitude below that published by de Oliveira *et al.* [175].

According to the results and the present EU-Directives 93/67/ECC on Risk Assessment for Existing Substances [179], DCF can be classified as “Harmful to aquatic organisms and may cause long term adverse effects in the aquatic environment”.

Information about DCF by-product samples and toxicity data are displayed for single species effects in Figure 23; the results were integrated according to Persoone *et al.* [97] in Figure 24. Generally, the results from *A. fischeri* (Figure 23) showed that six of nine DPs did not significantly influence the luminescence with an average residual toxicity of 0–16 %. Nevertheless, when bacteria were exposed to DP1, DP4 and DP5 samples, the luminescence inhibition greatly increased with an average residual toxicity of 56–91 %. Interestingly, compared to parent compound, toxicity in *A. fischeri* exposed to DP1 remained unchanged ($p > 0.05$).

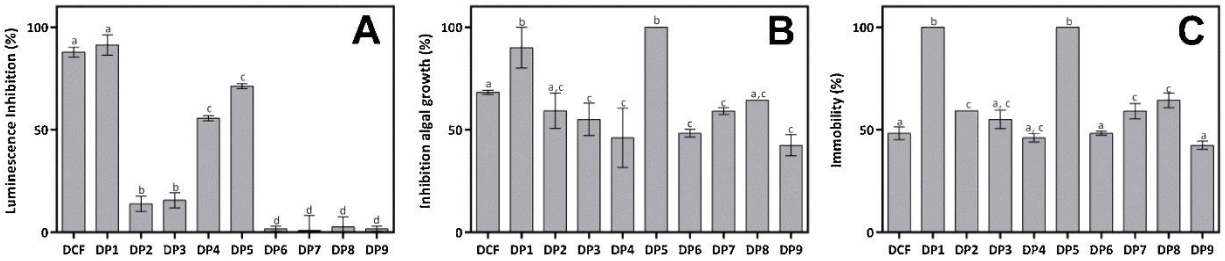


**Figure 23:** Toxicity results of freshly prepared DCF solution (50 mg $L^{-1}$; initial concentration) and its DP (50 mg $L^{-1}$; initial concentration) including *A. fischeri* luminescence inhibition after 30 min contact time (**A**), *R. subcapitata* inhibition of algal growth (**B**) and *D. magna* immobility after 48 h contact time (**C**); data with different letters (a–c) are significantly different (*Tukey's, $p < 0.05$*); error bars represent standard deviation (n = 3).

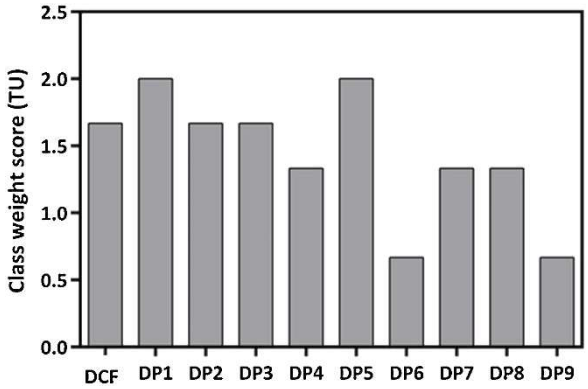


**Figure 24:** Class weight score according to Persoone *et al.* (2003) and hazard classification for DCF and its DPs: no acute toxicity (TU < 0.4); slight acute toxicity (0.4 ≤ TU < 1); acute toxicity (1 ≤ TU < 10).

To the best of our knowledge, scientific data on the aquatic toxicity of the DPs tested here is rather scarce. Nevertheless, there are several reports on DCF by-products that showed an increased toxicity compared to the parent compound in *A. fischeri*. However, the toxicity decreased following degradation of the intermediates [180], [181].

Data from *R. subcapitata* showed that DP1 and DP5 can be more toxic than DCF at the same concentration. However, average residual toxicity was always > 42 %, suggesting that continuous exposure to DPs may lead to more adverse effects in algae compared to DCF. Daphnids evidenced the same increasing toxicity trend of *R. subcapitata* with DP1 and DP5 deemed most toxic. In this context, the results agree with Schmitt-Jansen *et al.* [182] findings of an increase in the toxicity of DCF transformation products compared to the parent substance using *Scenedesmus vacuolatus*.

In regard to data integration [97] (Figure 24) the results confirmed DP1 and DP5 as the most toxic compounds (TU 2); DP2 and DP3 had the same toxicity as DCF, while the other by-products had reduced effects. However, data supported the general issue related to the presence of residual slight acute hazard in DCF and DPs with score > 0.4 TU.

## 5.6 Amoxicillin: Identification of Degradation Products and Antibiotic Activity

Amoxicillin (AMO) is among the most prescribed antibiotics for human use in Italy [183] and other European countries [184], which is a drug synthesized in large amounts and used in aquaculture farms to cope with the most common fish diseases. In Italy, it is estimated that more than 210 t are used annually, of which 86 ± 8% [185] are excreted in parental form with a theoretical environmental load estimated at around 190 t/year. Risk assessment studies for aquatic species and humans are under development, but despite the small amount of ecotoxicological data, some studies found it possible to establish compounds, such as AMO, in surface waters at non-negligible risk levels for aquatic species organisms [186], [187].

AMO has been detected at µg/L concentrations in the influent and effluent of WWTPs and surface water [188] [189], while its levels in pharmaceutical industry effluents may reach mg/L concentrations [190].

Although the treatment processes used in the plants shows high AMO removals [191], [192], [193], even if the percentage of removal depends on the duration of the treatment [194], at the same time, they have the disadvantage of increasing effluent toxicity and producing its transformation compounds, which may be more toxic than the product from which they derive [195]. As a consequence, WWTP effluents and

the practice of reusing sewage sludge in agriculture to recover nitrogen compounds useful for soil fertilization can contribute to its introduction into water bodies and its diffusion in the terrestrial environment of the degradation by-products (DPs) of the drug [63], [94], [97], [133]. Humans can be exposed to DPs through the consumption of aquatic organisms, agricultural products, or drinking water.

In this research, the DPs of AMO were investigated under the same chlorination process conditions used for DCF, in order to simulate the disinfection phase in WWTPs and reduce similar emerging pollutants [196], [197] at three different pH values.

In particular, a chromatographic profile of the possible DPs was obtained with an experiment at low concentrations of AMO (about $10^{-5}$ M), which were then isolated and structurally determined by repeating the chlorination experiment at concentrations levels at least 100 times higher. The structures of 16 isolated DPs, one of which was isolated for the first time, were determined by combining mass spectrometry, using as source a matrix-assisted laser desorption/ionization and as mass analyzer a time-of-flight analyzer (MALDI-MS/TOF) and nuclear magnetic resonance (NMR) data.

Microbial growth inhibition bioassays with *Escherichia coli* (ATCC 25922), *Klebsiella pneumoniae* (ATCC 20081), and *Staphylococcus aureus* (ATCC 6538) were performed to determine the changes in AMO antibacterial activity. *E. coli*, *K. pneumoniae*, and *S. aureus* were used as indicator microorganisms in the antimicrobial assays, since these bacteria are important human pathogens with high stability against antibiotics.

## 5.7 Chlorination Procedure and Product Isolation: Amoxicillin

Amoxicillin (1 g, 2.74 mmol), dissolved in milliQ water (2 L), was treated for 5 min with 5% hypochlorite (molar ratio AMO/NaOCl 1:2; concentration spectroscopically determined at a $\lambda_{max}$ of 292 nm, $\varepsilon$ = 350 $dm^3$/mol cm) at room temperature [88]. The pH of the solution increased immediately from the initial pH of 8.0 to 10.5, and the pH remained at this value during the reaction. After 5 min, the solution was quenched using an excess of thiosulphate, with respect to NaOCl, and dried by lyophilization, and the residue was dissolved in a saturated $Na_2CO_3$ solution and extracted with ethyl acetate (EA) (Figure 25). The EA fraction (351 mg) was separated with the silica gel

column chromatography (CC) using a gradient of methylene chloride/methanol (100:0 to 10:90, v/v) to yield 15 fractions. The EA5 fraction (25 mg), eluted with methylene chloride/methanol (90:10, v/v), was analysed via HPLC using a Supelcosil LC-18 column, 25 cm × 4.6 mm ID, and 5 µm particles. The solvent system was a gradient of acetonitrile/tetrahydrofuran/water (A, 30:10:60, v/v/v) and acetonitrile/water (B, 60:40, v/v), starting with 0% B for 1 min and installing a gradient to obtain 100% B over 20 min, at a solvent flow rate of 1.5 mL/min. The column effluent was monitored at 360 nm. Identification of DP6 and DP4 was achieved by comparison with standard compounds. The fraction EA7 (33 mg), eluted with methylene chloride/methanol (75:25, v/v), was analysed via HPLC using a Supelcosil LC-8 column, 15 cm × 4.6 mm I.D., and 5 µm particles. The solvent system used was a gradient of acetic acid/methanol (A, 1:99, v/v) and acetic acid/water (B, 1:99, v/v), starting with 65% B for 1 min and installing a gradient to obtain 100% A over 25 min and returning to 65% B for 5 min at a solvent flow rate of 1.5 mL/min. The column effluent was monitored at 280 nm. Identification of DP7 and DP8 was achieved by comparison with standard compounds. The fraction EA8 (29 mg), eluted with methylene chloride/methanol (70:30, v/v), was dried, dissolved in an appropriate volume of methylene chloride (100 µL), and analysed using a gas chromatograph with a flame ionization detector (Shimadzu 2010 series, Milano, Italy). The gas chromatograph was equipped with an Equity$^{TM}$-5 capillary column (30 m × 0.25 mm I.D. × 0.25 µm film thickness). The following parameters were set during the experiments: detector temperature, 340 °C, carrier gas, helium (25 cm/s), injected samples, and 1.0 µL, introduced into the injector using an AOC-20i auto sampler (Shimadzu, Milano, Italy) and heated to 225 °C with a split ratio of 100:1. The initial temperature was 40 °C with a 2 min hold, followed by an 8 °C/min ramp to 300 °C, with a 2 min hold. Identification of DP9 and DP10 was achieved by comparison with standard compounds.

The aqueous fraction (W, 959 mg) was dried by lyophilization, re-dissolved in methanol, and separated with the silica gel CC using a gradient of ethyl acetate/methanol (100:0 to 0:100, v/v) to yield 27 fractions. The fraction W8 (39 mg), eluted with ethyl acetate/methanol (70:30, v/v), was analysed via HPLC using a Discovery RP-Amide C16 column, 15 cm × 4.6 mm I.D., and 5.0 µm particles. The solvent system used was a mixture of 0.1% trifluoroacetic acid in acetonitrile/water (25:75), at a solvent flow rate of 1.0 mL/min. The column effluent was monitored at

254 nm. The identification of DP1—DP3 and DP5 was achieved by comparison with a standard compound. The W13 fraction (78 mg), eluted with ethyl acetate/methanol (60:40, v/v), was dried, dissolved in an appropriate volume of water/ethanol (50:50, v/v), and analysed using a Shimadzu 2010 series GC FID (Shimadzu, Milano, Italy). The gas chromatograph was equipped with an 80/120 Carbopack$^{TM}$ B AW/6.6% PEG 20M (2 m × 2 mm I.D., glass). The following parameters were set during the experiments: carrier gas, nitrogen, injected samples, and 1.0 µL, introduced into the injector using an AOC-20i auto sampler (Shimadzu, Milano, Italy). The initial temperature was 80 °C with a 2 min hold, followed by a 4 °C/min ramp to 200 °C with a 2 min hold. The identification of DP11, DP14, and DP15 was achieved by comparison with a standard compound. The fraction W15 (131 mg), eluted with ethyl acetate/methanol (50:50, v/v), was analysed via HPLC using an octadecyl-silica ODS (2) column (15 cm × 4.6 mm I.D.). The solvent system was a mixture of acetic acid, tetrahydrofuran, methanol, and water (1/2/10/87, v/v/v/v) at a solvent flow rate of 1.0 mL/min. The column effluent was monitored at 264 nm. The identification of compound DP13 was achieved by comparison with a standard compound. The fraction W22 (23 mg), eluted with methanol, was analysed via HPLC with an electron capture detector (ECD), using a RP-18 column (25 cm × 4.6 mm ID). The solvent system used was a mixture of 25% hexadecyltrimethylammonium chloride, $KH_2PO_4$, water, and methanol (1:7.5:500:500, v/w/v/v) at a solvent flow rate of 1.5 mL/min. The identification of DP12 was achieved by comparison with a standard compound [198].

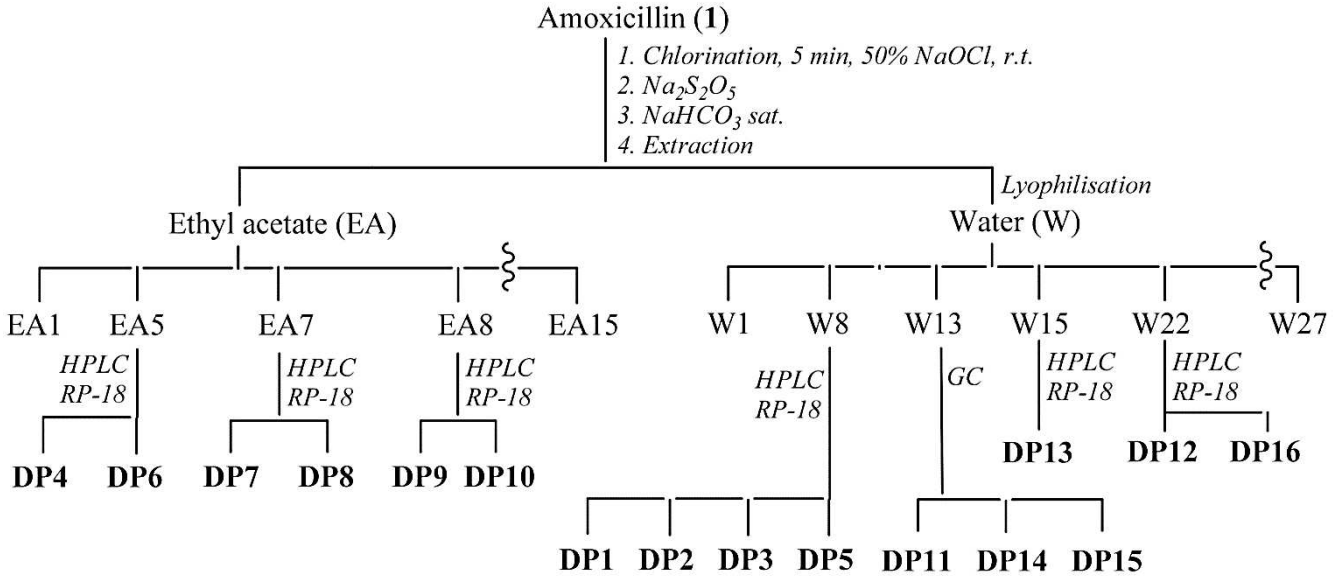


**Figure 25:** The isolation of all identified compounds (DP1–DP16).

## 5.8 Results and discussion

### 5.8.1 Chlorination Experiments

A $10^{-5}$ M AMO solution was treated for 10 min with 10% hypochlorite (molar ratio AMO/NaOCl 1:1 concentration, spectroscopically determined $\lambda_{max}$ 292 nm, ε 350 $dm^3$/mol cm) at room temperature [89], [102], [103], simulating the conditions used in a typical WWTP. The experiment was repeated at pH = 3 in a common $H_3PO_4/KH_2PO_4$ (20 mM) buffer (Figure 26a), at pH = 7 in $KH_2PO_4/K_2HPO_4$ (20 mM) buffer (Figure 26b) and at pH = 9 (Figure 27a). The presence of AMO was quantified using a Lambda 12 UV-Vis spectrophotometer (Perkin Elmer, 940 Winter Street, Waltham, MA 02451, USA). Absorbance peaks were determined at 230 nm (Figure 27b). The absorbance values were converted into concentration using a calibration curve prepared from standard solutions with known AMO concentrations. In this latter case, the pH of the solution, measured and recorded continuously by a pH-meter, increased immediately from the initial pH of 8.0 to 10.5, and the pH remained at this value during the reaction.

The measurements of the AMO concentration as a function of time at the two different buffered pH values show how degradation was greater at pH = 7, with a percentage of about 80% after just 20–25 min of treatment. When pH = 3, it was just under with the same time. Regardless of the pH value, the AMO concentration remained practically constant in the absence of NaOCl, with a degradation percentage of no more than 5–7% at the higher pH.

It is interesting to note that the presence of AMO practically disappeared after 15 min when it was in contact with hypochlorite. Thus, it remained almost constant in its absence. Hypochlorite, on the other hand, decomposed faster than AMO degraded, reducing by more than 95% after just 10 min, which indicates how all the active species presented in the solution contributed to drug degradation.

The measurements of the quantity of non-degraded AMO clearly shows how the percentage of degradation rapidly increased to 60% with a NaOCl/AMO ratio of 0.5, which was almost total with a NaOCl/AMO ratio = 0.75. The data reported in the literature for other emerging micropollutants generally observed longer reaction times, even in the order of hours. Oxidant concentrations even doubled that of the pollutant to ensure the complete mineralization of the latter, which was not infrequently after a double or triple treatment [89], [102], [103], [104].

An aliquot of the solution was taken every 5 min, quenched by sodium thiosulphate excess, filtered, dried by lyophilization, and dissolved in a saturated sodium bicarbonate solution before being extracted with ethyl acetate. The course of the reaction was monitored by HPLC. The main degradation by-products (DP4 and DP6—DP10 for the ethyl acetate fraction and DP1—DP3, DP5 and DP11—DP16 for the aqueous fraction) were identified by comparing their retention times with those of commercially available standard compounds or isolated by performing preparative experiments with an AMO solution at a concentration higher than $10^{-3}$ M treated with 5% hypochlorite at room temperature for 5 min. The degradation by-products obtained were isolated via column chromatography and HPLC and completely characterized using NMR and mass spectrometry (MS) analysis. DP1—DP16 were isolated in relative percentages of 1.01, 0.89, 2.25, 2.02, 1.56, 1.36, 2.21, 2.05, 3.01, 2.24, 1.25, 1.11, 1.23, 1.45, 2.25, and 0.23%, respectively. The plausible mechanism of their formation from AMO is shown in Figure 28. DP16, isolated for the first time, was determined by combining mass spectrometry (MS) and nuclear magnetic resonance (NMR) data.

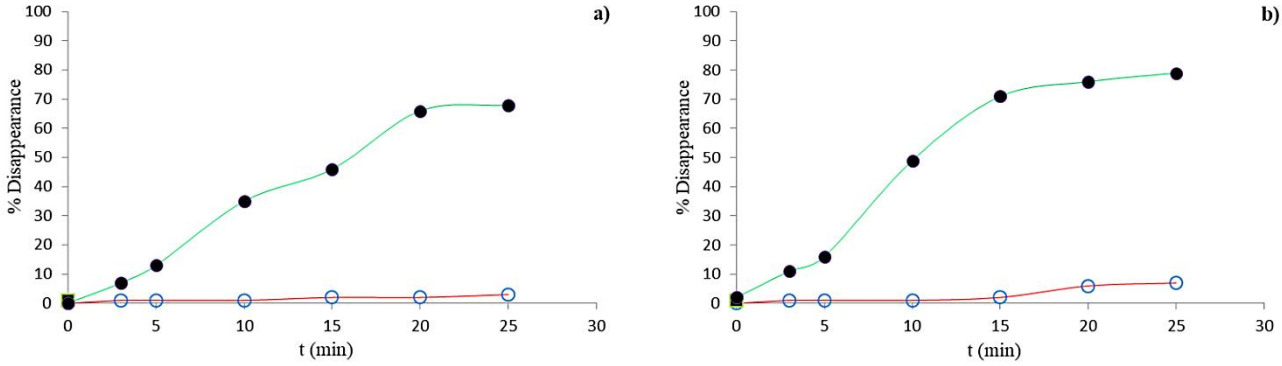


**Figure 26:** Time-conversion plot for the reaction of amoxicillin (AMO) with one equivalent NaOCl at buffered pH = 3.0 (**a**) and pH = 7 (**b**). ●: AMO consumption by reaction with NaOCl (green); ○: Disappearance of AMO in the absence of NaOCl (red).

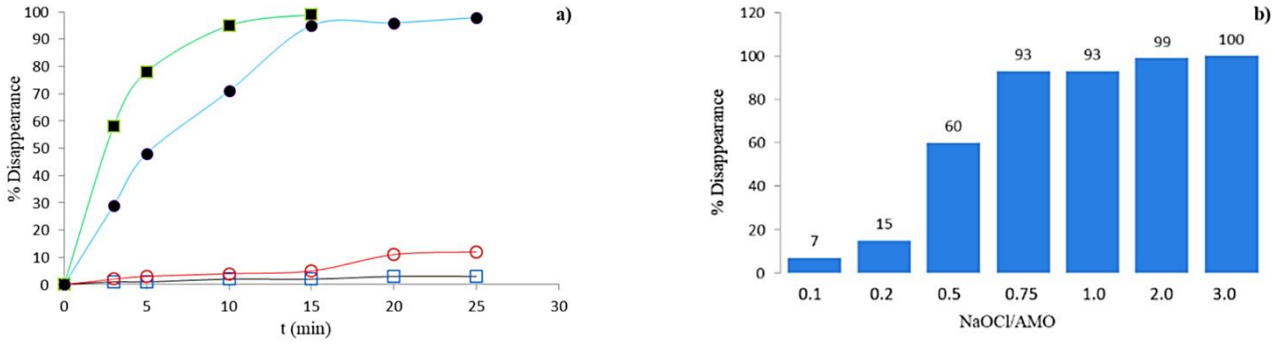


**Figure 27:** (**a**) Time-conversion plot for the reaction of AMO with one equivalent NaOCl at pH = 9.0. ■: NaOCl consumption in the presence of AMO (green); ●: AMO consumption by reaction with NaOCl (blue); □: Disappearance of NaOCl in the absence of AMO (red); ○: Disappearance of AMO in the absence of NaOCl (black); (**b**) AMO disappearance by NaOCl at pH basic no-buffered after a 5 min reaction.

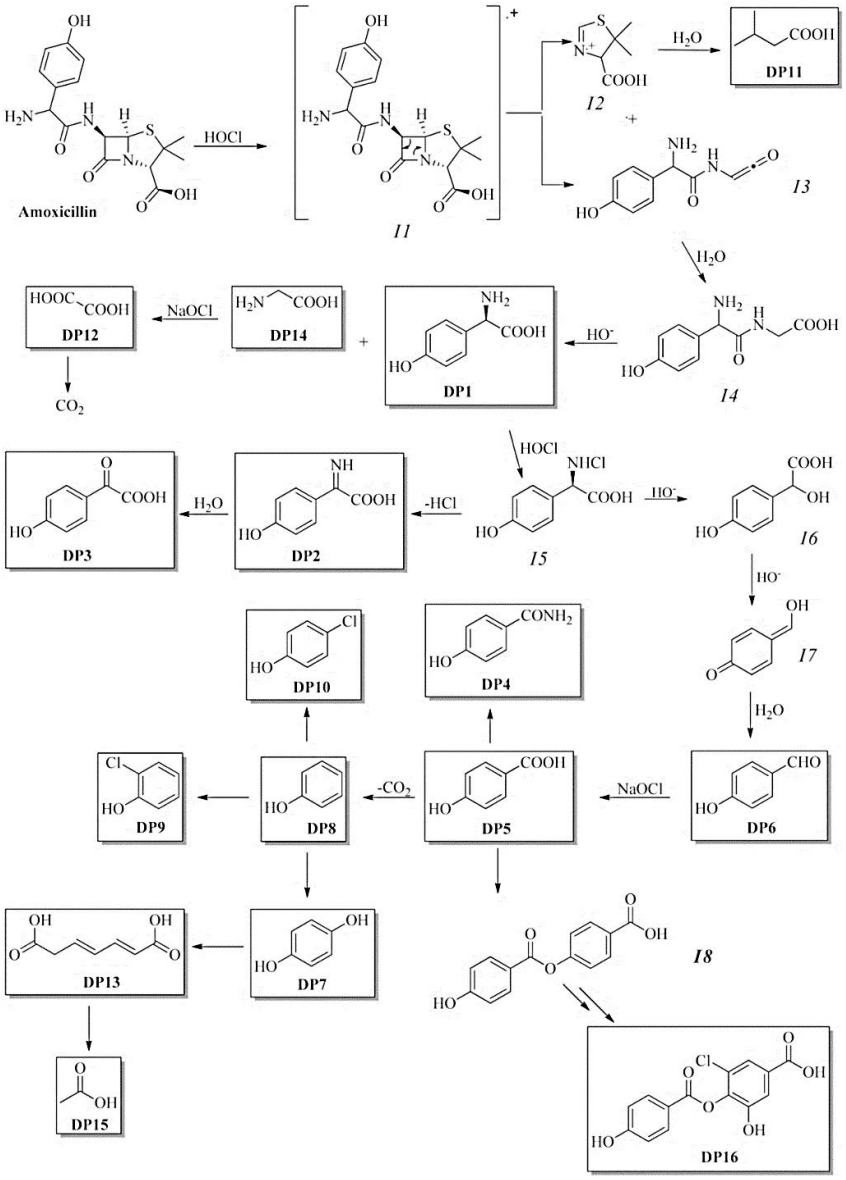


**Figure 28:** Plausible mechanism for the formation of DP1—DP16.

### 5.8.2 Structural Elucidation

AMO chlorination-produced degradation by-products DP1—DP16 were isolated by chromatographic processes and identified on the basis of their physical features. In AMO treatment with an unbuffered pH value, the changes of the drug were monitored with HPLC. Its main degradation by-products (DP1—DP16) were identified by comparing their retention times with those of the standard compounds and by employing NMR and MS analyses. The concentrations of DP1—DP16 were at a maximum after 5 min and were in the range of 3.01–0.89%.

The first three DPs (DP1—DP3) were $C_6C_2$ skeletal compounds obtained from the hydrolysis of the amide bond of the phenylethanoic acid residue and the subsequent oxidation of the alkyl chain. The DP4—DP6 had a $C_6C_1$ skeleton and, thus, it was easy to hypothesize that they were products derived from the decarboxylation of the previous three. Moreover, the DP7—DP10 had a $C_6C_1$ skeleton with an oxidized or chlorinated aromatic ring. DP11—DP15 products were di- or mono-carboxylic acids, which were final oxidation products. A separate discussion should be had for DP16, which is a phenylbenzoic ester chlorinated on the alcoholic part and clearly obtained from the esterification of two oxidation by-products.

The reaction could start by a single-electron transfer from the lone electron pair of the amino group to HClO, which formed the corresponding radical cation and chloride. This aminyl radical cation (*I1*) could undergo a β-lactam cycle when two fragments, *I2* and *I3*, formed. The first fragment formed via hydrolysis and gave DP11. The *I3* fragment first hydrolyzed the ketene function to a carboxylic function, giving the intermediate *I4* that led to DP1 and DP14. The second fragment oxidized to DP12 and $CO_2$. From the product DP1, it was possible to obtain DP2—DP3 with a $C_6C_2$ skeleton, DP4—DP6 with a $C_6C_1$ skeleton, and DP7—DP10 with a $C_6C_0$ skeleton through a series of oxidations, decarboxylations, and chlorations. Finally, DP13 and DP15 was obtained by opening the aromatic ring. A slightly different argument to justify DP16, the synthesis of which could come from the chlorination and subsequent oxidation of intermediate *I8*, in turn was obtainable from the esterification of two DP5 molecules.

### 5.8.3 Antibiotic Activity Results

Figure 29 shows the antimicrobial activity of AMO and its DPs against *S. aureus*. Partial activity was developed at 5 mg/L AMO when the inhibition did not exceed 28% for the parent compound.

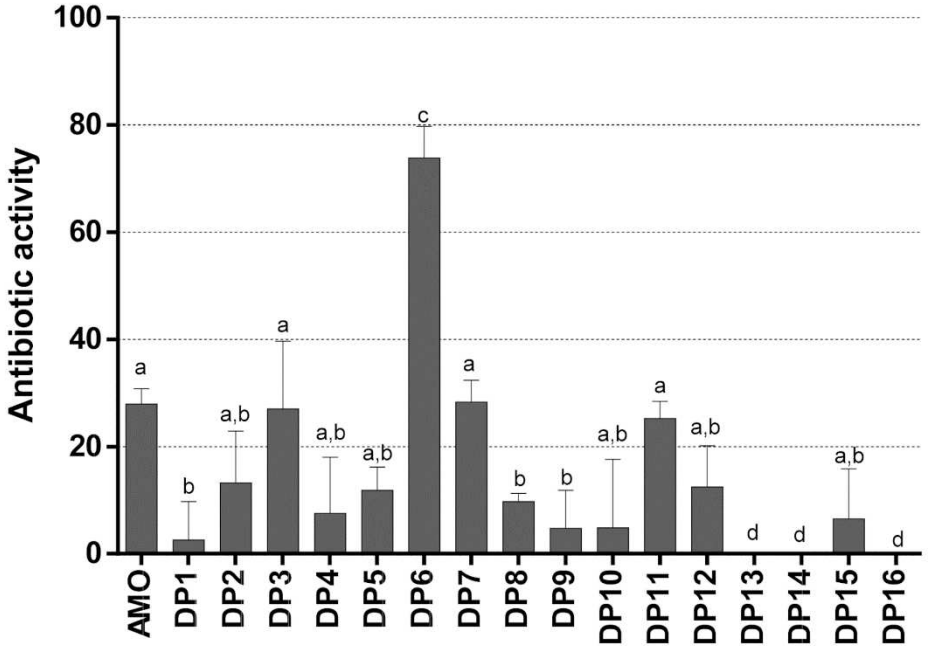


**Figure 29:** Antibacterial activity of AMO and its DPs against *S. aureus*. Groups with the same letter were not significantly different (*Tukey post hoc, $p < 0.05$*).

It was evident that 56% of DPs showed residual activity to *S. aureus* and this was more pronounced for DP6, where activity was exclusively due to oxidation by-products with 74% of antibiotic activity. DP1, DP8, and DP9 showed decreased antibiotic activity. Only DP13, DP14, and DP16 were revealed to have no antibiotic effects.

Similar tests with *E. coli* and *K. pneumoniae* revealed that both bacteria were resistant at 5 mg/L AMO, with no significant antimicrobial activity (data not shown). The related DPs appeared to have no antibiotic and/or toxic effect against *E. coli* and *K. pneumoniae* (data not shown).

According to Dimitrakopoulou *et al.* [106], *E. coli* and *K. pneumoniae* revealed a resistance up to 25 mg/L AMO, even if the suggested ranges for Minimum Inhibitory Concentrations (MICs) were 0.25–128 mg/L for Enterobacteriaceae (*i.e.*, *E. coli* and *K. pneumoniae*) [199].

## 5.9 Conclusions

This research investigated the fate of Diclofenac (DCF) and Amoxicillin (AMO) following disinfection treatment by chlorination. The reaction was carried out by simulating the conditions of a typical WWTP, using excess sodium hypochlorite and, in the case of amoxicillin, 3 different pH values. After chlorination treatment, chromatographic techniques were used to isolate, respectively, 14 disinfection by-products for DCF and 16 for AMO, which were fully characterized by MS and NMR analyses. Just over 40 % of DCF underwent complete mineralization, while ∼20 % was recovered and unchanged and almost 39 % was transformed into at least 14 disinfection by-products. Instead, AMO underwent almost complete mineralization: 95–96 % at pH 9, almost 80% at pH 7, and just under 70 % at pH 3 after only a few minutes of treatment.

Nine new compounds generated and isolated from DCF are by-products chlorinated at the aromatic ring (DP1−DP7, DP9) or in the side chain (DP8). Three of these appear to contain two (DP5−DP7) or three (DP8) units of DCF. The ecotoxicological evaluation made it possible to measure the biological effect of DPs; DP1 and DP5 present the highest potential to generate significant adverse effects on aquatic organisms, sometimes greater than parent compound. Effects are strictly concentration-dependent, thus effects in real wastewater could be of limited impact, but gaps into the knowledge still remained about their potential interactive adverse effects not yet explored.

On the other hand, the antibiotic activity of amoxicillin was measured by exploiting the different sensitivity of 3 bacterial strains. With regard to *E. coli* and *K. pneumoniae*, no antimicrobial activity occurred, regardless of how low AMO concentrations were or how low transformation by-products were. Conversely, *S. aureus* is less resistant to AMO, and this effect remained partially or totally in its reaction by-products. It is already known from the literature that amoxicillin is degraded by at least 75 % in WWTPs, but it was not clear what formed or the possible toxicity of these by-products.

# CHAPTER 6

In this chapter, part of the results based on original contributions published in [200] and submitted and MDPI (applied sciences) are presented.

## 6.1 Rare Earth Elements (REEs) in AOPs: a new frontier to remove pollutants

The persistence of emerging contaminants and above all the formation of unwanted by-products, a phenomenon which has already been widely discussed in previous chapters, represent an important challenge linked to water purification considering the high difficulty in removing them. To address these problems, several advanced oxidation processes (AOPs) have been developed. In particular, a new frontier is represented by the use of rare earth elements (REEs) as catalysts in AOPs and therefore their implementation in wastewater treatment could be thought of in the future. The REEs are a group of seventeen chemical elements in the periodic table, the 15 lanthanides from lanthanum (La) to lutetium (Lu), to which scandium (Sc) and yttrium (Y) are added since the latter tend to occur in the same mineral deposits with lanthanides and exhibit similar chemical properties. The chemical, metallurgical, and physical properties of the REEs are governed by their electron configuration. These properties make them suitable to be used in AOPs, where they can enhance the performance of the processes [55], [56]. In contrast to element Y, the lanthanides are characterized by the progressive filling of the 4f orbital [201]. Due to the low energy of these electrons, they do not directly participate in the bonding when forming compounds with other elements. As a consequence, this leads to a significant similarity in the chemical reactivity of the lanthanides. This uniform reactivity pattern is evident consistently throughout geochemical processes, rather than being unique to each individual element [201], [202].

In Table 4, the essential details encompassing the atomic numbers and intricate valence shell electronic configurations pertaining to the distinctive set of REEs are provided.

| Element | Atomic Number | Valence Shell Electronic Configuration |
|---|---|---|
| **Y** | 39 | [Ar] 3d1 4s2 |
| **La** | 57 | [Ar] 4d1 5s3 |
| **Ce** | 58 | [Xe] 4f1 5d1 6s2 |
| **Pr** | 59 | [Xe] 4f3 5d0 6s2 |
| **Nd** | 60 | [Xe] 4f4 5d0 6s2 |
| **Pm** | 61 | [Xe] 4f5 5d0 6s2 |
| **Sm** | 62 | [Xe] 4f6 5d0 6s2 |
| **Eu** | 63 | [Xe] 4f7 5d0 6s2 |
| **Gd** | 64 | [Xe] 4f7 5d1 6s2 |
| **Tb** | 65 | [Xe] 4f9 5d0 6s2 |
| **Dy** | 66 | [Xe] 4f10 5d0 6s2 |
| **Ho** | 67 | [Xe] 4f11 5d0 6s2 |
| **Er** | 68 | [Xe] 4f12 5d0 6s2 |
| **Tm** | 69 | [Xe] 4f13 5d0 6s2 |
| **Yb** | 70 | [Xe] 4f14 5d0 6s2 |
| **Lu** | 71 | [Xe] 4f14 5d1 6s2 |

**Table 4:** Atomic Number and Valence Shell Electronic Configuration of the Rare Earth Elements.

This chapter focuses on the use of REEs as catalysts for the degradation of ECs from wastewater, since their use, which is currently in place for wastewater treatment, lacks processing and economic sustainability.

## 6.2 Potential Environmental Impacts of REE-Based Catalysts

As for the use of REEs in AOPs, different perspectives are to be considered. Further improvement needs to be implemented in water treatments; as of now, several methods have been adopted that increase efficiency and provide better handling of waste, such as Fenton-like oxidation processes [203]. Studies focused on the use of lanthanides have demonstrated an improvement in wastewater treatments, as their use can produce on average 30% less sludge compared to other alternatives such as iron and aluminum [204]. The use of REEs could represent an alternative for reducing 9wastelands generated by sludge [204] and improving the removal of organic pollutants by enhancing photocatalytic activity [55].

Moreover, care should be taken to avoid the loss and transfer of particles into the environment, contributing to the anthropogenic input of REEs. The authors of [205] found that the mixture of lanthanides used in wastewater treatment had an antagonistic behavior, which could reduce their environmental impact. However, up to now, the knowledge of the toxicity of REEs is very limited, as the environmental fate is highly dependent on the system, such as the presence of organic matter, pH,

and presence of cations [206] which influence the speciation, which, by extension influences the bioaccumulation and bioavailability. Because of the lack of knowledge regarding the potential effects of REEs, the regulation for the discharge of REEs is still lacking. In contrast, many restrictions regarding the presence of organic pollutants have been applied globally [207].

## 6.3 REE-Based AOPs for pharmaceuticals removal

Pharmaceutical toxic compounds can end up in wastewater via many routes, such as via their consumption by humans or their use in agriculture. Therefore, it is essential to discover effective ways for decomposing these hazardous compounds in wastewater. The use of REEs has been shown by several studies to be potentially useful. Numerous researchers utilized REEs in various forms as heterogeneous catalysts in AOPs (Table 5).

Nie *et al.* [208] carried out a Fenton-like reaction, at 30 °C, to take complete degradation of the antibiotic sulfamethoxazole (SMX), in the simultaneous presence of $LaFeO_3$ and $H_2O_2$ at pH values ranging between 5.5 and 7.14. It was found that the SMX removal efficiency increased with the increase of the catalyst load and then reached a constant value when the $LaFeO_3$ concentration was above 1.4 g/L. Furthermore, it was investigated that the $LaFeO_3$ could be reused for at least 10 cycles and the reused catalyst kept the catalytic activity nearly as efficient as the fresh one.

Ref. [209] investigated the photocatalytic activity for degradation of carbamazepine and caffeine using MIL-125-$NH_2$, $LaFeO_3$, and $LaFeO_3$/MIL-125-$NH_2$ photocatalysts under solar simulator at ambient temperatures. $LaFeO_3$/MIL-125-$NH_2$ composite exhibited higher carbamazepine and caffeine degradation than MIL-125-$NH_2$ MOF and $LaFeO_3$ perovskite and this is highlighted through the calculation of pseudo-first-order kinetics equation. $LaFeO_3$/MIL-125-$NH_2$ composite photocatalysts prepared by the self-assembly method have shown excellent and promising results in the degradation of pharmaceutical compounds.

Chen *et al.* (2022) [210] used $LaFeO_3$/lignin-biochar (LFO/LG) catalysts prepared by a sol–gel pyrolysis to evaluate the degradation of ofloxacin (OFX) under visible light irradiation. The pure LaFeO3 (LFO) and the pure lignin-biochar (LG) were tested and prepared under the same conditions to compare which one had the best performance. The whole process was operated at a constant temperature in the

presence of $H_2O_2$ (30 wt%) and all experiments were carried out under different initial pH, revealing later an optimal photodegradation efficiency at pH values above 6. In addition, the morphology, microstructure, energy band structure, and photoelectrochemical behavior of the composite catalysts were characterized and the relationship with catalytic performance was explained. Pure LFO has almost no adsorption of OFX when the system was left in the dark to reach a saturation adsorption state and the degradation efficiency for LFO is only 53.4% after a 75-min degradation reaction. Instead, LFO-LG samples showed a significant adsorption effect on OFX, and the degradation efficiency was also improved up to 95.6%.

In the study of [211], the electrochemical degradation of dipyrone using cerium catalysts was not effective during a two-hour electrolysis. However, the use of a $CeO_2$/C gas diffusion electrode degraded all of the dipyrone in 20 min with 26% mineralization at −1.3 V, and after only 5 min with 57% mineralization at −1.1 V when the Fenton process was employed. The authors declared that ceria acts as an oxygen buffer leading to an increase in the local oxygen concentration, facilitating $H_2O_2$ formation and consequently improving the dipyrone degradation. $FeCeO_x$ can remove 83% of diclofenac in a heterogenous Fenton process and can be reused due to its chemical stability [212].

A heterogeneous Fenton catalyst, $Ce^0$-$Fe^0$-reduced graphene oxide (Ce–Fe–RGO), showed good catalytic performance and adsorption of sulfamethazine [213]. Ferrum-doped $CeO_2$ nanosheets with various Fe/Ce ratios were evaluated for the Fenton-like degradation of salicylic acid (SA). The 2% Fe-doped $CeO_2$ nanosheets showed the highest concentration of surface oxygen vacancies and catalytic activity under the optimum reaction conditions due to the complex adsorption of SA and $H_2O_2$ on the surface $Ce^{3+}$. The catalytic activity of the nanosheets could be recovered, and so they could be reused in new cycles [214]. A surface of graphite felt loaded with $CeO_x$ accelerated the mineralization of carbamazepine via an E-peroxone process [215].

The $Fe^0$/$CeO_2$ nanocomposite enhanced the removal of tetracycline (TC) in the Fenton oxidation process and could be reused for further cycles. The authors suggested a synergistic effect between nanoscale $Fe^0$ and $CeO_2$ [51].

Hu *et al.* [216] tried out for the first time the use of cobalt (Co) and REE gadolinium (Gd) to investigate the removal of two antibiotics from wastewater, ciprofloxacin (CIP) and tetracycline. In particular, the sponge-like structure of Co- and Gd-modified biochar (MBC) was conducive to studying its adsorption capacity due to

the presence of metal oxides and functional groups. Furthermore, the influence of pH on the absorption of antibiotics was studied by varying the pH between 3 and 11. It was observed that at pH 9, the antibiotic adsorption capacity of MBC was greatly increased. These data suggested that MBC is an innovative and effective adsorbent for the removal of antibiotics from complex contaminated water.

Luan *et al.* [217] synthesized photocatalysts $Er_2FeSbO_7$, $BiTiSbO_6$, or N-TO by solid-state method to degrade enrofloxacin (ENR), a common antibiotic able to effectively kill Gram-positive and Gram-negative bacteria and mycoplasma under visible light irradiation. A new photocatalyst provided by $Er_2FeSbO_7/BiTiSbO_6$ heterojunction (EBH) was prepared for the first time by the thermal solvent method and tested. It was observed that the photocatalytic activity among the four photocatalysts was as follows: EBHP > $Er_2FeSbO_7$ > $BiTiSbO_6$ > N-TO. Therefore, it can be concluded that the EBHP process can be a potent method for treating pharmaceutical wastewater that is polluted by ENR.

FeOCl doped with Y or La showed efficient Fenton catalytic activity for ibuprofen degradation under simulated solar light [218]. Tungsten oxide composites ($WO_3$) doped with La, Gd, or Er showed an enhanced photocatalytic degradation of organic dyes compared to the pure composites [219].

Sharmin *et al.* (2022) [220] synthesized 10% Gd-doped BiFeO3 nanoparticles (BGFO) via a simple and cost-effective hydrothermal technique at a lower reaction temperature of 160 °C. Following this approach, the synthesized nanoparticles exhibited photocatalytic activity towards the degradation of pharmaceutical pollutants such as ciprofloxacin (CIP) and levofloxacin (LFX) under simulated solar irradiation.

In general, the studies highlighted the use of diverse catalysts to improve the efficiency of removing pharmaceutical compounds. Each study focused on targeting specific pharmaceutical compounds; this targeted approach allowed for a more accurate evaluation of the catalyst's performance against particular contaminants. Among the studies conducted on CIP removal, the highest removal percentage (>99%) within a timeframe of 180 min was achieved by the study utilizing the MBC catalyst [216].

The pH can play a significant role in the reactivity and adsorption behavior of both the catalyst and the target compound. The studies reported a range of pH values,

including pH 4, 5, 6.48, and 9, indicating that different pH levels can be effective depending on the specific catalyst and target compound.

Furthermore, the temperature of the reaction can influence the reaction kinetics and the stability of the catalyst. It was generally observed that moderate temperatures (20–25 °C) were preferred to strike a balance between reaction rates and energy consumption.

The pharmaceutical degradation studies highlighted the potential of Fenton-based processes for wastewater treatment, showcasing the reusability of $FeCeO_x$ [210], the catalytic performance and adsorption properties of Ce-Fe-RGO [213], and the degradation capabilities of ferrum-doped $CeO_2$ nanosheets [51]. The results emphasize the versatility and effectiveness of Fenton processes in removing pharmaceutical compounds, offering promising solutions for the treatment of wastewater contaminated with these contaminants.

| Catalyst Doped REE | Target | Dose of Catalyst | Dose of Target | Time (min) | Conditions | Proposed Mechanism | Removal (%) | Reference |
|---|---|---|---|---|---|---|---|---|
| **$LaFeO_3$** | Sulfamethoxazole | 1.4 g/L | 3 mg/L | 120 | pH = 6.48, T = 30 °C | Production of •OH and superoxide radicals ($O_2^-$/HOO) | 100% | [208] |
| **$LaFeO_3$/MIL-125-$NH_2$** | Carbamazepine (CBZ) and Caffeine (CAF) | 250 mg/L | 5 mg/L CBZ and 1 mg/L CAF | 60 | Visible light | Production of •OH and $O_2^-$ | 74% CBZ<br>87% CAF | [209] |
| **$LaFeO_3$/lignin-biochar (LFO/LG)** | Ofloxacin (OFX) | 250 mg/L | 30 mg/L | 75 | Visible light, addition of $H_2O_2$ | Production of •OH | 95.60% | [210] |
| **$CeO_2$/C gas diffusion electrode (GDE)** | Dipyrone | - | 100 mg/L | 20 | - | Production of •OH | 100% | [211] |
| **$FeCeO_x$** | Diclofenac | 0.5 g/L | 20 mg/L | 40 | pH = 5, addition of $H_2O_2$, ambient temperature | Production of •OH | 83% | [212] |
| **$CeO_2$ nanosheets doped with Fe** | Salicylic acid | 250 mg/L | 50 mg/L | 120 | Addition of $H_2O_2$, pH = 4, T = 55 °C | Production of superoxide radicals ($O_2^-$/HOO) | 96% by 2wt% Fe-$CeO_2$ | [214] |
| **$CeO_x$ modified graphite felt** | Carbamazepine | - | 10 mg/L | 60 | pH = 5, T = 25 °C | Production of •OH | 69.40% | [215] |
| **Sponge-like structure of Co- and Gd-modified biochar (MBC)** | Ciprofloxacin (CIP)/Tetracycline (TC) | 1.1 g/L | 20 mg/L | 180 | pH = 9 | - | 99% of CIP or TC | [216] |
| **$Er_2FeSbO_7$/$BiTiSbO_6$ heterojunction (EBH) catalyst** | Enrofloxacin (ENR) | 0.75 g/L | 0.025 mM | 150 | Visible light, T = 20 °C, | Production of •OH | 99,16% | [217] |
| **FeOCl doped with Y or LA** | Ibuprofen | 0.5 g/L | 5 mg/L | 20 | Neutral pH, addition of $H_2O_2$, room temperature, dark | Production of •OH | 84–82% by 0.9wt% FeOCl/La and 1.2wt% FeOCl/Y, respectively | [218] |
| **Gd doped $BiFeO_3$ nanoparticles (BGFO)** | Ciprofloxacin (CIP)/Levofloxacin (LFX) | - | - | 240 | Solar illumination | Production of $O_2^-$ | 80%/79% | [220] |

**Table 5:** REE catalysts used for pharmaceutical degradation.

### 6.3.1 Levofloxacin: a preliminary study

The presence of antibiotics in the aquatic environment and their potential impact on the development of antibiotic-resistant bacteria is a significant concern in the scientific community. In addition, many drugs can exert their inhibitory effect against degrading microorganisms present in water purification plants (activated sludge), thus compromising the quality of the water product that comes out [221]. The antibiotics whose presence is often found in water belong to tetracyclines, sulphonamides, macrolides, lincosamides and quinolones. More specifically, this chapter presents the preliminary results regarding the degradation of a quinolone antibiotic that is a member of a large group of broad-spectrum bacteriocidal that share a bicyclic core structure related to the substance 4-quinolone. The most popular quinolones are fluoroquinolones (FQs) (with a fluorine atom on C6) which include ciprofloxacin, lomefloxacin, norfloxacin, ofloxacin, moxifloxacin and levofloxacin (Figure 30).

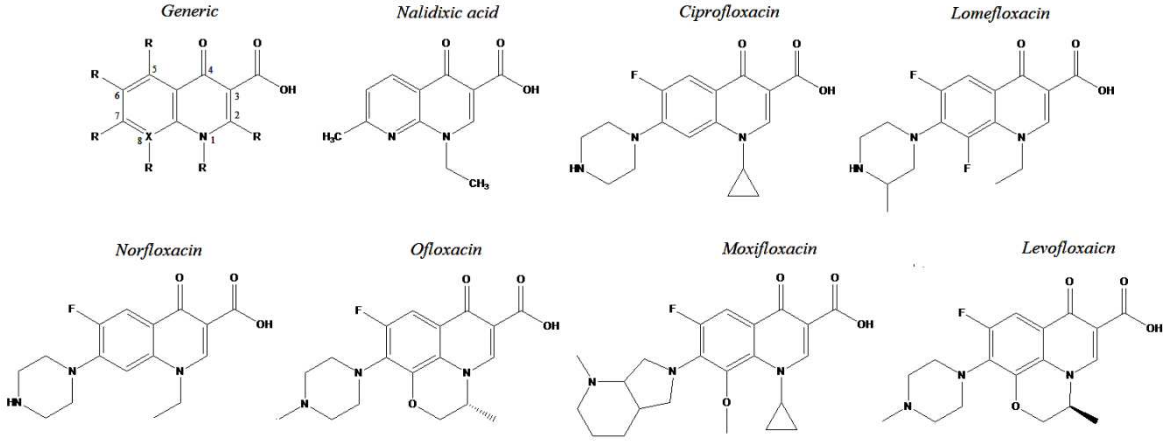


**Figure 30:** Chemical structure of the main quinolones.

According to literature, ciprofloxacin was the most consumed second-generation quinolone in 24 countries; levofloxacin was the most consumed in Bulgaria, Cyprus, Hungary and Italy; and ofloxacin was the most consumed in France [222].

This preliminary investigation focuses precisely on the degradation in water of the fluoroquinolone levofloxacin, as a chemical target, by means of AOPs. The same process was then also performed on a biological target, *i.e.* on a Levofloxacin-resistant strain of enterococci (*Enterococcus faecalis* ATCC 29212). The persistence

of the enterococci strains was then evaluated through inactivation bacterial test using the technique for inclusion of the inoculum on a suitable selective substrate.

The aim of the study was to evaluate the performance effectiveness of the AOP process in degrading the two targets, exploiting the principle of heterogeneous photocatalysis which requires the addition of catalysts.

Heterogeneous photocatalysis is a chemical process involving the use of semiconductors as catalysts to promote chemical reactions via interaction with near-ultraviolet (UV) or solar visible irradiation. In the specific case study, REEs-based nanopowders, such as cerium, lanthanum and a combination of cerium doped with lanthanum, were used as semiconductors in the photocatalytic process, under simulated solar irradiation conditions, to promote the generation of reactive oxygen species (ROS) and degrade the chosen targets.

## 6.4 Materials and Methods

### 6.4.1 Reagents and chemicals

Levofloxacin (98.0%) were purchased from Sigma Aldrich (Milan, Italy). All chemicals were analytical grade and used as received without further purification. Deionized water was used throughout the experiments. The reaction was carried out using a phosphate buffer with sodium dihydrogen phosphate/disodium hydrogen phosphate ($NaH_2PO_4/Na_2HPO_4$) to keep the pH constant at 7.00. MeOH:10 mM $CH_3COONH_4$ (70:30 v/v) mixture was used as the mobile phase in the HPLC column, flowing at 1 mL/min through a Luna Phenomenex® C18 (250 4.6 mm; 5 m) column. Per run, a volume of 20 μL of the sample was injected and disclosed with a U.V. detector set at 295 nm. The precursors for the design of REEs catalyst were cerium nitrate hexahydrate ($Ce(NO_3)_3 \cdot 6H_2O$, 99%; Sigma Aldrich) and lanthanum nitrate hexahydrate ($La(NO_3)_3 \cdot 6H_2O$, 99.9%; Sigma Aldrich). For the preparation of the Enterococci selective agars, Tryptic Soy Broth (TSB, Difco, Becton-Dickenson Labs) and Slanetz & Bartley agar without TTC (Biolife, Italy) were used.

### 6.4.2 Catalyst preparation procedure: Cerium and Lanthanum nanopowders

Co-precipitation method was used to synthesized single cerium/lanthanum oxide nanopowders ($CeO_2$, $La_2O_3$) and the lanthanum cerate nanopowders coded as LC10 ($La_{0.1}Ce_{0.9}O_{2-\delta}$) [223], [224]. Cerium nitrate ($Ce(NO_3)_3 \cdot 6H_2O$, 99%; Sigma Aldrich) and lanthanum nitrate hexahydrate ($La(NO_3)_3 \cdot 6H_2O$, 99.9%; Sigma Aldrich) were mixed in Milli Q water up to a final concentration of 0.2 M in a beaker for 30 min. Then both precursors were mixed in beaker for 30 min at room temperature. Precipitation was performed at room temperature. Aqueous ammonia was added dropwise to the mixture under constant magnetic stirring. The precipitates were collected at pHs 8-8.5 using pH meter (Mettler Toledo FE20-Basic Five Easy™). The stirring was continued for 15 min after the completion of precipitation. The best pH condition for co-precipitation technique was found to be around pH ~8; justification for such a choice was substantiated through thermal and phase analyses. The obtained light yellow-coloured colloidal solutions were washed with Milli Q water followed by four cycles of centrifugation at a speed of 3000 rpm (for 15 min). The resultant products were then dried in an oven at 110 °C for 8 h and crushed to powders. The oven-dried precursors were calcined at 850 °C for 2 h in air atmosphere to obtain the mixed oxide nanopowders.

### 6.4.3 Photocatalytic degradation experiments

All photoreaction experiments were carried out in a jacketed custom made photoreactor. The reactor consisted of a 100 mL cylindrical Pyrex glass reactor vessel equipped with solar simulator (SS) lamp that provides illumination approximating natural sunlight. This device is a solar radiation simulator (Xenon lamp) and the irradiation source having a light power of 250 $W/m^2$, with a spectral wavelength range of 320 - 430 nm. The UV-A part of the solar spectrum is responsible of the activation of REEs nanopowders in photocatalytic processes. The temperature was kept constant at 25 °C by circulating the cooling water continuously into the modified double-hinge photoreactor. Furthermore, the solutions were kept in constant magnetic mixing during the execution of the photocatalytic oxidation experiments (60 min dark + 180 min light).

The photocatalytic oxidation of the pharmaceutical was evaluated by adding 0.5 g/L of photocatalysts ($CeO_2$, $La_2O_3$, LC10) into the levofloxacin solution with an initial concentration of 1 mg/L. The same procedure was adopted for the photocatalytic oxidation of the biological target (*Enterococcus faecalis* ATCC 29212) starting from an initial concentration of $10^6$ CFU/mL. The stirred mixture was left for 60 min in the dark to establish an equilibrium of adsorption between drug/bacteria and the catalyst. At defined time intervals (dark; 0, 5, 10, 15, 30, 60, 120, 180 min), aliquots were sampled and centrifuged at 3000 rpm for 20 min so as not to create interference with subsequent chemical quantification on the HPLC instrument.

### 6.4.4 Bacterial count and inactivation test

Levofloxacin resistance phenotypes were tested by Kirby–Bauer method according to standard recommendations [225]. The test allowed the selection of the *Enterococcus faecalis* ATCC 29212 strain as resistant to levofloxacin, therefore it was possible to use it as a biological target in the photocatalytic oxidation experiments.

Briefly, the colonies, before AOP treatment, were transferred to appropriate culture broth for growing. Bacterial strains were grown to exponential phase in Tryptic Soy Broth at 37 °C overnight. After 24h, via spectrophotometric method at 590 nm, the density was adjusted to obtain a suspension of 0.5 McFarland (standard turbidity) corresponding approximately to 1–2 × $10^8$ CFU/mL suspension. The inactivation experiment was conducted by spiking an aliquot of bacterial suspension with an initial density of $10^8$ CFU/mL to the reaction solution, already added with the catalyst, in order to dilute it up to a concentration of $10^6$ CFU/mL. The stirred mixture was then sampled after 60 minutes in the dark and then at time intervals of 0, 5, 10, 15, 30, 60, and 180 minutes. Subsequently, through the technique for inclusion of the inoculum in a solidifiable substrate ("Pour Plate"), the sample to be analyzed was inoculated into an empty sterile 90 mm Petri dish, then adding the agarized substrate (12-15 ml) kept in fusion at 45-46°C. For this procedure, a selective medium for the isolation and enumeration of fecal streptococci (Slanetz & Bartley agar) was used. The inactivation of total (initial concentration 1.0 × $10^6$ CFU/mL) Enterococci was evaluated after 24 hours incubation on this substrate. Bacterial count was performed in triplicate.

## 6.5 Results and discussions

### 6.5.1 Kinetic results

Heterogeneous photocatalysis (with $CeO_2$, $La_2O_3$ and LC10) of a levofloxacin solution with an initial concentration of 1 mg/L was carried out under artificial irradiation simulating solar light. Before undertaking the levofloxacin photodegradation studies, a control experiment was carried out under dark conditions. Under these conditions, a slight degradation is observable in the systems using cerium (A, C). No degradation was observed in the system using lanthanum (B). The degradation profile of levofloxacin during heterogeneous photocatalysis reactions was monitored using High-Performance Liquid Chromatography - Ultra Violet (HPLC-UV).

The direct irradiation of the levofloxacin solution was conducted for 180 min with regular sampling at determined intervals time. HPLC-UV analysis show a gradual degradation for levofloxacin and a steady decrease in the concentrations versus the time of irradiation.

Due to their similar degradation trend photocatalysis degradations seem to be modelled with a first-order kinetic according to the following equation:

$$\mathrm{Ln}\,(C_t) = \mathrm{Ln}\,(C_0) - k*t$$

The plot of $C/C_0$ ratio (where C is the concentration of the compound at time t, $C_0$ is its initial concentration) versus irradiation time, suggests the first-order kinetics of the photocatalysis reaction (Figure 31).

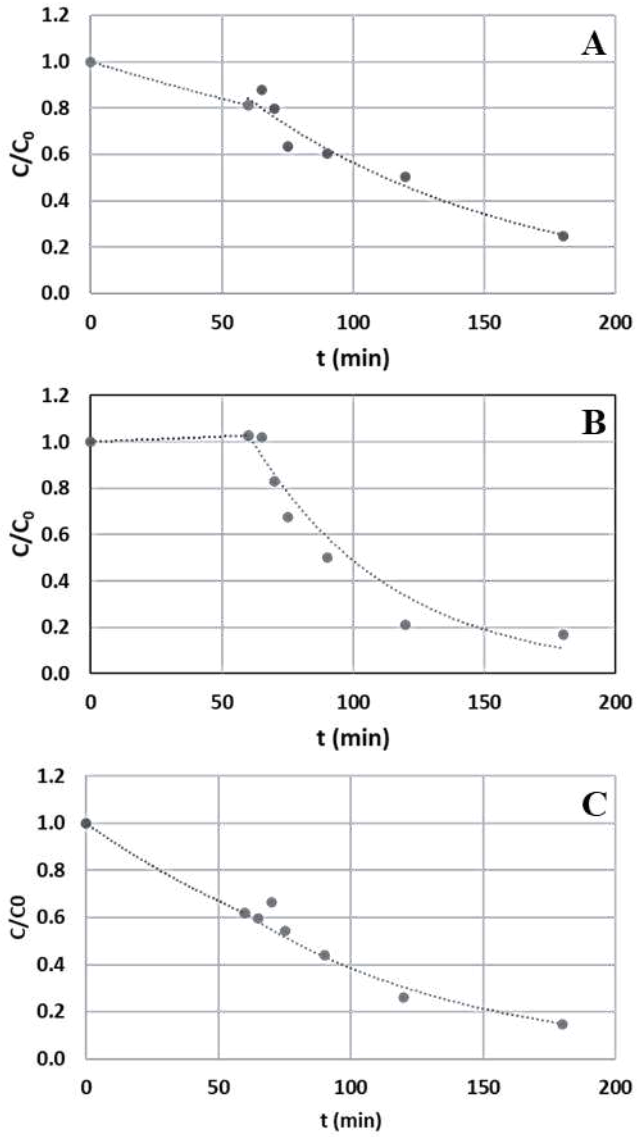


**Figure 31:** Removal of Levofloxacin as a function of time during photocatalytic treatment at pH 7 in the presence of the catalysts $CeO_2$ (**A**), $La_2O_3$ (**B**) and LC10 (**C**). Average results of duplicate measurements are shown.

Kinetic results demonstrated that catalyst $CeO_2$ is capable to degrading 75% of the target compound in 120 min of irradiation. In the dark its degradation capacity is only 19%. With catalyst $La_2O_3$ the degradation is faster with a removal rate of 83% after 120 min. Lanthanum cerate nanopowders coded as LC10 show a degradation efficiency of 85% in 120 min. Probably, regarding the combined catalyst, the greatest contribution in the removal of the drug is provided by lanthanum alone. Even in the dark phase LC10 shows the best adsorption response with a removal percentage of 38%.

### 6.5.2 Inactivation kinetic results

Preliminary tests were carried out to evaluate the multiple contribution of simulated solar radiation coupled with 0.5 g/L of REE-catalysts in AOP process aimed to degrading target bacteria. The inactivation profiles of levofloxacin-resistant *Enterococcus faecalis* ATCC 29212 strain starting from an initial concentration of $1.0 \times 10^6$ CFU/mL are shown in Figure 32. Heterogeneous photocatalysis (with $CeO_2$, $La_2O_3$ and LC10) on bacteria does not show significant effects on their inactivation in the dark phase. Under these conditions, a slight degradation is observable in the SS/$La_2O_3$ system.

Approximately 2.5 log unit enterococci inactivation was observed after 60 min of experiments for SS/$CeO_2$ system. After 60 minutes, the process completely removes all bacterial cells.

The SS/$La_2O_3$ system, on the other hand, shows a higher degradation rate given that the enterococci inactivation occurs only after 5 minutes through a drastic decrease of approximately 2.1 log unit enterococci starting from the dark phase.

Finally, the SS/LC10 system follows an inactivation kinetics of the biological target very similar to that found for the SS/$CeO_2$ system. Also in this case the process removes the biological target after 60 minutes of activity with an inactivation rate equal approximately to 2.5 log units of enterococci.

Similarly to the tests conducted on the photodegradation of the drug levofloxacin, this analysis on bacterial inactivation, using the same catalysts, shows how even for the case of the biological target the most effective system is the one that uses lanthanum alone. In the SS/$La_2O_3$ system the best performance in the dark phase is also observed.

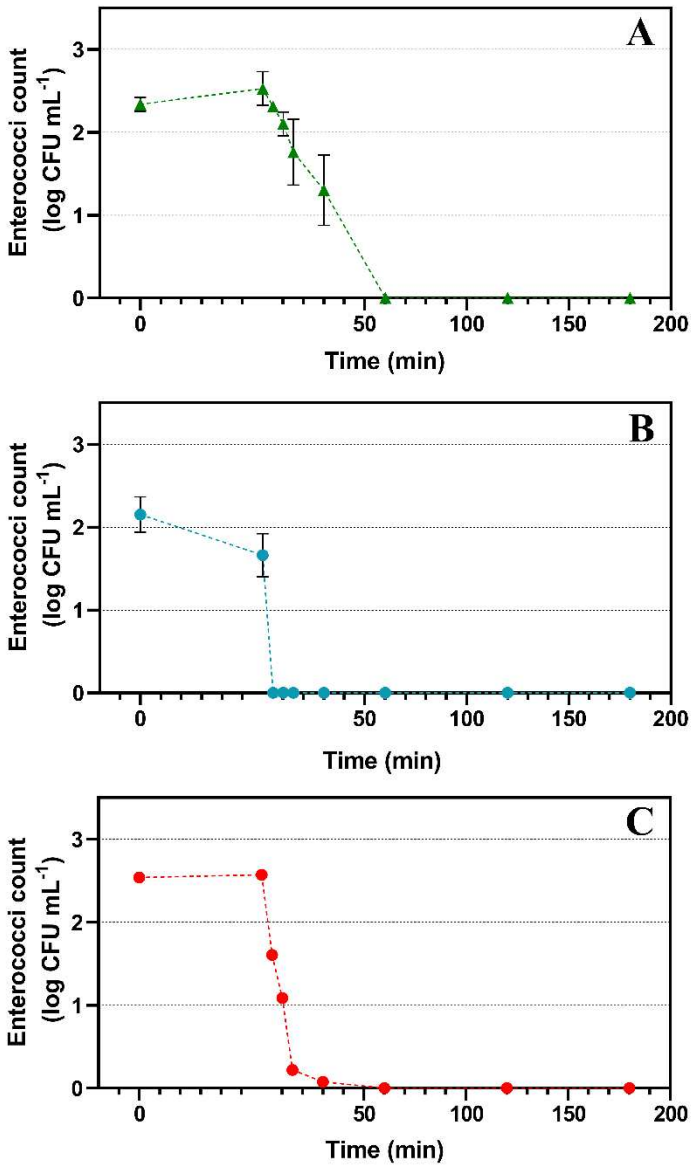


**Figure 32:** Effect of simulated solar radiation coupled with 0.5 g/L of REE-catalysts on the inactivation of levofloxacin-resistant *Enterococcus faecalis* ATCC 29212 strain. (**A**) $CeO_2$, (**B**) $La_2O_3$ and (**C**) LC10. Results are shown as logarithm of CFU $mL^{-1}$.

## 6.6 Conclusions

REEs have been shown to be promising for removing hazardous organic compounds from aqueous solutions, such as wastewater. The effectiveness of REEs in this regard depends mainly on the presence of oxygen vacancies and the concentration of REE ions in the catalysts. Specifically, the metal oxide surfaces promote the decomposition of hydrogen peroxide, which leads to the formation of hydroxide species responsible for the degradation of organic compounds.

The preliminary study on the degradation of the drug levofloxacin presented in this chapter highlights how REE-based catalysts can play an important role in the removal of emerging contaminants. At first kinetic results on chemical target demonstrated that catalyst $CeO_2$ is capable to degrading 75% of the target compound in 120 min of irradiation. In the dark its degradation capacity is only 19%. With catalyst $La_2O_3$ the degradation is faster with a removal rate of 83% after 120 min. Lanthanum cerate nanopowders coded as LC10 show a degradation efficiency of 85% in 120 min. Secondly, heterogeneous photocatalysis on biological target has highlighted that the best disinfection system is SS/$La_2O_3$ which shows a drastic decrease of approximately 2.1 log units of enterococci starting from the dark phase up to 5 minutes of the process. The SS/$CeO_2$ and SS/LC10 systems have almost overlapping bacterial inactivation kinetics and allow the removal of the biological target after 60 minutes of treatment with an inactivation rate equal to approximately 2.5 log units of enterococci. Ultimately the SS/$La_2O_3$ system shows the best degradation performance in kinetic terms both with regards to the chemical and biological target.

The combination of rare earth elements (REEs) with catalysts in AOPs is attracting great interest due to the exceptional properties of rare earths. Furthermore, AOPs that include REE combined catalysts and other parameters should be chosen based on the nature of the contaminants and the acid-base properties of the wastewater to be treated. Overall, the application of REEs as catalysts in water purification represents a promising field of research and development, as these elements have the potential to revolutionize wastewater treatment. It is also important to also address the challenges related to their availability and environmental impact, in fact being able to produce clean water without generating traces of persistent toxins remains a challenging objective.

# GENERAL CONCLUSIONS & OUTLOOK

The field of wastewater treatment is dynamic and constantly evolving, demanding tailored solutions that account for specific local conditions and requirements. Proper wastewater management is critical to protecting human health and the environment, and requires a holistic approach that takes into account the specific challenges of each situation. To ensure the safe reuse of wastewater, strict guidelines and regulations could be established, water quality carefully monitored, and advanced treatment systems used. Nowadays, available data relating to the effectiveness of removal of emerging contaminants (ECs) in WWTPs allow us to conclude that a substantial part of these exits secondary wastewater treatment unchanged and therefore conventional WWTPs does not constitute a safe primary barrier against the spread of these contaminants. Furthermore, it is clear that the presence and transformation of pharmaceuticals in wastewater has become an issue of growing environmental concern. In this thesis, in fact, particular attention was given to the transformation by-products deriving from simulated chlorination processes which imitate the same normally present in purification plants. It has been observed that transformation by-products can have similar or even more powerful biological effects than the original compound, therefore ecotoxicological analysis represents in this regard an indispensable tool for assessing health and environmental risk.

The application of new efficient water management strategies is a key element to increase water productivity. Advanced oxidation processes (AOPs) appear to be a valid alternative for the treatment of such biologically persistent wastewaters because they are based on the formation of highly reactive and non-selective free radicals (especially hydroxyl radical, HO•) which are capable of mineralising almost all organic contaminants. AOPs can be effective for removing a wide range of ECs, including pharmaceuticals and personal care products (PPCPs), and other pollutants. AOPs can be adapted to meet specific objectives, for example to improve the performance of the entire WWTP in the future, a possible option could be to apply AOPs before (pre-treatment, to increase biodegradability) or after (post -treatment, to improve water quality) a biological treatment. Each of these AOPs offers unique advantages and limitations, making them suitable for different water treatment

scenarios. In particular, AOPs in heterogeneous phase involve the use of catalysts that allow the chemical oxidation reactions to be accelerated and the quantity of oxidizing reagents required to be reduced. Recently, the application of Rare Earth Elements (REEs) in AOPs has gained growing interest. Heterogeneous catalysts doped with REEs are a class of catalysts that incorporate these elements into a solid support or substrate, typically a metal oxide, to enhance their catalytic activity for various chemical reactions. This possible application is discussed in the last chapter of this thesis with particular attention to the degradation of pharmaceutical products (Levofloxacin) and the removal of antibiotic-resistant bacteria (*E. faecalis*) using nanopowders of cerium, lanthanum and a combination of the two. The combination of REEs with catalysts in AOPs is attracting great interest due to the exceptional properties of rare earths and therefore their implementation in WWTPs could be thought of in the future. Overall, the application of REEs as catalysts in water purification represents a promising field of research and development, as these elements have the potential to revolutionize wastewater treatment. However, one of the main obstacles to large-scale implementation of AOPs is their cost, which includes both energy consumption and capital costs for installing and operating the reactors. It is important to consider these factors when choosing an AOP, particularly if you are aiming for a large-scale application.

In addition to the observations made in this thesis, it is essential to consider further critical challenges and potential solutions in the realm of wastewater treatment and the reuse of treated wastewater:

*Energy Efficiency in AOPs:* While advanced oxidation processes (AOPs) have demonstrated their efficacy, they often come with a substantial energy demand, particularly in larger applications. This presents a pressing issue, calling for ongoing research aimed at improving the energy efficiency of AOPs. Innovations in reactor design, the incorporation of renewable energy sources, and process optimization are potential solutions to reduce energy consumption and minimize the environmental footprint of these processes.

*Scaling AOPs for Large-Scale Application:* One of the practical challenges we face is scaling up AOPs for broader use, requiring considerable infrastructure and resources. To address this challenge, collaborative efforts involving governmental bodies, research institutions, and the private sector should be encouraged. Together,

these stakeholders can work on developing standardized and cost-effective AOP systems that are well-suited for widespread deployment.

*Ecological Impact of AOPs:* AOPs generate highly reactive radicals, raising concerns about potential ecological consequences in receiving waters. To mitigate this issue, research should aim to better understand the fate of these radicals in natural ecosystems and devise strategies to minimize any unintended harm to non-target organisms.

*Sustainable Sourcing of REEs:* The application of Rare Earth Elements (REEs) in AOPs highlights the importance of sustainable sourcing. Efforts should focus on promoting responsible mining practices and establishing recycling programs for REEs, particularly from end-of-life products. These initiatives can reduce environmental harm and reduce the reliance on new mining.

*Public Awareness and Policy Advocacy:* A persistent challenge is the limited public awareness regarding responsible wastewater management and the potential risks associated with emerging contaminants. Advocacy for informed policy-making and public awareness campaigns is instrumental in promoting responsible wastewater management practices. These efforts contribute to safer water reuse and a healthier environment.

*International Collaboration:* Many emerging contaminants transcend national borders, necessitating global cooperation. International collaboration among researchers, regulatory bodies, and governments is vital for the exchange of best practices, data, and technologies to address emerging contaminants on a global scale.

*Continuous Monitoring and Research:* The dynamic nature of the wastewater treatment field necessitates continuous monitoring and research. New contaminants may emerge over time, and ongoing research is crucial to adapt treatment technologies and stay ahead of new challenges. This commitment to research and innovation ensures the continued protection of human health and the environment.

In conclusion, by addressing these critical challenges and considering potential solutions, we can further enhance the effectiveness of wastewater treatment and work toward a more sustainable and environmentally responsible future. These efforts collectively contribute to safeguarding both human health and the environment, underlining the dynamic and evolving nature of wastewater treatment.

# *References*


1. Shiklomanov, I.A., *World water resources: a new appraisal and assessment for the 21st century.* 1998.
2. Winpenny, J., *et al.*, *The wealth of waste: the economics of wastewater use in agriculture.* Water Reports, 2010(35).
3. Organization, W.H., *WHO guidelines for the safe use of wasterwater excreta and greywater*. Vol. 1. 2006: World Health Organization.
4. Qadir, M., *et al.*, *The challenges of wastewater irrigation in developing countries.* Agricultural water management, 2010. **97**(4): p. 561-568.
5. Trinh, L.T., *et al.*, *Exploring the potential for wastewater reuse in agriculture as a climate change adaptation measure for Can Tho City, Vietnam.* Agricultural Water Management, 2013. **128**: p. 43-54.
6. Jackson, J. and R. Sutton, *Sources of endocrine-disrupting chemicals in urban wastewater, Oakland, CA.* Science of the total environment, 2008. **405**(1-3): p. 153-160.
7. Jaramillo, M.F. and I. Restrepo, *Wastewater reuse in agriculture: A review about its limitations and benefits.* Sustainability, 2017. **9**(10): p. 1734.
8. Verlicchi, P., M. Al Aukidy, and E. Zambello, *Occurrence of pharmaceutical compounds in urban wastewater: removal, mass load and environmental risk after a secondary treatment—a review.* Science of the total environment, 2012. **429**: p. 123-155.
9. Verlicchi, P., *et al.*, *Hospital effluent: investigation of the concentrations and distribution of pharmaceuticals and environmental risk assessment.* Science of the total environment, 2012. **430**: p. 109-118.
10. Lombardo-Agüí, M., *et al.*, *Multiresidue analysis of quinolones in water by ultra-high perfomance liquid chromatography with tandem mass spectrometry using a simple and effective sample treatment.* Journal of separation science, 2014. **37**(16): p. 2145-2152.
11. Carrotte-Lefebvre, I., *et al.*, *Contact allergy to octocrylene: first 2 cases.* Contact Dermatitis, 2003. **48**(1): p. 45-55.
12. Chen, C.-Y., *et al.*, *Non-conventional water reuse in agriculture: A circular water economy.* Water Research, 2021. **199**: p. 117193.
13. Rosen, S. and J.R. Vincent, *Household water resources and rural productivity in Sub-Saharan Africa: A review of the evidence*. Vol. 673. 1999: Citeseer.
14. Nkue Nouwezem, D.J. and G. Libralato, *Integrated Water Resources Management: From Spring to Reuse*, in *Clean Water and Sanitation*, W. Leal Filho, *et al.*, Editors. 2022, Springer International Publishing: Cham. p. 357-369.
15. *AQUASTAT*, FAO, Editor. 2021.
16. *World Economic Forum*. Global Risks 10th ed. 2015.
17. Ali, I. and H.Y. Aboul-Enein, *Chiral pollutants: distribution, toxicity and analysis by chromatography and capillary electrophoresis*. 2005: John Wiley & Sons.
18. *Water Reuse within a Circular Economy Context*. 2020, UNESCO & WSSM.
19. Helmer, R. and I. Hespanhol, *Water pollution control: a guide to the use of water quality management principles*. 1997: CRC Press.

20. Jiménez Cisneros, B.E., *et al.*, *Freshwater resources.* 2014.
21. Doorenbos, J. and W. Pruitt, *Crop water requirements. FAO irrigation and drainage paper 24.* Land and Water Development Division, FAO, Rome, 1977. **144**(1).
22. Oller, I., S. Malato, and J. Sánchez-Pérez, *Combination of advanced oxidation processes and biological treatments for wastewater decontamination—a review.* Science of the total environment, 2011. **409**(20): p. 4141-4166.
23. Bartram, J. and R. Ballance, *Water quality monitoring: a practical guide to the design and implementation of freshwater quality studies and monitoring programmes*. 1996: CRC Press.
24. Bitton, G., *Wastewater microbiology*. 2005: John Wiley & Sons.
25. Deblonde, T., C. Cossu-Leguille, and P. Hartemann, *Emerging pollutants in wastewater: a review of the literature.* International journal of hygiene and environmental health, 2011. **214**(6): p. 442-448.
26. Pal, A., *et al.*, *Impacts of emerging organic contaminants on freshwater resources: review of recent occurrences, sources, fate and effects.* Science of the total environment, 2010. **408**(24): p. 6062-6069.
27. Chhaya, T. Raychoudhury, and S.K. Prajapati, *Bioremediation of pharmaceuticals in water and wastewater.* Microbial bioremediation & biodegradation, 2020: p. 425-446.
28. WHO, *Pharmaceuticals in drinking-water*. 2012.
29. Bottoni, P., S. Caroli, and A.B. Caracciolo, *Pharmaceuticals as priority water contaminants.* Toxicological & Environmental Chemistry, 2010. **92**(3): p. 549-565.
30. Nikolaou, A., S. Meric, and D. Fatta, *Occurrence patterns of pharmaceuticals in water and wastewater environments.* Analytical and bioanalytical chemistry, 2007. **387**: p. 1225-1234.
31. Mompelat, S., B. Le Bot, and O. Thomas, *Occurrence and fate of pharmaceutical products and by-products, from resource to drinking water.* Environment international, 2009. **35**(5): p. 803-814.
32. Filby, A.L., *et al.*, *Health impacts of estrogens in the environment, considering complex mixture effects.* Environmental health perspectives, 2007. **115**(12): p. 1704-1710.
33. Thorpe, K.L., *et al.*, *Relative potencies and combination effects of steroidal estrogens in fish.* Environmental science & technology, 2003. **37**(6): p. 1142-1149.
34. Sumpter, J.P. and A.C. Johnson, *Lessons from endocrine disruption and their application to other issues concerning trace organics in the aquatic environment.* Environmental science & technology, 2005. **39**(12): p. 4321-4332.
35. Zhou, S., *et al.*, *Drug bioactivation covalent binding to target proteins and toxicity relevance.* Drug metabolism reviews, 2005. **37**(1): p. 41-213.
36. Escher, B.I., *et al.*, *In vitro assessment of modes of toxic action of pharmaceuticals in aquatic life.* Environmental science & technology, 2005. **39**(9): p. 3090-3100.
37. Morley, N.J., *Environmental risk and toxicology of human and veterinary waste pharmaceutical exposure to wild aquatic host–parasite relationships.* Environmental Toxicology and Pharmacology, 2009. **27**(2): p. 161-175.
38. Celiz, M.D., J. Tso, and D.S. Aga, *Pharmaceutical metabolites in the environment: analytical challenges and ecological risks.* Environmental Toxicology and Chemistry, 2009. **28**(12): p. 2473-2484.
39. Schwarzenbach, R.P., *et al.*, *Global water pollution and human health.* Annual review of environment and resources, 2010. **35**: p. 109-136.

40. Balasuriya, A., *Coastal area management: Biodiversity and ecological sustainability in Sri Lankan perspective*, in *Biodiversity and climate change adaptation in tropical islands*. 2018, Elsevier. p. 701-724.
41. Ambulkar, A. and J.A. Nathanson, *Wastewater treatment.* Encyclopedia Britannica, 2021.
42. Hreiz, R., M.A. Latifi, and N. Roche, *Optimal design and operation of activated sludge processes: State-of-the-art.* Chemical Engineering Journal, 2015. **281**: p. 900-920.
43. Comninellis, C., *et al.*, *Advanced oxidation processes for water treatment: advances and trends for R&D.* Journal of Chemical Technology & Biotechnology: International Research in Process, Environmental & Clean Technology, 2008. **83**(6): p. 769-776.
44. Skoumal, M., *et al.*, *Mineralization of paracetamol by ozonation catalyzed with Fe2+, Cu2+ and UVA light.* Applied Catalysis B: Environmental, 2006. **66**(3-4): p. 228-240.
45. Poyatos, J.M., *et al.*, *Advanced oxidation processes for wastewater treatment: state of the art.* Water, Air, and Soil Pollution, 2010. **205**: p. 187-204.
46. Ribeiro, A.R., *et al.*, *An overview on the advanced oxidation processes applied for the treatment of water pollutants defined in the recently launched Directive 2013/39/EU.* Environment international, 2015. **75**: p. 33-51.
47. Andreozzi, R., *et al.*, *Advanced oxidation processes (AOP) for water purification and recovery.* Catalysis today, 1999. **53**(1): p. 51-59.
48. Aieta, E.M., *et al.*, *Advanced Oxidation Processes for Treating Groundwater Contaminated With TCE and PCE: Pilot-Scale Evaluations.* Journal-American Water Works Association, 1988. **80**(5): p. 64-72.
49. Xu, X., *et al.*, *An overview on the application of advanced oxidation processes for the removal of naphthenic acids from water.* Critical Reviews in Environmental Science and Technology, 2017. **47**(15): p. 1337-1370.
50. Hoigné, J. and H. Bader, *Rate constants of reactions of ozone with organic and inorganic compounds in water—I: non-dissociating organic compounds.* Water Research, 1983. **17**(2): p. 173-183.
51. Zhang, N., *et al.*, *Ceria accelerated nanoscale zerovalent iron assisted heterogenous Fenton oxidation of tetracycline.* Chemical Engineering Journal, 2019. **369**: p. 588-599.
52. Oliverio, M., *et al.*, *Erbium salts as non-toxic catalysts compatible with alternative reaction media.* Sustainability, 2018. **10**(3): p. 721.
53. Zinatloo-Ajabshir, S., M. Emsaki, and G. Hosseinzadeh, *Innovative construction of a novel lanthanide cerate nanostructured photocatalyst for efficient treatment of contaminated water under sunlight.* Journal of Colloid and Interface Science, 2022. **619**: p. 1-13.
54. Ambaye, T.G., *et al.*, *Emerging technologies for the recovery of rare earth elements (REEs) from the end-of-life electronic wastes: a review on progress, challenges, and perspectives.* Environmental Science and Pollution Research, 2020. **27**: p. 36052-36074.
55. Chan, S.H.S., *et al.*, *Recent developments of metal oxide semiconductors as photocatalysts in advanced oxidation processes (AOPs) for treatment of dye waste-water.* Journal of Chemical Technology & Biotechnology, 2011. **86**(9): p. 1130-1158.
56. Bokare, A.D. and W. Choi, *Review of iron-free Fenton-like systems for activating H2O2 in advanced oxidation processes.* Journal of hazardous materials, 2014. **275**: p. 121-135.

57. Onozuka, K., *et al.*, *Perovskite-type La2Ti2O7 mesoporous photocatalyst.* Journal of Solid State Chemistry, 2012. **192**: p. 87-92.
58. Assila, O., *et al.*, *Degradation of pollutants in water by Fenton-like oxidation over LaFe-catalysts: Optimization by experimental design.* Microporous and Mesoporous Materials, 2023. **349**: p. 112422.
59. Song, J., *et al.*, *Insights into mechanism of catalytic ozonation of cinnamyl alcohol over core–shell Fe3O4@ SiO2@ La2O3 catalyst.* Separation and Purification Technology, 2022. **282**: p. 119969.
60. Fatta-Kassinos, D., M.I. Vasquez, and K. Kümmerer, *Transformation products of pharmaceuticals in surface waters and wastewater formed during photolysis and advanced oxidation processes–degradation, elucidation of by-products and assessment of their biological potency.* Chemosphere, 2011. **85**(5): p. 693-709.
61. Rosal, R., *et al.*, *Identification of intermediates and assessment of ecotoxicity in the oxidation products generated during the ozonation of clofibric acid.* Journal of Hazardous Materials, 2009. **172**(2-3): p. 1061-1068.
62. Sirtori, C., *et al.*, *Effect of water-matrix composition on Trimethoprim solar photodegradation kinetics and pathways.* Water research, 2010. **44**(9): p. 2735-2744.
63. Romanucci, V., *et al.*, *Disinfection by-products and ecotoxic risk associated with hypochlorite treatment of irbesartan.* Science of The Total Environment, 2020. **712**: p. 135625.
64. Luongo, G., *et al.*, *LC and NMR studies for identification and characterization of degradation by-products of olmesartan acid, elucidation of their degradation pathway and ecotoxicity assessment.* Molecules, 2021. **26**(6): p. 1769.
65. Luongo, G., *et al.*, *Secondary Effects of Hypochlorite Treatment on the Emerging Pollutant Candesartan: The Formation of Degradation By-products and Their Toxicological Profiles.* Molecules, 2021. **26**(11): p. 3422.
66. Luongo, G., *et al.*, *Complete Characterization of Degradation By-products of Olmesartan Acid, Degradation Pathway, and Ecotoxicity Assessment.* Applied Sciences, 2021. **11**(12): p. 5393.
67. Siciliano, A., *et al.*, *Newly Discovered Irbesartan Disinfection By-products via Chlorination: Investigating Potential Environmental Toxicity.* Applied Sciences, 2023. **13**(14): p. 8170.
68. Zenker, A., *et al.*, *Bioaccumulation and biomagnification potential of pharmaceuticals with a focus to the aquatic environment.* Journal of environmental management, 2014. **133**: p. 378-387.
69. Yaghmaeian, K., G. Moussavi, and A. Alahabadi, *Removal of amoxicillin from contaminated water using NH4Cl-activated carbon: Continuous flow fixed-bed adsorption and catalytic ozonation regeneration.* Chemical Engineering Journal, 2014. **236**: p. 538-544.
70. Rivera-Utrilla, J., *et al.*, *Pharmaceuticals as emerging contaminants and their removal from water. A review.* Chemosphere, 2013. **93**(7): p. 1268-1287.
71. Ibáñez, M., *et al.*, *Removal of emerging contaminants in sewage water subjected to advanced oxidation with ozone.* Journal of hazardous materials, 2013. **260**: p. 389-398.
72. Kim, S., *et al.*, *Removal of contaminants of emerging concern by membranes in water and wastewater: A review.* Chemical Engineering Journal, 2018. **335**: p. 896-914.
73. Delgado-Moreno, L., *et al.*, *Innovative application of biobed bioremediation systems to remove emerging contaminants: Adsorption, degradation and bioaccesibility.* Science of the Total Environment, 2019. **651**: p. 990-997.

74. Kanakaraju, D., B.D. Glass, and M. Oelgemöller, *Advanced oxidation process-mediated removal of pharmaceuticals from water: A review.* Journal of environmental management, 2018. **219**: p. 189-207.
75. Ladhari, A., *et al.*, *Sartans: What they are for, how they degrade, where they are found and how they transform.* Sustainable Chemistry and Pharmacy, 2021. **20**: p. 100409.
76. Hollender, J., *et al.*, *Comprehensive micropollutant screening using LC-HRMS/MS at three riverbank filtration sites to assess natural attenuation and potential implications for human health.* Water research X, 2018. **1**: p. 100007.
77. Fekadu, S., *et al.*, *Pharmaceuticals in freshwater aquatic environments: A comparison of the African and European challenge.* Science of the total Environment, 2019. **654**: p. 324-337.
78. Fick, J., *et al.*, *Results from the Swedish National Screening Programme 2010 Subreport 3. Pharmaceuticals*. 2011, IVL Svenska Miljöinstitutet.
79. Minguez, L., *et al.*, *Toxicities of 48 pharmaceuticals and their freshwater and marine environmental assessment in northwestern France.* Environmental Science and Pollution Research, 2016. **23**: p. 4992-5001.
80. Bayer, A., *et al.*, *Behavior of sartans (antihypertensive drugs) in wastewater treatment plants, their occurrence and risk for the aquatic environment.* Environmental Science and Pollution Research, 2014. **21**(18): p. 10830-10839.
81. Schwabe, U. and D. Paffrath, *Report on Pharmaceutical Prescriptions*. 2013, Springer: Berlin/Heidelberg, Germany.
82. Letzel, T., *et al.*, *LC–MS screening techniques for wastewater analysis and analytical data handling strategies: Sartans and their transformation products as an example.* Chemosphere, 2015. **137**: p. 198-206.
83. Al-Rajab, A.J., *et al.*, *Investigation of the presence of pharmaceuticals and personal care products (PPCPs) in groundwater of Jazan area, Saudi Arabia.* Tropical Journal of Pharmaceutical Research, 2018. **17**(10): p. 2061-2066.
84. Patel, M., *et al.*, *Pharmaceuticals of emerging concern in aquatic systems: chemistry, occurrence, effects, and removal methods.* Chemical reviews, 2019. **119**(6): p. 3510-3673.
85. ISO, I., *8692:2012. Water quality - fresh water algal growth inhibition test with unicellular green algae.* 2012.
86. ISO, I., *11348-3. Water quality-Determination of the inhibitory effect of water samples on the light emission of Vibrio fischeri (Luminescent bacteria test)-Part 3: Method using freeze-dried bacteria.* International Organization for Standardization, London, UK, 2007.
87. ISO, E., *Water quality—Determination of the inhibition of the mobility of Daphnia magna Straus (Cladocera, Crustacea)—Acute toxicity test.* EN ISO, 2012. **6341**: p. 1996.
88. Bedner, M. and W.A. MacCrehan, *Transformation of acetaminophen by chlorination produces the toxicants 1, 4-benzoquinone and N-acetyl-p-benzoquinone imine.* Environmental science & technology, 2006. **40**(2): p. 516-522.
89. Romanucci, V., *et al.*, *Disinfection by-products and Ecotoxic risk associated with hypochlorite treatment of tramadol.* Molecules, 2019. **24**(4): p. 693.
90. Zhang, M., *et al.*, *A simple method for removal of carbon nanotubes from wastewater using hypochlorite.* Scientific reports, 2019. **9**(1): p. 1284.

91. Carpinteiro, I., *et al.*, *Free chlorine reactions of angiotensin II receptor antagonists: Kinetics study, transformation products elucidation and in-silico ecotoxicity assessment.* Science of The Total Environment, 2019. **647**: p. 1000-1010.
92. Mutha, V.A.K., *et al.*, *Degradation study of irbesartan: Isolation and structural elucidation of novel degradants.* Journal of Pharmaceutical and Biomedical Analysis, 2018. **157**: p. 180-188.
93. Shah, R.P., A. Sahu, and S. Singh, *Identification and characterization of degradation products of irbesartan using LC–MS/TOF, MSn, on-line H/D exchange and LC–NMR.* Journal of pharmaceutical and biomedical analysis, 2010. **51**(5): p. 1037-1046.
94. Luongo, G., *et al.*, *Peracetic acid vs. sodium hypochlorite: Degradation and transformation of drugs in wastewater.* Molecules, 2020. **25**(10): p. 2294.
95. Cousaert, N., *et al.*, *Efficient, protection-free Suzuki–Miyaura synthesis of ortho-biphenyltetrazoles.* Tetrahedron letters, 2005. **46**(38): p. 6529-6532.
96. Rao, K.V.P., *et al.*, *A novel approach for the conversion of primary amides into tetrazoles by using tributyltin chloride and sodium azide in the presence of DMF.* Synlett, 2007. **2007**(08): p. 1289-1293.
97. Persoone, G., *et al.*, *A practical and user-friendly toxicity classification system with microbiotests for natural waters and wastewaters.* Environmental Toxicology: An International Journal, 2003. **18**(6): p. 395-402.
98. Cui, H., *et al.*, *Toxicity of 17 disinfection by-products to different trophic levels of aquatic organisms: ecological risks and mechanisms.* Environmental Science & Technology, 2021. **55**(15): p. 10534-10541.
99. Prasse, C., U. von Gunten, and D.L. Sedlak, *Chlorination of phenols revisited: unexpected formation of α, β-unsaturated C4-dicarbonyl ring cleavage products.* Environmental science & technology, 2020. **54**(2): p. 826-834.
100. Grbović, G., *et al.*, *Synthesis, characterisation and aquatic ecotoxicity of the UV filter hexyl 2-(4-diethylamino-2-hydroxybenzoyl) benzoate (DHHB) and its chlorinated by-products.* Environmental chemistry, 2015. **13**(1): p. 119-126.
101. Kumaraswamy, K., *et al.*, *Isolation and characterization of novel degradation products of valsartan by nmr and high resolution mass spectroscopy: Development and validation of valsartan by UPLC.* Asian J. Chem, 2020. **32**: p. 1064-1068.
102. Zarrelli, A., *et al.*, *Chemical fate and genotoxic risk associated with hypochlorite treatment of nicotine.* Science of the total environment, 2012. **426**: p. 132-138.
103. Zarrelli, A., *et al.*, *Ecotoxicological evaluation of caffeine and its derivatives from a simulated chlorination step.* Science of the total environment, 2014. **470**: p. 453-458.
104. Trincado, M., *et al.*, *Domino Rhodium/Palladium-Catalyzed Dehydrogenation Reactions of Alcohols to Acids by Hydrogen Transfer to Inactivated Alkenes.* Chemistry–A European Journal, 2010. **16**(9): p. 2751-2757.
105. Siciliano, A., *et al.*, *Amoxicillin in water: Insights into relative reactivity, by-product formation, and toxicological interactions during chlorination.* Applied Sciences, 2021. **11**(3): p. 1076.
106. Dimitrakopoulou, D., *et al.*, *Degradation, mineralization and antibiotic inactivation of amoxicillin by UV-A/TiO2 photocatalysis.* Journal of environmental management, 2012. **98**: p. 168-174.

107. Trampuž, M., G. Stavber, and B. Likozar, *Catalyst-free aza-Michael addition for C–N coupling in active pharmaceutical ingredient synthesis: Modelling of thermodynamic, reaction kinetics and mass transfer considerations.* Chemical Engineering Journal, 2019. **374**: p. 924-936.
108. Grom, M., *et al.*, *Modelling chemical kinetics of a complex reaction network of active pharmaceutical ingredient (API) synthesis with process optimization for benzazepine heterocyclic compound.* Chemical Engineering Journal, 2016. **283**: p. 703-716.
109. Robnik, B., *et al.*, *Understanding and kinetic modeling of complex degradation pathways in the solid dosage form: the case of saxagliptin.* Pharmaceutics, 2019. **11**(9): p. 452.
110. Lofrano, G., *et al.*, *Emerging concern from short-term textile leaching: a preliminary ecotoxicological survey.* Bulletin of environmental contamination and toxicology, 2016. **97**: p. 646-652.
111. Medici, A., *et al.*, *Octocrylene: from sunscreens to the degradation pathway during chlorination processes: formation of by-products and their ecotoxicity assessment.* Molecules, 2022. **27**(16): p. 5286.
112. Berardesca, E., *et al.*, *Review of the safety of octocrylene used as an ultraviolet filter in cosmetics.* Journal of the European Academy of Dermatology and Venereology, 2019. **33**: p. 25-33.
113. de Groot, A.C. and D.W. Roberts, *Contact and photocontact allergy to octocrylene: a review.* Contact dermatitis, 2014. **70**(4): p. 193-204.
114. Bennàssar, A., *et al.*, *Two cases of photocontact allergy to the new sun filter octocrylene.* Dermatology online journal, 2009. **15**(12).
115. Karlsson, I., *et al.*, *Clinical and experimental studies of octocrylene's allergenic potency.* Contact Dermatitis, 2011. **64**(6): p. 343-352.
116. Mokh, S., *et al.*, *Chromatographic methods for the determination of a broad spectrum of UV filters in swimming pool water.* Environmental Science and Pollution Research, 2022: p. 1-12.
117. Nakayama, S.F., *et al.*, *Worldwide trends in tracing poly-and perfluoroalkyl substances (PFAS) in the environment.* TrAC Trends in Analytical Chemistry, 2019. **121**: p. 115410.
118. Cheung, M.Y., S. Liang, and J. Lee, *Toxin-producing cyanobacteria in freshwater: A review of the problems, impact on drinking water safety, and efforts for protecting public health.* Journal of Microbiology, 2013. **51**: p. 1-10.
119. Kahn, G. and J.R. Vercellotti. *CARB 100-Commercial applications of powdered activated carbons for decolorizing food products such as fruit juice concentrates and sugar*. in *Abstracts of Papers of the American Chemical Society*. 2008. AMER CHEMICAL SOC 1155 16TH ST, NW, WASHINGTON, DC 20036 USA.
120. Vieira, W.T., *et al.*, *Endocrine-disrupting compounds: Occurrence, detection methods, effects and promising treatment pathways—A critical review.* Journal of Environmental Chemical Engineering, 2021. **9**(1): p. 104558.
121. Valdez-Carrillo, M., *et al.*, *Pharmaceuticals as emerging contaminants in the aquatic environment of Latin America: a review.* Environmental Science and Pollution Research, 2020. **27**: p. 44863-44891.
122. Snow, D.D., *et al.*, *Detection, occurrence and fate of emerging contaminants in agricultural environments.* Water Environment Research, 2012. **84**(10): p. 764-785.

123. de Oliveira, M., *et al.*, *Pharmaceuticals residues and xenobiotics contaminants: occurrence, analytical techniques and sustainable alternatives for wastewater treatment.* Science of the total environment, 2020. **705**: p. 135568.
124. Li, P., *et al.*, *Occurrence and fate of antibiotic residues and antibiotic resistance genes in a reservoir with ecological purification facilities for drinking water sources.* Science of the Total Environment, 2020. **707**: p. 135276.
125. Jean, J., *et al.*, *Identification and prioritization of bioaccumulable pharmaceutical substances discharged in hospital effluents.* Journal of environmental management, 2012. **103**: p. 113-121.
126. Mills, L.J. and C. Chichester, *Review of evidence: are endocrine-disrupting chemicals in the aquatic environment impacting fish populations?* Science of the total environment, 2005. **343**(1-3): p. 1-34.
127. Zhou, Y., *et al.*, *Occurrence, abundance, and distribution of sulfonamide and tetracycline resistance genes in agricultural soils across China.* Science of the Total Environment, 2017. **599**: p. 1977-1983.
128. Parliament, I., *Law 9 December 1998 n. 426.* New Interventions in the Environmental Field, 1998.
129. ISO, I., *10253:2016. Water quality - Marine Algal Growth Inhibition Test with Skeletonema sp. and Phaeodactylum tricornutum.* 2016.
130. Brausch, J.M. and G.M. Rand, *A review of personal care products in the aquatic environment: environmental concentrations and toxicity.* Chemosphere, 2011. **82**(11): p. 1518-1532.
131. Gago-Ferrero, P., *et al.*, *First determination of UV filters in marine mammals. Octocrylene levels in Franciscana dolphins.* Environmental science & technology, 2013. **47**(11): p. 5619-5625.
132. Duis, K., T. Junker, and A. Coors, *Review of the environmental fate and effects of two UV filter substances used in cosmetic products.* Science of The Total Environment, 2022. **808**: p. 151931.
133. Luongo, G., *et al.*, *Oxidation of diclofenac in water by sodium hypochlorite: Identification of new degradation by-products and their ecotoxicological evaluation.* Journal of Pharmaceutical and Biomedical Analysis, 2021. **194**: p. 113762.
134. Kasprzyk-Hordern, B., R.M. Dinsdale, and A.J. Guwy, *The occurrence of pharmaceuticals, personal care products, endocrine disruptors and illicit drugs in surface water in South Wales, UK.* Water research, 2008. **42**(13): p. 3498-3518.
135. Gabarrón, S., *et al.*, *Evaluation of emerging contaminants in a drinking water treatment plant using electrodialysis reversal technology.* Journal of hazardous materials, 2016. **309**: p. 192-201.
136. Huerta-Fontela, M., M.T. Galceran, and F. Ventura, *Occurrence and removal of pharmaceuticals and hormones through drinking water treatment.* Water research, 2011. **45**(3): p. 1432-1442.
137. Boix, C., *et al.*, *Biotransformation of pharmaceuticals in surface water and during waste water treatment: Identification and occurrence of transformation products.* Journal of hazardous materials, 2016. **302**: p. 175-187.
138. Christensen, F., *Pharmaceuticals in the environment—a human risk?* Regulatory toxicology and pharmacology, 1998. **28**(3): p. 212-221.
139. Stuer-Lauridsen, F., *et al.*, *Environmental risk assessment of human pharmaceuticals in Denmark after normal therapeutic use.* Chemosphere, 2000. **40**(7): p. 783-793.
140. Merlin, C., *et al.*, *Persistence and dissemination of the multiple-antibiotic-resistance plasmid pB10 in the microbial communities of wastewater sludge microcosms.* Water research, 2011. **45**(9): p. 2897-2905.

141. Andersson, D.I. and D. Hughes, *Evolution of antibiotic resistance at non-lethal drug concentrations.* Drug resistance updates, 2012. **15**(3): p. 162-172.
142. Boumendjel, A., *et al.*, *Occurrence of the synthetic analgesic tramadol in an African medicinal plant.* Angewandte Chemie International Edition, 2013. **52**(45): p. 11780-11784.
143. Fowler, P.A., *et al.*, *Impact of endocrine-disrupting compounds (EDCs) on female reproductive health.* Molecular and cellular endocrinology, 2012. **355**(2): p. 231-239.
144. Hess-Wilson, J. and K. Knudsen, *Endocrine disrupting compounds and prostate cancer.* Cancer letters, 2006. **241**(1): p. 1-12.
145. Austin, B., *Antibiotic pollution from fish farms: effects on aquatic microflora.* Microbiological Sciences, 1985. **2**(4): p. 113-117.
146. Miranda, C. and G. Castillo, *Resistance to antibiotic and heavy metals of motile aeromonads from Chilean freshwater.* Science of the total environment, 1998. **224**(1-3): p. 167-176.
147. Kovalakova, P., *et al.*, *Occurrence and toxicity of antibiotics in the aquatic environment: A review.* Chemosphere, 2020. **251**: p. 126351.
148. Klein, E.Y., *et al.*, *Global increase and geographic convergence in antibiotic consumption between 2000 and 2015.* Proceedings of the National Academy of Sciences, 2018. **115**(15): p. E3463-E3470.
149. ECDC. *Summary of the latest data on antibiotic consumption in the European Union*. 2016. CDC Atlanta, GA, USA.
150. Prevention, E.C.f.D., Control, and ECDC, *Antimicrobial consumption*. 2018, European Centre for Disease Control (ECDC) Stockholm.
151. Van Boeckel, T.P., *et al.*, *Global antibiotic consumption 2000 to 2010: an analysis of national pharmaceutical sales data.* The Lancet infectious diseases, 2014. **14**(8): p. 742-750.
152. Kotwani, A. and K. Holloway, *Trends in antibiotic use among outpatients in New Delhi, India.* BMC infectious diseases, 2011. **11**: p. 1-9.
153. Lofrano, G., *et al.*, *Photocatalytic degradation of the antibiotic chloramphenicol and effluent toxicity effects.* Ecotoxicology and environmental safety, 2016. **123**: p. 65-71.
154. McGettigan, P. and D. Henry, *Use of non-steroidal anti-inflammatory drugs that elevate cardiovascular risk: an examination of sales and essential medicines lists in low-, middle-, and high-income countries.* PLoS medicine, 2013. **10**(2): p. e1001388.
155. Iroko Pharmaceuticals, L., *Briefing Documents for FDA Joint Meeting of the Arthritis Advisory Committee (AAC) and Drug Safety and Risk Management Advisory Committee (DSARM).* Acesso em, 2016. **4**.
156. http://www.novartis.com/about-novartis/company-history/index.shtml.
157. Food, U. and D. Administration, *FDA Briefing Document, joint meeting of the Arthritis Advisory Committee and the Drug Safety and Risk Management Advisory Committee*. 2018.
158. Green, R.E., *et al.*, *Potential threat to Eurasian griffon vultures in Spain from veterinary use of the drug diclofenac.* Journal of Applied Ecology, 2016. **53**(4): p. 993-1003.
159. Prakash, V., *et al.*, *Catastrophic collapse of Indian white-backed Gyps bengalensis and long-billed Gyps indicus vulture populations.* Biological conservation, 2003. **109**(3): p. 381-390.
160. Oaks, J.L., *et al.*, *Diclofenac residues as the cause of vulture population decline in Pakistan.* Nature, 2004. **427**(6975): p. 630-633.

161. Zhang, Y., S.-U. Geißen, and C. Gal, *Carbamazepine and diclofenac: removal in wastewater treatment plants and occurrence in water bodies.* Chemosphere, 2008. **73**(8): p. 1151-1161.

162. Lonappan, L., *et al.*, *Diclofenac in municipal wastewater treatment plant: quantification using laser diode thermal desorption—atmospheric pressure chemical ionization—tandem mass spectrometry approach in comparison with an established liquid chromatography-electrospray ionization–tandem mass spectrometry method.* Journal of Chromatography A, 2016. **1433**: p. 106-113.

163. Sakshaug, S., *et al.*, *Drug Consumption in Norway 2007-2011.* A Statistical Presentation of the Drug Consumption in Norway during the Years, 2007. **2011**.

164. Ternes, T.A., *Occurrence of drugs in German sewage treatment plants and rivers.* Water research, 1998. **32**(11): p. 3245-3260.

165. Vieno, N. and M. Sillanpää, *Fate of diclofenac in municipal wastewater treatment plant—A review.* Environment international, 2014. **69**: p. 28-39.

166. Le Coadou, L., *et al.*, *Quality survey of natural mineral water and spring water sold in France: Monitoring of hormones, pharmaceuticals, pesticides, perfluoroalkyl substances, phthalates, and alkylphenols at the ultra-trace level.* Science of the Total Environment, 2017. **603**: p. 651-662.

167. Tapie, N., *et al.*, *Passive samplers for chemical substance monitoring and associated toxicity assessment in water.* Water Science and Technology, 2011. **63**(10): p. 2418-2426.

168. Aminot, Y., *et al.*, *Inputs and seasonal removal of pharmaceuticals in the estuarine Garonne River.* Marine Chemistry, 2016. **185**: p. 3-11.

169. López-Serna, R., *et al.*, *Occurrence of 95 pharmaceuticals and transformation products in urban groundwaters underlying the metropolis of Barcelona, Spain.* Environmental Pollution, 2013. **174**: p. 305-315.

170. Miyamoto, G., N. Zahid, and J.P. Uetrecht, *Oxidation of diclofenac to reactive intermediates by neutrophils, myeloperoxidase, and hypochlorous acid.* Chemical research in toxicology, 1997. **10**(4): p. 414-419.

171. Quintana, J.B., *et al.*, *Investigating the chlorination of acidic pharmaceuticals and by-product formation aided by an experimental design methodology.* Water Research, 2010. **44**(1): p. 243-255.

172. Dong, H., *et al.*, *Effects of bromide and iodide on the chlorination of diclofenac: Accelerated chlorination and enhanced formation of disinfection by-products.* Separation and Purification Technology, 2018. **193**: p. 415-420.

173. Földényi, R., S. Joó, and J. Tóth, *Adsorption of diclofenac on activated carbon and its hypochlorination in the presence of dissolved organic matter.* International Journal of Environmental Science and Technology, 2017. **14**: p. 1071-1080.

174. Soufan, M., M. Deborde, and B. Legube, *Aqueous chlorination of diclofenac: kinetic study and transformation products identification.* Water research, 2012. **46**(10): p. 3377-3386.

175. de Oliveira, L.L.D., *et al.*, *Acute and chronic ecotoxicological effects of four pharmaceuticals drugs on cladoceran Daphnia magna.* Drug and Chemical Toxicology, 2016. **39**(1): p. 13-21.

176. Ferrer, I., *et al.*, *Determination of drugs in surface water and wastewater samples by liquid chromatography–mass spectrometry: methods and preliminary results including toxicity studies with Vibrio fischeri.* Journal of Chromatography A, 2001. **938**(1-2): p. 187-197.

177. Ferrari, B.t., *et al.*, *Ecotoxicological impact of pharmaceuticals found in treated wastewaters: study of carbamazepine, clofibric acid, and diclofenac.* Ecotoxicology and environmental safety, 2003. **55**(3): p. 359-370.
178. Cleuvers, M., *Mixture toxicity of the anti-inflammatory drugs diclofenac, ibuprofen, naproxen, and acetylsalicylic acid.* Ecotoxicology and environmental safety, 2004. **59**(3): p. 309-315.
179. Commission, E., *Technical guidance document in support of Commission Directive 93/67/EEC on risk assessment for new notified substances and Commission Regulation (EC) No 1488/94 on risk assessment for existing substances*. 1996: OOPEC.
180. Calza, P., *et al.*, *Solar driven production of toxic halogenated and nitroaromatic compounds in natural seawater.* Science of the total environment, 2008. **398**(1-3): p. 196-202.
181. Diniz, M., *et al.*, *Ecotoxicity of ketoprofen, diclofenac, atenolol and their photolysis by-products in zebrafish (Danio rerio).* Science of the Total Environment, 2015. **505**: p. 282-289.
182. Schmitt-Jansen, M., *et al.*, *Phytotoxicity assessment of diclofenac and its phototransformation products.* Analytical and bioanalytical chemistry, 2007. **387**: p. 1389-1396.
183. Lalumera, G.M., *et al.*, *Preliminary investigation on the environmental occurrence and effects of antibiotics used in aquaculture in Italy.* Chemosphere, 2004. **54**(5): p. 661-668.
184. Jones, O., N. Voulvoulis, and J. Lester, *Aquatic environmental assessment of the top 25 English prescription pharmaceuticals.* Water research, 2002. **36**(20): p. 5013-5022.
185. García-Reiriz, A., P.C. Damiani, and A.C. Olivieri, *Different strategies for the direct determination of amoxicillin in human urine by second-order multivariate analysis of kinetic–spectrophotometric data.* Talanta, 2007. **71**(2): p. 806-815.
186. Calderón-Preciado, D., V. Matamoros, and J.M. Bayona, *Occurrence and potential crop uptake of emerging contaminants and related compounds in an agricultural irrigation network.* Science of the total environment, 2011. **412**: p. 14-19.
187. Straub, J.O., *Environmental risk assessment for new human pharmaceuticals in the European Union according to the draft guideline/discussion paper of January 2001.* Toxicology letters, 2002. **135**(3): p. 231-237.
188. Schreiber, F. and U. Szewzyk, *Environmentally relevant concentrations of pharmaceuticals influence the initial adhesion of bacteria.* Aquatic Toxicology, 2008. **87**(4): p. 227-233.
189. Andreozzi, R., *et al.*, *Antibiotics in the environment: occurrence in Italian STPs, fate, and preliminary assessment on algal toxicity of amoxicillin.* Environmental science & technology, 2004. **38**(24): p. 6832-6838.
190. Alaton, I.A., *et al.*, *Combined chemical and biological oxidation of penicillin formulation effluent.* Journal of Environmental management, 2004. **73**(2): p. 155-163.
191. Navalon, S., M. Alvaro, and H. Garcia, *Reaction of chlorine dioxide with emergent water pollutants: product study of the reaction of three β-lactam antibiotics with ClO2.* Water Research, 2008. **42**(8-9): p. 1935-1942.
192. Kurt, A., *et al.*, *Treatment of antibiotics in wastewater using advanced oxidation processes (AOPs).* Physico-chemical wastewater treatment and resource recovery, 2017. **175**.

193. Moles, S., *et al.*, *Towards the removal of antibiotics detected in wastewaters in the POCTEFA territory: occurrence and TiO2 photocatalytic pilot-scale plant performance.* Water, 2020. **12**(5): p. 1453.

194. Abbassi, B.E., *et al.*, *Antibiotics in wastewater: Their degradation and effect on wastewater treatment efficiency.* J Food Agric Environ, 2016. **14**(3-4): p. 95-9.

195. Calisto, V., *et al.*, *Direct photodegradation of carbamazepine followed by micellar electrokinetic chromatography and mass spectrometry.* Water research, 2011. **45**(3): p. 1095-1104.

196. Chusaksri, S., *et al.*, *Reactions of phenylurea compounds with aqueous chlorine: Implications for herbicide transformation during drinking water disinfection.* Journal of hazardous materials, 2012. **209**: p. 484-491.

197. Sandín-España, P., J. Magrans, and J. García-Baudín, *Study of clethodim degradation and by-product formation in chlorinated water by HPLC.* Chromatographia, 2005. **62**: p. 133-137.

198. Hurst, W.J., J. Mckim, and R. Martin Jr, *HPLC determination of oxalic acid in cocoa.* Journal of liquid chromatography, 1986. **9**(12): p. 2781-2789.

199. Andrews, J.M., *Determination of minimum inhibitory concentrations.* Journal of antimicrobial Chemotherapy, 2001. **48**(suppl_1): p. 5-16.

200. Saviano, L., *et al.*, *Catalytic Activity of Rare Earth Elements (REEs) in Advanced Oxidation Processes of Wastewater Pollutants: A Review.* Molecules, 2023. **28**(17): p. 6185.

201. Liu, S., *Electronic structure of rare earth metals.* Handbook on the physics and chemistry of rare earths, 1978. **1**: p. 233-335.

202. Been, E., *et al.*, *Electronic structure trends across the rare-earth series in superconducting infinite-layer nickelates.* Physical Review X, 2021. **11**(1): p. 011050.

203. Chong, M.N., *et al.*, *Recent developments in photocatalytic water treatment technology: a review.* Water research, 2010. **44**(10): p. 2997-3027.

204. Kajjumba, G.W. and E.J. Marti, *A review of the application of cerium and lanthanum in phosphorus removal during wastewater treatment: Characteristics, mechanism, and recovery.* Chemosphere, 2022: p. 136462.

205. Kajjumba, G.W., M. Attene-Ramos, and E.J. Marti, *Toxicity of lanthanide coagulants assessed using four in vitro bioassays.* Science of The Total Environment, 2021. **800**: p. 149556.

206. Gonzalez, V., *et al.*, *Environmental fate and ecotoxicity of lanthanides: are they a uniform group beyond chemistry?* Environment international, 2014. **71**: p. 148-157.

207. Ghadiri, M., *et al.*, *Computational simulation for transport of priority organic pollutants through nanoporous membranes.* Chemical Engineering & Technology, 2013. **36**(3): p. 507-512.

208. Nie, Y., *et al.*, *Enhanced Fenton-like degradation of refractory organic compounds by surface complex formation of LaFeO3 and H2O2.* Journal of hazardous materials, 2015. **294**: p. 195-200.

209. Younes, H.A., *et al.*, *Perovskite/metal-organic framework photocatalyst: A novel nominee for eco-friendly uptake of pharmaceuticals from wastewater.* Journal of Alloys and Compounds, 2023. **930**: p. 167322.

210. Chen, X., *et al.*, *Synergy effect between adsorption and heterogeneous photo-Fenton-like catalysis on LaFeO3/lignin-biochar composites for high efficiency degradation of ofloxacin under visible light.* Separation and Purification Technology, 2022. **280**: p. 119751.

211. Assumpção, M.H.M.T., *et al.*, *Degradation of dipyrone via advanced oxidation processes using a cerium nanostructured electrocatalyst material.* Applied Catalysis A: General, 2013. **462**: p. 256-261.
212. Chong, S., *et al.*, *Preparation of FeCeOx by ultrasonic impregnation method for heterogeneous Fenton degradation of diclofenac.* Ultrasonics sonochemistry, 2016. **32**: p. 231-240.
213. Wang, N., *et al.*, *A review on Fenton-like processes for organic wastewater treatment.* Journal of Environmental Chemical Engineering, 2016. **4**(1): p. 762-787.
214. Wang, W., *et al.*, *Fe doped CeO2 nanosheets as Fenton-like heterogeneous catalysts for degradation of salicylic acid.* Chemical Engineering Journal, 2018. **333**: p. 226-239.
215. Wang, X., *et al.*, *Electro-catalytic activity of CeO x modified graphite felt for carbamazepine degradation via E-peroxone process.* Frontiers of Environmental Science & Engineering, 2021. **15**: p. 1-10.
216. Hu, B., *et al.*, *Cobalt-gadolinium modified biochar as an adsorbent for antibiotics in single and binary systems.* Microchemical Journal, 2021. **166**: p. 106235.
217. Luan, J., *et al.*, *Synthesis and Property Examination of Er2FeSbO7/BiTiSbO6 Heterojunction Composite Catalyst and Light-Catalyzed Retrogradation of Enrofloxacin in Pharmaceutical Waste Water under Visible Light Irradiation.* Materials, 2022. **15**(17): p. 5906.
218. Shi, X., *et al.*, *FeOCl/Ln (Ln= La or Y): efficient photo-Fenton catalysts for ibuprofen degradation.* New Journal of Chemistry, 2019. **43**(41): p. 16273-16280.
219. Tahir, M.B. and M. Sagir, *Carbon nanodots and rare metals (RM= La, Gd, Er) doped tungsten oxide nanostructures for photocatalytic dyes degradation and hydrogen production.* Separation and Purification Technology, 2019. **209**: p. 94-102.
220. Sharmin, F. and M. Basith, *Highly efficient photocatalytic degradation of hazardous industrial and pharmaceutical pollutants using gadolinium doped BiFeO3 nanoparticles.* Journal of Alloys and Compounds, 2022. **901**: p. 163604.
221. Nzila, A., S.A. Razzak, and J. Zhu, *Bioaugmentation: an emerging strategy of industrial wastewater treatment for reuse and discharge.* International journal of environmental research and public health, 2016. **13**(9): p. 846.
222. Adriaenssens, N., *et al.*, *Consumption of quinolones in the community, European union/European Economic area, 1997–2017.* Journal of Antimicrobial Chemotherapy, 2021. **76**(Supplement_2): p. ii37-ii44.
223. Zhou, H.-P., *et al.*, *General and facile synthesis of ceria-based solid solution nanocrystals and their catalytic properties.* Journal of Solid State Chemistry, 2009. **182**(9): p. 2475-2485.
224. Singh, K., R. Kumar, and A. Chowdhury, *Synthesis of La-doped ceria nanoparticles: impact of lanthanum depletion.* Journal of materials science, 2016. **51**: p. 4134-4141.
225. EUCAST, *European Committee on Antimicrobial Susceptibility Testing*. 2014.